

ISSN : 2165-4069(Online)

ISSN : 2165-4050(Print)



IJARAI

International Journal of  
Advanced Research in Artificial Intelligence

Volume 2 Issue 9

[www.ijarai.thesai.org](http://www.ijarai.thesai.org)

A Publication of  
The Science and Information Organization



INTERNATIONAL JOURNAL OF  
ADVANCED RESEARCH IN ARTIFICIAL INTELLIGENCE



THE SCIENCE AND INFORMATION ORGANIZATION  
[www.thesai.org](http://www.thesai.org) | [info@thesai.org](mailto:info@thesai.org)



## Editorial Preface

### *From the Desk of Managing Editor...*

"The question of whether computers can think is like the question of whether submarines can swim." — Edsger W. Dijkstra, the quote explains the power of Artificial Intelligence in computers with the changing landscape. The renaissance stimulated by the field of Artificial Intelligence is generating multiple formats and channels of creativity and innovation.

This journal is a special track on Artificial Intelligence by The Science and Information Organization and aims to be a leading forum for engineers, researchers and practitioners throughout the world.

The journal reports results achieved; proposals for new ways of looking at AI problems and include demonstrations of effectiveness. Papers describing existing technologies or algorithms integrating multiple systems are welcomed. IJARAI also invites papers on real life applications, which should describe the current scenarios, proposed solution, emphasize its novelty, and present an in-depth evaluation of the AI techniques being exploited. IJARAI focusses on quality and relevance in its publications.

In addition, IJARAI recognizes the importance of international influences on Artificial Intelligence and seeks international input in all aspects of the journal, including content, authorship of papers, readership, paper reviewers, and Editorial Board membership.

The success of authors and the journal is interdependent. While the Journal is in its initial phase, it is not only the Editor whose work is crucial to producing the journal. The editorial board members, the peer reviewers, scholars around the world who assess submissions, students, and institutions who generously give their expertise in factors small and large— their constant encouragement has helped a lot in the progress of the journal and shall help in future to earn credibility amongst all the reader members.

I add a personal thanks to the whole team that has catalysed so much, and I wish everyone who has been connected with the Journal the very best for the future.

**Thank you for Sharing Wisdom!**

**Managing Editor**  
**IJARAI**  
**Volume 2 Issue 9 September 2013**  
**ISSN: 2165-4069(Online)**  
**ISSN: 2165-4050(Print)**  
**©2013 The Science and Information (SAI) Organization**

# Editorial Board

**Peter Sapaty - Editor-in-Chief**

**National Academy of Sciences of Ukraine**

Domains of Research: Artificial Intelligence

**Alaa F. Sheta**

**Electronics Research Institute (ERI)**

Domain of Research: Evolutionary Computation, System Identification, Automation and Control, Artificial Neural Networks, Fuzzy Logic, Image Processing, Software Reliability, Software Cost Estimation, Swarm Intelligence, Robotics

**Antonio Dourado**

**University of Coimbra**

Domain of Research: Computational Intelligence, Signal Processing, data mining for medical and industrial applications, and intelligent control.

**David M W Powers**

**Flinders University**

Domain of Research: Language Learning, Cognitive Science and Evolutionary Robotics, Unsupervised Learning, Evaluation, Human Factors, Natural Language Learning, Computational Psycholinguistics, Cognitive Neuroscience, Brain Computer Interface, Sensor Fusion, Model Fusion, Ensembles and Stacking, Self-organization of Ontologies, Sensory-Motor Perception and Reactivity, Feature Selection, Dimension Reduction, Information Retrieval, Information Visualization, Embodied Conversational Agents

**Liming Luke Chen**

**University of Ulster**

Domain of Research: Semantic and knowledge technologies, Artificial Intelligence

**T. V. Prasad**

**Lingaya's University**

Domain of Research: Bioinformatics, Natural Language Processing, Image Processing, Robotics, Knowledge Representation

**Wichian Sittiprapaporn**

**Maharakham University**

Domain of Research: Cognitive Neuroscience; Cognitive Science

**Yaxin Bi**

**University of Ulster**

Domains of Research: Ensemble Learning/Machine Learning, Multiple Classification Systems, Evidence Theory, Text Analytics and Sentiment Analysis

---

## Reviewer Board Members

- **Alaa Sheta**  
Electronics Research Institute (ERI)
- **Albert Alexander**  
Kongu Engineering College
- **Amir HAJJAM EL HASSANI**  
Université de Technologie de Belfort-Monbéliard
- **Amit Verma**  
Department in Rayat & Bahra Engineering College, Mo
- **Antonio Dourado**  
University of Coimbra
- **B R SARATH KUMAR**  
Lenora College of Engineering
- **Babatunde Opeoluwa Akinkunmi**  
University of Ibadan
- **Bestoun S.Ahmed**  
Universiti Sains Malaysia
- **Chien-Peng Ho**  
Information and Communications Research Laboratories, Industrial Technology Research Institute of Taiwan
- **David M W Powers**  
Flinders University
- **Dimitris Chrysostomou**  
Democritus University
- **Dr.Dhananjay R Kalbande**  
Mumbai University
- **Francesco Perrotta**  
University of Macerata
- **Frank Ibikunle**  
Covenant University
- **Grigoras Gheorghe**  
"Gheorghe Asachi" Technical University of Iasi, Romania
- **Guandong Xu**  
Victoria University
- **Haibo Yu**  
Shanghai Jiao Tong University
- **Jatinderkumar R. Saini**  
S.P.College of Engineering, Gujarat
- **Krishna Prasad Miyapuram**  
University of Trento
- **Luke Liming Chen**  
University of Ulster
- **Marek Reformat**  
University of Alberta
- **Md. Zia Ur Rahman**  
Narasaraopeta Engg. College, Narasaraopeta
- **Mokhtar Beldjehem**  
University of Ottawa
- **Monji Kherallah**  
University of Sfax
- **Nitin S. Choubey**  
Mukesh Patel School of Technology Management & Eng
- **Rajesh Kumar**  
National University of Singapore
- **Rajesh K Shukla**  
Sagar Institute of Research & Technology-Excellence, Bhopal MP
- **Rongrong Ji**  
Columbia University
- **Said Ghoniemy**  
Taif University
- **Samarjeet Borah**  
Dept. of CSE, Sikkim Manipal University
- **Sana'a Wafa Tawfeek Al-Sayegh**  
University College of Applied Sciences
- **Saurabh Pal**  
VBS Purvanchal University, Jaunpur
- **Shahaboddin Shamshirband**  
University of Malaya
- **Shaidah Jusoh**  
Zarqa University
- **Shrinivas Deshpande**
- **SUKUMAR SENTHILKUMAR**  
Universiti Sains Malaysia
- **T C.Manjunath**  
HKBK College of Engg
- **T V Narayana Rao**  
Hyderabad Institute of Technology and Management
- **T. V. Prasad**

Lingaya's University

- **Vitus S.W Lam**  
Domains of Research
- **VUDA Sreenivasarao**  
St. Mary's College of Engineering &  
Technology
- **Vishal Goyal**
- **Wei Zhong**  
University of south Carolina Upstate
- **Wichian Sittiprapaporn**  
Mahasarakham University
- **Yaxin Bi**

University of Ulster

- **Yuval Cohen**  
The Open University of Israel
- **Zhao Zhang**  
Deptment of EE, City University of Hong  
Kong
- **Zne-Jung Lee**  
Dept. of Information management, Huafan  
University
- **Zhigang Yin**  
Institute of Linguistics, Chinese Academy of  
Social Sciences

# CONTENTS

**Paper 1: An Efficient Routing Protocol under Noisy Environment for Mobile Ad Hoc Networks using Fuzzy Logic**

*Authors: Supriya Srivastava, A. K. Daniel*

**PAGE 1 – 6**

**Paper 2: Genetic Algorithm Utilizing Image Clustering with Merge and Split Processes Which Allows Minimizing Fisher Distance Between Clusters**

*Authors: Kohei Arai*

**PAGE 7 – 13**

**Paper 3: Secure Copier Which Allows Reuse Copied Documents with Sorting Capability in Accordance with Document Types**

*Authors: Kohei Arai*

**PAGE 14 – 18**

**Paper 4: Bi-Directional Reflectance Distribution Function: BRDF Effect on Un-mixing, Category Decomposition of the Mixed Pixel (MIXEL) of Remote Sensing Satellite Imagery Data**

*Authors: Kohei Arai*

**PAGE 19 – 23**

**Paper 5: Visualization of 5D Assimilation Data for Meteorological Forecasting and Its Related Disaster Mitigations Utilizing Vis5D of Software Tool**

*Authors: Kohei Arai*

**PAGE 24 – 29**

**Paper 6: Comparative Study Among Least Square Method, Steepest Descent Method, and Conjugate Gradient Method for Atmospheric Sounder Data Analysis**

*Authors: Kohei Arai*

**PAGE 30 – 37**

**Paper 7: An Approach with Support Vector Machine using Variable Features Selection on Breast Cancer Prognosis**

*Authors: Sandeep Chaurasia, Dr. P Chakrabarti*

**PAGE 38 – 42**

**Paper 8: A Discrete Mechanics Approach to Gait Generation on Periodically Unlevel Grounds for the Compass-type Biped Robot**

*Authors: Tatsuya Kai, Takeshi Shintani*

**PAGE 43 – 51**

**Paper 9: The Paradox of the Fuzzy Disambiguation in the Information Retrieval**

*Authors: Anna Bryniarska*

**PAGE 52 – 58**

# An Efficient Routing Protocol under Noisy Environment for Mobile Ad Hoc Networks using Fuzzy Logic

Supriya Srivastava<sup>1</sup> and A. K. Daniel<sup>2</sup>

<sup>1,2</sup>Computer Science & Engineering Department M M M Engineering College, Gorakhpur U.P. (India)

**Abstract**—A MANET is a collection of mobile nodes communicating and cooperating with each other to route a packet from the source to their destinations. A MANET is used to support dynamic routing strategies in absence of wired infrastructure and centralized administration. In this paper, we propose a routing algorithm for the mobile ad hoc networks based on fuzzy logic to discover an optimal route for transmitting data packets to the destination. This protocol helps every node in MANET to choose next efficient successor node on the basis of channel parameters like environment noise and signal strength. The protocol improves the performance of a route by increasing network life time, reducing link failure and selecting best node for forwarding the data packet to next node.

**Keywords**—Fuzzy Logic; Noise; Signal Strength; MANET

## I. INTRODUCTION

Mobile ad hoc network is a collection of mobile devices which can communicate through wireless links. The task of routing protocol is to direct packets from source to destination. This is particularly hard in mobile ad hoc networks due to the mobility of the network elements and lack of centralized control. Source routing is a routing technique in which the sender of a packet determines the complete sequence of nodes through which it forwards the packet. The sender explicitly lists this route in the packet's header, identifying each forwarding "hop" by the address of the next node to which to transmit the packet on its way to the destination host. When a host needs a route to another host, it dynamically determines one based on cached information and on the results of a route discovery protocol, unlike conventional routing protocols.

Routing in MANET using the shortest hop count is not a sufficient condition to construct high-quality routes, because minimum hop count routing often chooses routes that have significantly less capacity than the best routes that exist in the network [1]. The routes selected based on hop count alone may be of bad quality since the routing protocols do not ignore weak quality links which are typically used to connect to remote nodes. The weak quality of a link can be the result of under considered metrics like Energy, SNR, Packet Loss, Maximum available bandwidth, load etc. The links usually have poor signal-to-noise ratio (SNR), hence higher frame error rates and lower throughput [2] [3].

All real measurements in any network are disturbed by noise. This includes electronic noise, but can also include external events that affect the measured phenomenon—wind,

vibrations, gravitational attraction of the moon, variations of temperature, variations of humidity, etc., depending on its measurement and of the sensitivity of the device. It is not possible to reduce the noise by controlling the environment.

Otherwise, when the characteristics of the noise are known and are different from the signals, it is possible to filter it or to process the signal. In MANET, it is always needed to choose a channel with lower noise that result in reduction of number of dropped packets to increase the quality of service. The possibility that a packet will drop due to poor signal of the assigned transmission channel is called as "Dropped Call". The dropped packet rate is dependent on the following factors:

- The Channel Capacity
- Level of Traffic in the system
- Probability that noise is above unavoidable frequency.
- Probability that Residual Energy of nodes is below threshold
- Probability that Signal Strength is below Receiver threshold.
- Probability that Signal is below the specified Co-Channel interference level.

The proposed approach is called An Efficient Routing Protocol under Noisy Environment for Mobile Ad Hoc Networks using Fuzzy Logic (ERP). In this paper, the proposed protocol enhances Dynamic Source Routing protocol by considering Signal strength and Noise constraints to improve its performance. The fuzzy logic based technique uses two important parameters as noise factor and signal strength for route selection that results in best possible combinations to choose a route. The proposed protocol defines how a fuzzy logic based technique is effective to select routes, avoid link failure and increase network lifetime. A control mechanism like fuzzy logic is used to make mobile nodes intelligent. Fuzzy logic is basically the extension of crisp logic that includes the intermediate values between absolutely true and absolutely false. It has the efficiency to solve the system uncertainties.

The rest of the paper is organized as follows: related work and design issue in Section 2, the proposed protocol in Section 3, validation and analysis in Section 4 and finally Conclusion in Section 5.

## II. DESIGN ISSUES AND RELATED WORK

The movement of the nodes, packet collision and bad channel condition are the various reasons for the data packets to loss. Packet losses are subjected to occur due to continuous period of intermittent failure during the communication between nodes. The fading conditions cause certain nodes to completely lose their connectivity. Signal-to-Noise ratio is an important issue over a link; the links that usually have bad signal-to-noise ratio (SNR) have higher frame error rates and lower throughput, resulting in link failure. Signal-to-noise ratio (SNR or S/N) compares the level of a desired signal to the level of background noise [4].

- SNR is defined as the ratio of signal power to the noise power. A ratio higher than 1:1 indicates more signal than noise.

$$SNR = \frac{P_{Signal}}{P_{noise}}$$

Where  $P$  is average power

- Both signal and noise power must be measured at the same and equivalent points in a system, and within the same system bandwidth. If the signal and the noise are measured across the same impedance, then the SNR can be obtained by calculating the square of the amplitude ratio:

$$SNR = \frac{P_{Signal}}{P_{noise}} = \left(\frac{A_{Signal}}{A_{noise}}\right)^2$$

Where  $A$  is root mean square (RMS) of amplitude

- In decibels, the SNR is defined as

$$SNR_{dB} = 10 \log_{10} \left( \frac{P_{Signal}}{P_{noise}} \right) \\ = P_{signal, dB} - P_{noise, dB}$$

- Noise Limited System,  $\mu \rightarrow 0$

Here, we are considering only noise limited system, so the effect of receiver threshold signal can be considered and also assumed that there will not be any Co-Channel interference. In such a case,  $\mu \rightarrow 0$  and the expression for dropped packet rate is

$$D = \sum_{n=0}^N a_n D_n = \sum_{n=0}^N a_n [1 - (1 - \delta)^n]$$

- Interference Limited System,  $\delta \rightarrow 0$

Here, we are consider only interference-limited system, so the effect of Co-Channel interference can be considered and also assumed that there will not be any kind of noise which is introducing in the system. In such a case,  $\delta \rightarrow 0$  and the expression for dropped packet rate is

$$D = \sum_{n=0}^N a_n D_n = \sum_{n=0}^N a_n [1 - (1 - \mu)^n]$$

Many algorithms have been proposed for route selection in Mobile Ad-Hoc network in recent years. Some of them are:

**Devi M. [5]** propose a fuzzy based route recovery technique. It consists of two phases, Proactive failure discovery, and Route failure recovery. Nodes in the network estimate the metrics Link Expiration Time (LET), Received Signal Strength (RSS), Available Band Width (ABW) and Residual Energy (RE) and using fuzzy logic, the type of node is estimated as weak, normal or strong.

**Fuad Alnajjar et al. [4]** has proposed a mechanism to provide an efficient QoS routing protocol to enhance the performance of existing routing protocols in Mobile ad hoc network environment.

**Supriya Srivastava et al [6]** proposes an Energy-Efficient Routing protocol that will improve the utilization of link by balancing the energy consumption between utilized and underutilized nodes. It also proposed a method for maintenance of the route during a link failure.

**Junghwi Jeon et al. [7]** have proposed a fast route recovery scheme to solve the link failure problem caused by node movement, packet collision or bad channel condition.

**Merlinda Drini [8]** explained that the mobility of the nodes, packet collision and bad channel condition are the various reasons for the data packets to fail. Packet losses are subjected to occur due to continuous period of intermittent failure during the communication between nodes. The fading conditions cause certain nodes to completely lose their connectivity.

**Nityananda Sarma et al. [9]** have proposed a simple model for computing link stability and route stability based on received signal strengths.

**Tomonori Kagi et al. [10]** have proposed a reliability improvement method in mobile ad hoc networks by applying network coding encoded by a relay node. Therefore, reliability is improved without requiring the source node to send redundant encoding packets.

**Srinivas Sethi et al [11]** have proposed an Optimized Reliable Ad hoc On-demand Distance Vector (ORAODV) scheme that offers quick adoption to dynamic link conditions, low processing and low network utilization in ad hoc network.

**V. Ramesh et al [12]** have proposed a dynamic source routing protocol in which the mobile node uses signal power strength from the received packets to predict the link breakage time, and sends a warning to the source node of the packet if the link is soon-to-be-broken.

**Khalid Zahedi et al [13]** have proposed and implemented a new approach for solving the problem of link breakages in MANET in Dynamic Source Routing (DSR) routing protocol.

**Senthilkumar Maruthamuthu et al [14]** have discussed the new protocol QPHMP-SHORT with multiple QoS

constraints based on the QoS parameters namely delay, jitter, bandwidth, and cost metrics between source and destination.

### III. PROPOSED MODEL FOR NODE SELECTION USING FUZZY LOGIC BASED TECHNIQUE

The proposed protocol uses Fuzzy based decision making technique to verify the status of a node. As an outcome of fuzzy decision rules, the node status can be considered as Little Strong, Strong, Very Strong, Lower Medium, Medium, Higher Medium, Little Weak, Weak, and Very Weak. Before a node transmits the data to the next node, it checks the status of that node. This estimated decision is stored in a routing table and is exchanged among all neighbors using a status flag with RREQ message. Data packets are transmitted through intermediate nodes that are in the routing table, whenever the source node sends data to the destination. If the status of a node is Little Weak, Weak or Very Weak then the sending does not transmit the packet to that node, if the status of a node is Lower Medium, Medium or Higher then that node is considerable for receiving the packet from sender node but if the status of a node is Little Strong, Strong, Very Strong then the sending node will choose this node for efficient data packet transmission. The process of node selection consists of two input functions that transform the system inputs into fuzzy sets such as Noise Factor and Signal Strength of paths between any two nodes. Fuzzy set for Noise Factor and Signal Strength in the protocol can be defined as,

$$A = \{(d, \mu_A(n))\}, n \in N_s$$

And

$$B = \{(e, \mu_B(s))\}, s \in S_i$$

Where,

$N_s$  are universe of discourse for Noise and  $S_i$  is a universe of discourse for Signal Strength,  
 $n$  and  $s$  are particular elements of  $N_s$  and  $S_i$  respectively,  
 $\mu_A(n)$ ,  $\mu_B(s)$  are membership functions, find the degree of membership of the element in a given set.

Membership functions for Noise and Signal Strength are defined from Figure 1, as follows:

$$\mu_A(n) = \left\{ \begin{array}{ll} 0, & \text{if } n > TH_2 \\ (n - TH_1) / TH_1 - TH_2, & \text{if } TH_1 \geq n \geq TH_2 \\ 1, & \text{if } n \leq TH_1 \end{array} \right\}$$

$$\mu_B(s) = \left\{ \begin{array}{ll} 0, & \text{if } s \leq TH_1 \\ (TH_1 - s) / TH_1 - TH_2, & \text{if } TH_1 < s < TH_2 \\ 1, & \text{if } s \geq TH_2 \end{array} \right\}$$

Where,

$TH_1$  = Threshold to activate system

$TH_2$  = Threshold which identifies the level of activeness

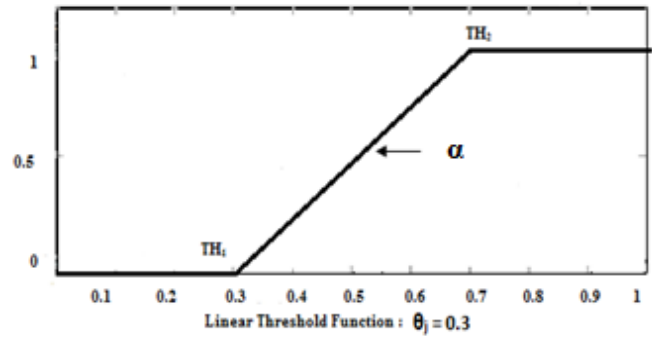


Fig. 1. Graph showing minimum and maximum threshold for any input variable

A fuzzy relation is a relation between elements of  $N_s$  and elements of  $S_i$ , described by a membership function,

$$\mu_{N_s \times S_i}(n, s), n \in N_s \text{ and } s \in S_i$$

Now applying AND fuzzy operator i.e.  $\min(\wedge)$  on fuzzy relation,

$$\begin{aligned} \mu_A(n) \wedge \mu_B(s) &= \min(\mu_A(n), \mu_B(s)) \\ &= \left\{ \begin{array}{ll} \mu_A(n), & \text{if and only if } \mu_A(n) \leq \mu_B(s) \\ \mu_B(s), & \text{if and only if } \mu_A(n) \geq \mu_B(s) \end{array} \right\} \end{aligned}$$

#### A. Rule Evaluation

The proposed protocol is a fuzzy logic based protocol for the selection of successor node for data packet transmission. The process of route selection consists of two input functions that transform the system inputs into fuzzy sets such as Noise Factor and Signal Strength of paths between any two nodes.

The Table 1 of Input Function uses three membership functions to show the varying degrees of input variables.

TABLE I. INPUT FUNCTION

Input	Membership		
Noise Factor	Light	Medium	Heavy
Signal Strength	Weak	Adequate	Strong

In Table 2, 9 membership functions are defined that represent the varying output memberships of the fuzzy output defined for each of the rules in the rule set and the graph for the same is shown in Figure 2.

Then an aggregation of these fuzzy probabilistic values into a single fuzzy output is represented in a detailed rule-set (Table 3).

TABLE II. OUTPUT FUNCTION

Output	Membership
Output Memberships	Little Strong, Strong, Very Strong, Lower Medium, Medium, Higher, Medium, Little Weak, Weak, Very Weak

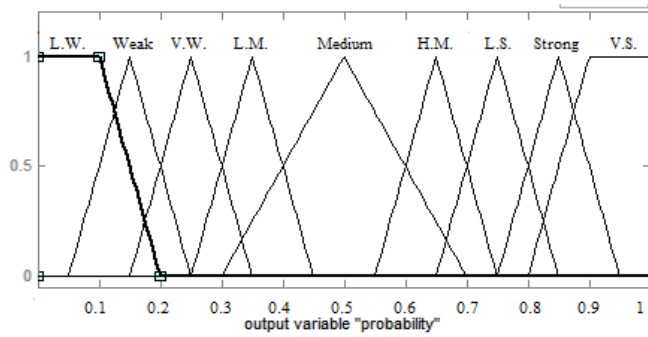


Fig. 2. Graph showing all possible probabilities of output variable

**B. The Proposed Rule set**

The given protocol defines all the possible combinations of the different membership functions for the two input variables that results in 9 rules for the fuzzy inference shown in Table 3.

TABLE III. RULE SET TABLE

Noise Factor	Signal Strength	Output Memberships
Light	Weak	Higher Medium
Light	Adequate	Strong
Light	Strong	Very Strong
Medium	Weak	Little Weak
Medium	Adequate	Medium
Medium	Strong	Little Strong
Heavy	Weak	Very Weak
Heavy	Adequate	Weak
Heavy	Strong	Lower Medium

- Rule 1**  
IF Noise Factor is Light AND Signal Strength is Weak  
THEN output membership is Higher Medium
- Rule 2**  
IF Noise Factor is Light AND Signal Strength is Adequate  
THEN output membership is Strong
- Rule 3**  
IF Noise Factor is Light AND Signal Strength is Strong  
THEN output membership is Very Strong
- Rule 4**  
IF Noise Factor is Medium AND Signal Strength is Weak  
THEN output membership is Little Weak
- Rule 5**  
IF Noise Factor is Medium AND Signal Strength is Adequate  
THEN output membership is Medium
- Rule 6**  
IF Noise Factor is Medium AND Signal Strength is Strong  
THEN output membership is Little Strong
- Rule 7**  
IF Noise Factor is Heavy AND Signal Strength is Weak  
THEN output membership is Very Weak
- Rule 8**  
IF Noise Factor is Heavy AND Signal Strength is Adequate  
THEN output membership is Weak
- Rule 9**  
IF Noise Factor is Heavy AND Signal Strength is Strong  
THEN output membership is Lower Medium

**IV. VALIDATION AND ANALYSIS**

Let us consider a network of 5 nodes and 6 edges.

Now suppose the noise factor at each edge as:

$$N_s = \{0.1, 0.3, 0.4, 0.7, 0.8, 0.9\}$$

And the signal strength at each edge as:

$$S_i = \{0.2, 0.3, 0.5, 0.6, 0.9, 0.1\}$$

A membership function based on the noise at each edge and its graphical representation is shown in Figure-3

$$\mu_{\text{Noise}}(n) = \left. \begin{cases} 0, & \text{if } \text{Noise}(n) \geq 0.8 \text{ (TH}_2\text{)} \\ (0.8 - \text{Noise}(n))/0.2, & \text{if } 0.6 < \text{Noise}(n) < 0.8 \\ 1, & \text{if } \text{Noise}(n) \leq 0.6 \end{cases} \right\}$$

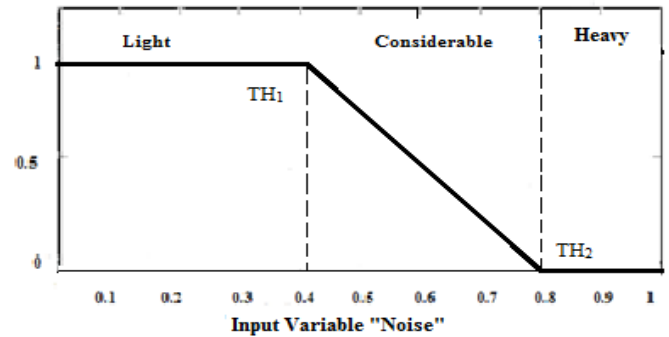


Fig. 3. Graph showing membership functions for input variable "Noise"

A membership function based on the Signal Strength at each edge and its graphical representation is shown in Figure-4

$$\mu_{\text{Signal}}(s) = \left. \begin{cases} 0, & \text{if } \text{Signal}(s) \leq 0.3 \text{ (TH}_1\text{)} \\ (\text{Signal}(s) - 0.3)/0.4, & \text{if } 0.3 < \text{Signal}(s) < 0.7 \\ 1, & \text{if } \text{Signal}(s) \geq 0.7 \end{cases} \right\}$$

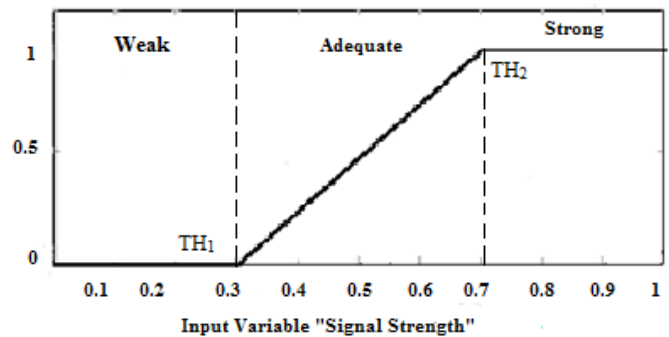


Fig. 4. Graph showing membership functions for input variable "Signal Strength"

Now calculate the degree of membership of Noise and Signal Strength using the above defined membership functions for both of these input variables which are shown in Table 4 and Table 5.

TABLE IV. DEGREE OF MEMBERSHIP OF NOISE

Noise (Ns)	Degree of Lightness
0.1	1
0.3	1
0.4	1
0.7	0.5
0.8	0
0.9	0

In Table 4 for the Noise factors {0.1, 0.3, 0.4, 0.7, 0.8, 0.9} the degree of memberships are {1, 1, 1, 0.5, 0, 0} respectively. According to fuzzy output the memberships of the above noise factors are,

**{0.1| weak, 0.3| weak, 0.4| weak, 0.7|Considerable, 0.8| Considerable, 0.9| heavy}**

TABLE V. DEGREE OF MEMBERSHIP OF SIGNAL STRENGTH

Signal (Si)	Degree of Strongness
0.2	0
0.3	0
0.5	0.5
0.6	0.75
0.9	1
01	1

In Table 5 for the Signal Strengths {0.2, 0.3, 0.5, 0.6, 0.9, 1} the degree of memberships are {0, 0, 0.5, 0.75, 1, 1} respectively. According to fuzzy output the memberships of the above Signal Strengths are,

**{0.2| weak, 0.3| weak, 0.4| Adequate, 0.7| Adequate, 0.8| Strong, 0.9| Strong}**

Now create Table 6 that shows the fuzzy relation between membership functions of noise factor and signal strength.

TABLE VI. FUZZY RELATION ON MEMBERSHIP VALUE OF SIGNAL STRENGTH AND NOISE

$\frac{Si}{Ns}$	0.2	0.3	0.5	0.6	0.9	1
0.1	1 $\wedge$ 0	1 $\wedge$ 0	1 $\wedge$ 0.5	1 $\wedge$ 0.75	1 $\wedge$ 1	1 $\wedge$ 1
0.3	1 $\wedge$ 0	1 $\wedge$ 0	1 $\wedge$ 0.5	1 $\wedge$ 0.75	1 $\wedge$ 1	1 $\wedge$ 1
0.4	1 $\wedge$ 0	1 $\wedge$ 0	1 $\wedge$ 0.5	1 $\wedge$ 0.75	1 $\wedge$ 1	1 $\wedge$ 1
0.7	0.5 $\wedge$ 0	0.5 $\wedge$ 0	0.5 $\wedge$ 0.5	0.5 $\wedge$ 0.75	0.5 $\wedge$ 1	0.5 $\wedge$ 1
0.8	0 $\wedge$ 0	0 $\wedge$ 0	0 $\wedge$ 0.5	0 $\wedge$ 0.75	0 $\wedge$ 1	0 $\wedge$ 1
0.9	0 $\wedge$ 0	0 $\wedge$ 0	0 $\wedge$ 0.5	0 $\wedge$ 0.75	0 $\wedge$ 1	0 $\wedge$ 1

The result of the AND ( $\wedge$ ) operation process on membership values of Signal Strength and Noise shown in Table 7.

TABLE VII. RESULT AFTER AND FUZZY OPERATION

$\frac{Si}{Ns}$	0.2	0.3	0.5	0.6	0.9	1
0.1	0	0	0.5	0.75	1	1
0.3	0	0	0.5	0.75	1	1
0.4	0	0	0.5	0.75	1	1
0.7	0	0	0.5	0.5	0.5	0.5
0.8	0	0	0	0	0	0
0.9	0	0	0	0	0	0

The possible combinations of distance and energy with higher membership value shown in Table 8:

TABLE VIII. OUTPUT TABLE

$\frac{Si}{Ns}$	0.9	1
0.1	1	1
0.3	1	1
0.4	1	1

The degree of membership of noise and signal is shown in Table 9.

TABLE IX. OUTPUT TABLE WITH THE DEGREE OF MEMBERSHIP

Noise (Ns)	Degree membership of (Noise)	Signal (Si)	Degree of Strongness of (Signal)
0.1	Light	0.9	Strong
0.3	Light	1	Strong
0.4	Light		

The output memberships for these values are “Very Strong” as “Noise is Light and Signal strength is strong”. Now all the resultant possible combinations of noise and signal strength are:

- Noise factor = 0.1 and Signal strength = 0.9
- Noise factor = 0.1 and Signal strength = 1
- Noise factor = 0.3 and Signal strength = 0.9
- Noise factor = 0.3 and Signal strength = 1
- Noise factor = 0.4 and Signal strength = 0.9
- Noise factor = 0.4 and Signal strength = 1.

The effective edge to be selected can have any of the above combinations. But the perfect combination among all combinations is when noise factor is 0.1 and signal strength is 1, which will be perfect for transmission of data packet to next successor node.

#### A. Performance Evaluation

The proposed protocol is a fuzzy logic based protocol for the efficient successive edge selection for data packet transmission. The best possible outcomes obtained from the above proposed fuzzy logic based protocol helps a mobile Ad-Hoc network to choose an efficient edge on the basis of parameters like environment noise and signal strength. The protocol improves the performance of a route by increasing network life time, reducing link failure and selecting best node for forwarding the data packet to next node.

#### V. CONCLUSIONS

The proposed protocol an Efficient Routing Protocol under Noisy Environment for Mobile Ad Hoc Networks using Fuzzy Logic (ERP) is efficient for transmission of data. The status of the node is verified before a node transmits the data to the

next node. The designed fuzzy logic controller determines, best outcome from all the possible combinations of offered signal strength and noise. If the status is normal or strong, then it transmits the packet to the next node. The validation shows that the fuzzy based effective edge selection technique increases packet delivery ratio, decreases link failure, lowers error rate and increases throughput.

#### REFERENCES

- [1] Wing Ho Yuen, Heung-no Lee and Timothy D. Andersen "A simple and effective cross layer networking system for Mobile Ad Hoc Networks", in: PIMRC 2002, vol. 4, September 2002, pp. 1952-1956.
- [2] H.M. Tsai, N. Wisitpongphan, and O.K. Tonguz, "Link-quality aware AODV protocol," in Proc. IEEE International Symposium on Wireless Pervasive Computing (ISWPC) 2006, Phuket, Thailand, January 2006
- [3] E. Royer and C.-K. Toh, "A review of current routing protocols for Ad Hoc mobile wireless networks," IEEE Personal Communications Magazine, vol. 6, No. 2, April 1999.
- [4] Fuad Alnajjar and Yahao Chen "SNR/RP aware routing algorithm cross-layer design for MANET" in International Journal of Wireless & Mobile Networks (IJWMN), Vol 1, No 2, November 2009.
- [5] H Devi M. and V. Rhymend Uthariaraj "Fuzzy based route recovery technique for Mobile Ad Hoc Networks" in European Journal of Scientific Research ISSN 1450-216X Vol.83 No.1 (2012), pp.129-143.
- [6] Supriya Srivastava, A.K. Daniel "Energy-efficient position based routing protocol for MANET in proceedings of International Conference in computing, engineering and information technology (ICCEIT), 2012.
- [7] Junghwi Jeon., Kiseok Lee., and Cheeha Kim., "Fast route recovery scheme for Mobile Ad Hoc Networks", IEEE International Conference on Information Networking, 2011.
- [8] Merlinda Drini & Tarek Saadawi . "Modeling wireless channel for Ad-Hoc network routing protocol", ISCC Marakech Morocco, July 2008, Page(s): 549-555
- [9] Nityananda Sarma., and Sukumar Nandi., "Route stability based QoS routing in mobile Ad Hoc networks", IEEE international Conference on Emerging Trends in Engineering and Technology, 2008.
- [10] Tomonori Kagi., and Osamu Takahashi., "Efficient reliable data transmission using network coding in MANET multipath routing environment", Springer, KES, 2008.
- [11] Srinivas Sethi., and Siba K. Udgata., "Optimized and reliable AODV for MANET", International Journal of Computer Applications, 2010.
- [12] V.Ramesh., Dr.P.Subbaiah., and K.Sangeetha Supriya., "Modified DSR (Preemptive) to reduce link breakage and routing overhead for MANET using Proactive Route Maintenance (PRM)", Global Journal of Computer Science and Technology, 2010.
- [13] Khalid Zahedi., and Abdul Samad Ismail., "Route maintenance approach for link breakage prediction in mobile Ad Hoc networks", International Journal of Advanced Computer Science and Applications ((IJACSA), 2011.
- [14] Senthilkumar Maruthamuthu., and Somasundaram Sankaralingam., "QoS aware power and hop count constraints routing protocol with mobility prediction for MANET using SHORT", International Journal of Communications, Network and System Sciences, 2011.

# Genetic Algorithm Utilizing Image Clustering with Merge and Split Processes Which Allows Minimizing Fisher Distance Between Clusters

Kohei Arai<sup>1</sup>

Graduate School of Science and Engineering  
Saga University  
Saga City, Japan

**Abstract**—Genetic algorithm utilizing image clustering with merge and split processes which allows minimizing Fisher distance between clusters is proposed. Through experiments with simulation and real remote sensing satellite imagery data, it is found that the proposed clustering method is superior to the conventional k-means and ISODATA clustering methods in comparison to the geographic maps and classification results from Maximum Likelihood classification method.

**Keyword**—image clustering; clustering; genetic algorithm; Fisher distance

## I. INTRODUCTION

There are hierarchical and non-hierarchical clustering methods. In particular, k-means and ISODATA clustering methods are well known as conventional clustering methods with relatively high clustering performance. One of the problems of the conventional clustering methods is poor clustering performance when the data distributions are overlapped and when the data distribution is concave shape, not convective. Also Genetic Algorithm: GA clustering with fitness function of Fisher distance between clusters or some other definition of distance is proposed.

The clustering method proposed here is GA based clustering with merge and split of the cluster. Therefore, it is possible to minimize fitness function (Fisher distance, in this case) through GA process. Also it is possible to refine the clusters created through GA process by merge and split process like ISODATA.

The following section describes the proposed GA based clustering with merge and split process followed by some experiments. Then conclusion is described together with some discussions.

## II. PROPOSED METHOD

### A. GA Based Clustering Method

GA allows minimization of fitness function which is defined as distance between clusters, in general. GA based clustering performance depends on the definition of fitness function.

Fundamental scheme for the GA based image clustering is shown in Figure 1.

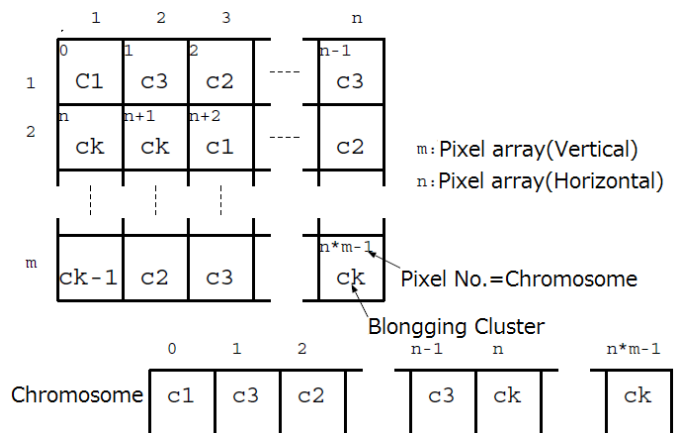


Fig. 1. Fundamental scheme for the GA based clustering

Image data is expressed with two dimensional  $m$  by  $m$  matrixes. Chromosome is defined as pixel, at first. Then selection of chromosome has to be done (based on elite selection strategy in this case). Through cross over, and mutation processes, chromosome is updated by minimizing fitness function such as distance between clusters. Thus chromosome represents cluster number, finally. Conversion can be defined with difference of chromosome between the previous and the current chromosomes. The proposed clustering method introduces Fisher distance (Ratio of within cluster variance and between cluster variance) as fitness function.

### B. Problem Discription

Basically, GA provides one of local minima, not global optimum solution. Therefore, clustering performance is not good enough. In particular, data distributions in feature space are overlapped as shown in Figure 2. It should consist of three clusters. It, however, they are overlapped each other. Therefore, it is not easy to make clusters. Furthermore, data distributions are concave shape, not convective shape Figure 3 shows conceptual illustration of process flow of the proposed merge and split procedure. In this case, cluster #1 is distributed as concave shape. If GA based cluster is applied to the data with the number of cluster is two. Then cluster #1 includes not only cluster #1 of data but also cluster #2 data at first. The number of clusters then increased from two to three. After that GA based clustering is applied to the data results in three clusters.

Finally, two clusters are merged to cluster #1 results in appropriate two clusters.

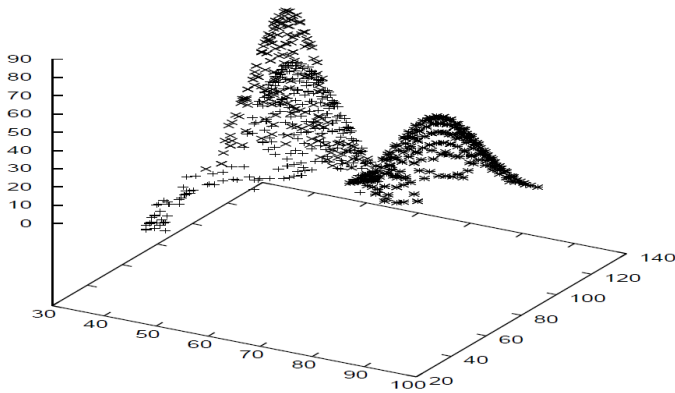


Fig. 2. Well overlapped data distribution in feature space

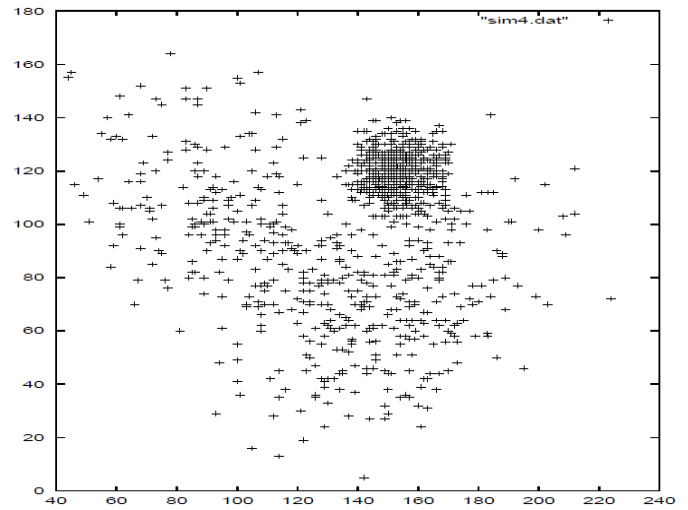


Fig. 4. Data distribution of two clusters in feature space

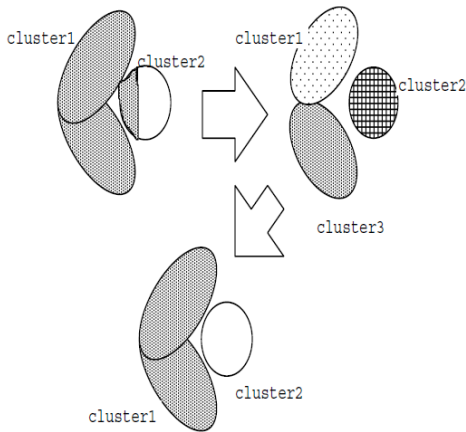


Fig. 3. Example of concave shaped data distribution in feature space.

### III. EXPERIMENTS

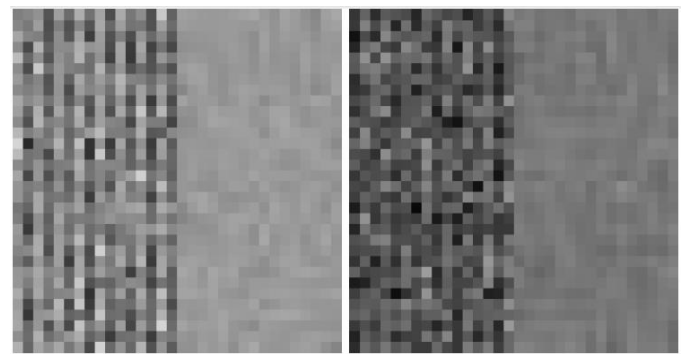
#### A. Preliminary Simulations

In order to create the aforementioned situation of data distribution like Figure 3, two clusters of simulation data is created. The simulation data is generated manually and is distributed as shown in Figure 4 in two dimensional feature spaces which are corresponding to two bands, Band 1 and Band 2. The image consists of 32 by 32 pixels. Two clusters of simulation imagery data of Band 1 and Band 2 are shown in Figure 5 (a) and (b), respectively.

The clustered result by k-means clustering is shown in Figure 6 while the clustered result from the proposed method is shown in Figure 7. In the proposed method, the parameters for GA are as follows,

- Decreasing factor for elite selection strategy: 0.75
- Cross over probability: 0.6
- Mutation probability: 0.03,
- Range for iteration: 1000 to 3000

Meanwhile, clustered resultant images for k-means and the proposed GA based clustering methods are shown in Figure 8.



(a)Band 1

(b)Band 2

Fig. 5. Two clusters simulation imagery data

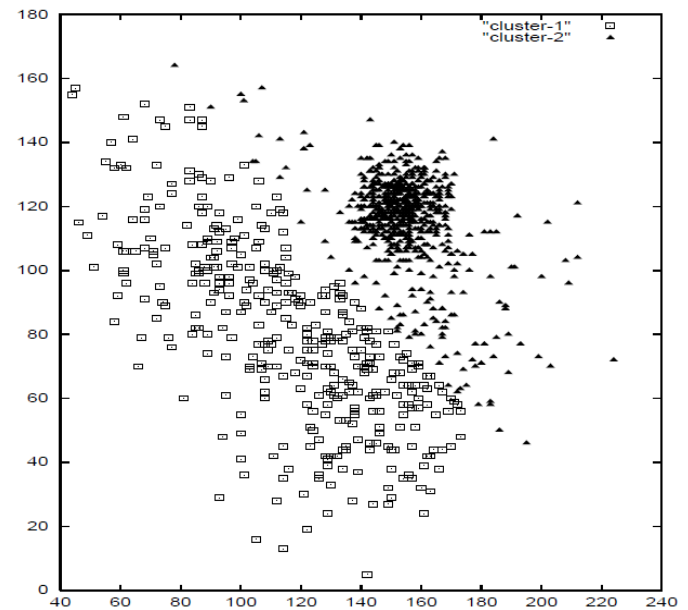


Fig. 6. Clustered result by k-means clustering method on two dimensional feature plane (Percent Correct Clustering: PCC is 86.5%)

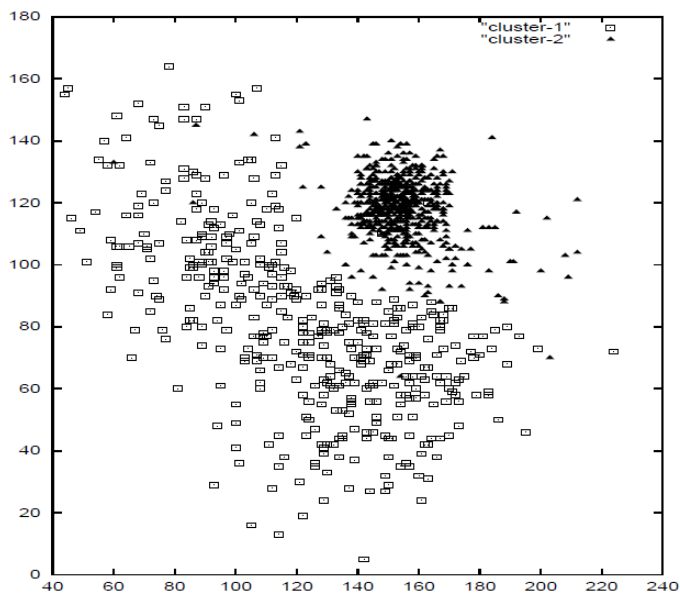


Fig. 7. Clustered result by the proposed GA based method on two dimensional feature plane (PCC=93.1%)

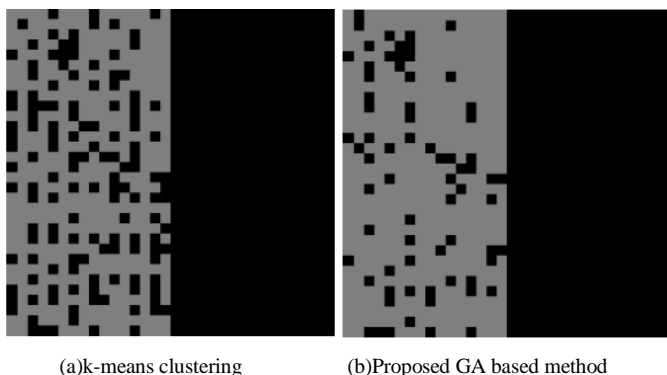


Fig. 8. Clustered image data

Relation between Fisher distances after and before the merge and split process is shown in Figure 9. Fisher distance is increased remarkably by the GA algorithm.

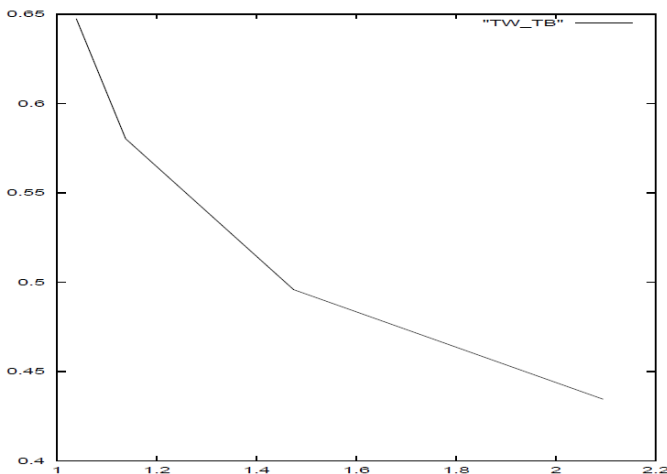


Fig. 9. Relation between Fisher distances after and before the merge and split process

### B. Experiments with Remote Sensing Satellite Images

Landsat-5 TM image data of Saga city, Kyushu Japan which is acquired on 21 May 1985 is used for experiments. Figure 10 shows just two bands of images while Figure 11 shows data distribution on two dimensional feature plane. The number of clusters is set as two.

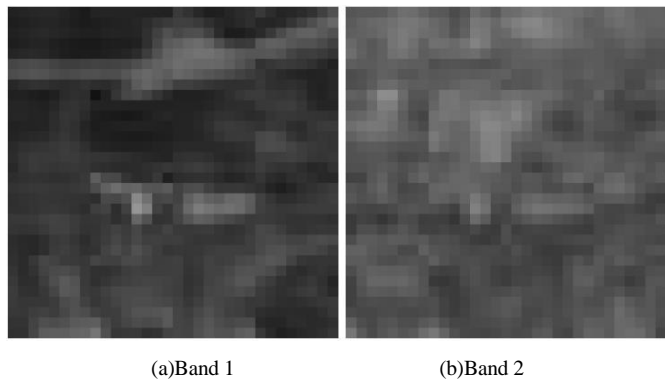


Fig. 10. Landsat-5 TM image used for experiments (Original image #1)

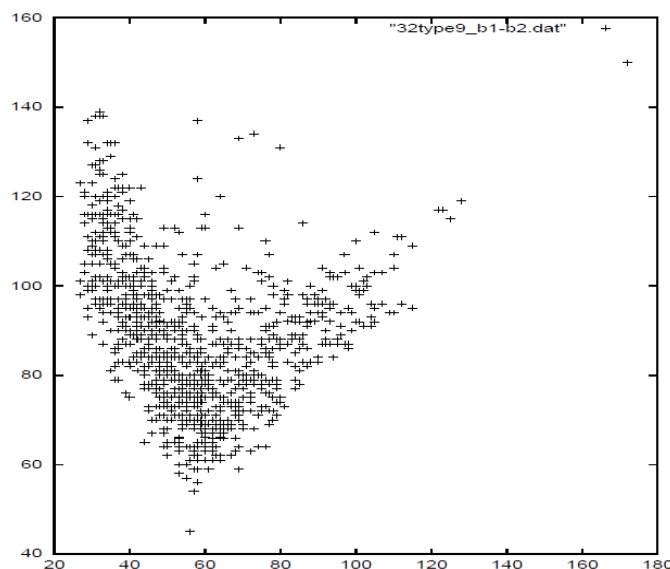
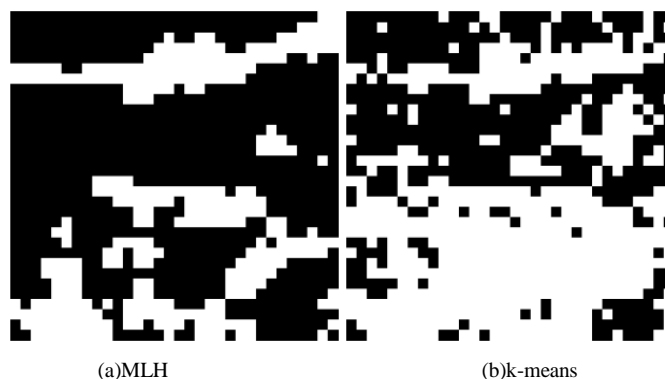


Fig. 11. Data distribution on two dimensional feature plane.

Maximum Likelihood classification: MLH is applied to the data, first. Then k-means, ISODATA and the proposed GA based clustering methods are applied. Figure 12 shows the clustered results of these methods.



(a)MLH (b)k-means

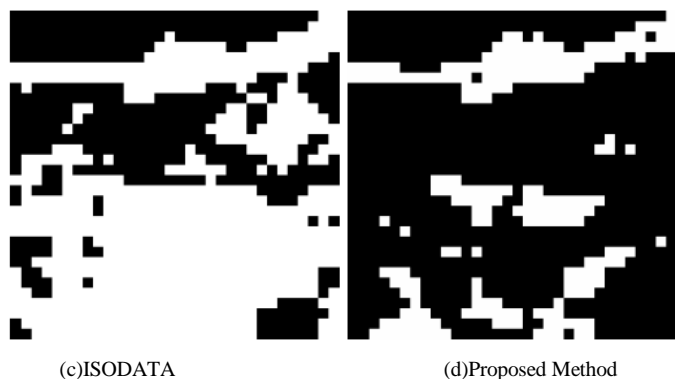


Fig. 12. Clustered images

The clustered resultant image of the proposed GA based method is very similar to that from MLH classification method while these from the conventional clustering methods, k-means and ISODATA differ from that from MLH classification method. On the other hand, the clustered result on the two dimensional feature plane for k-means, ISODATA, and the proposed methods are shown in Figure 13.

Same experiment is conducted with the different portion of the same satellite image data. Images of Band 1 and 2 are shown in Figure 14. Data distribution on two dimensional feature plane is shown in Figure 15. Using this image data, comparison among the aforementioned three clustering methods is conducted. k-means, ISODATA and the proposed GA based clustering methods are applied. Figure 16 shows the clustered results of these methods.

The clustered resultant image of the proposed GA based method is very similar to that from MLH classification method while these from the conventional clustering methods, k-means and ISODATA differ from that from MLH classification method. On the other hand, the clustered result on the two dimensional feature plane for k-means, ISODATA, and the proposed methods are shown in Figure 17.

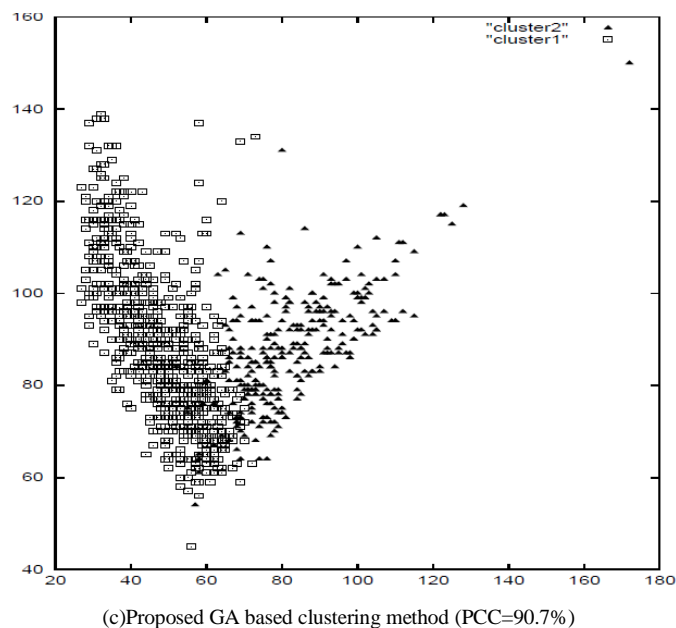
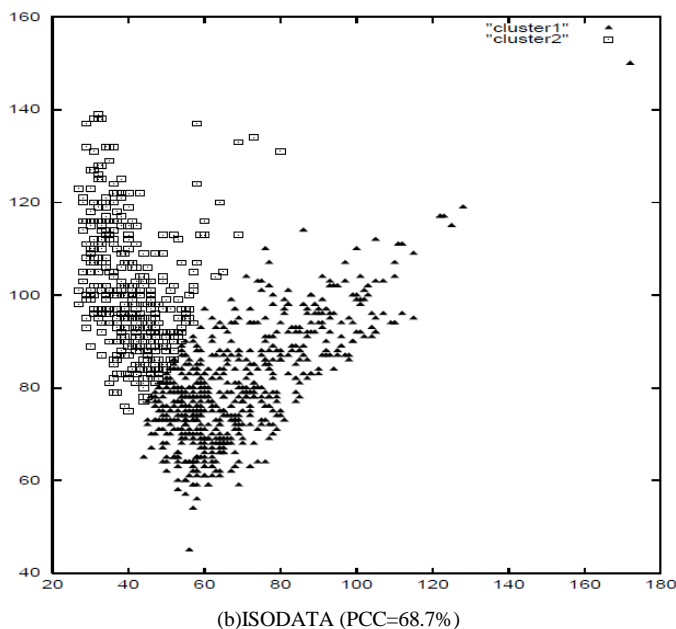
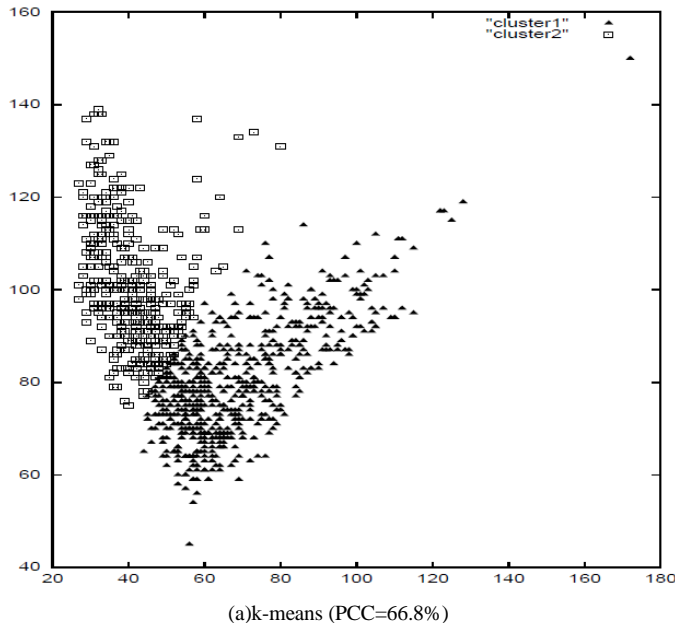


Fig. 13. Clustered results on two dimensional feature plane

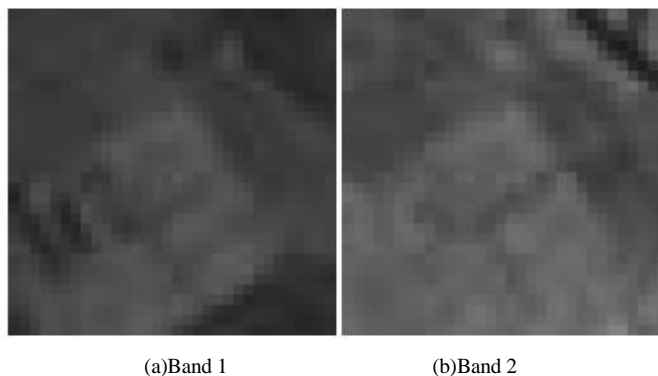
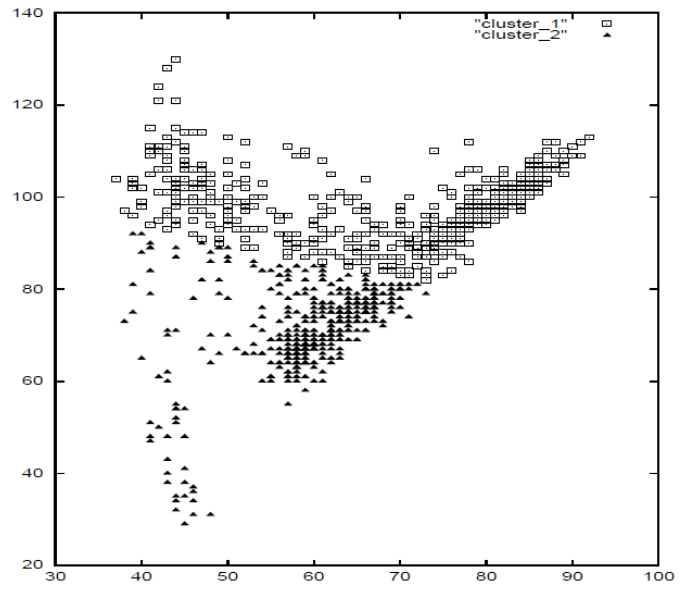
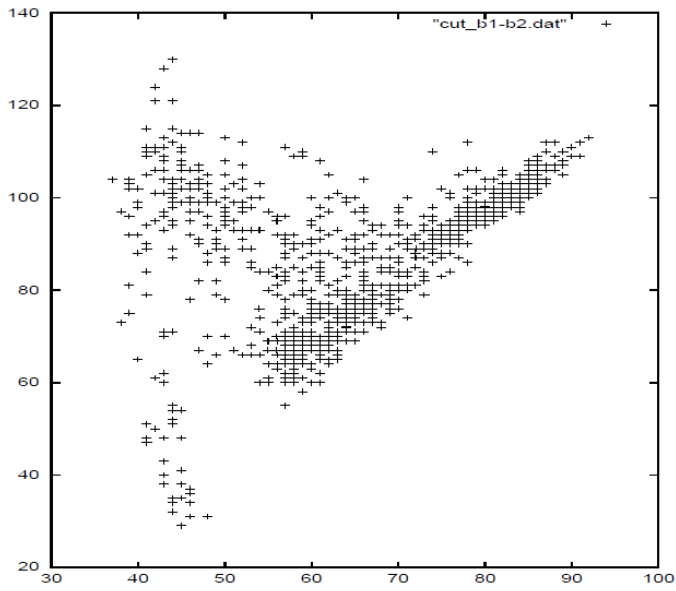


Fig. 14. Another portion of Landsat-5 TM image data (Original image #2)



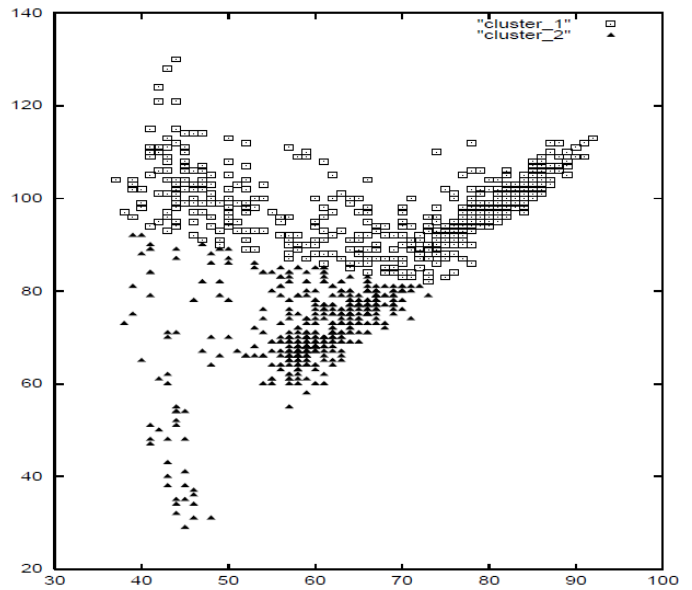
(a) k-means (PCC=64.6%)

Fig. 15. Data distribution on two dimensional feature plane



(a) MLH

(b) k-means



(b) ISODATA (PCC=64.7%)



(c) ISODATA

(d) Proposed method

Fig. 16. Clustered image

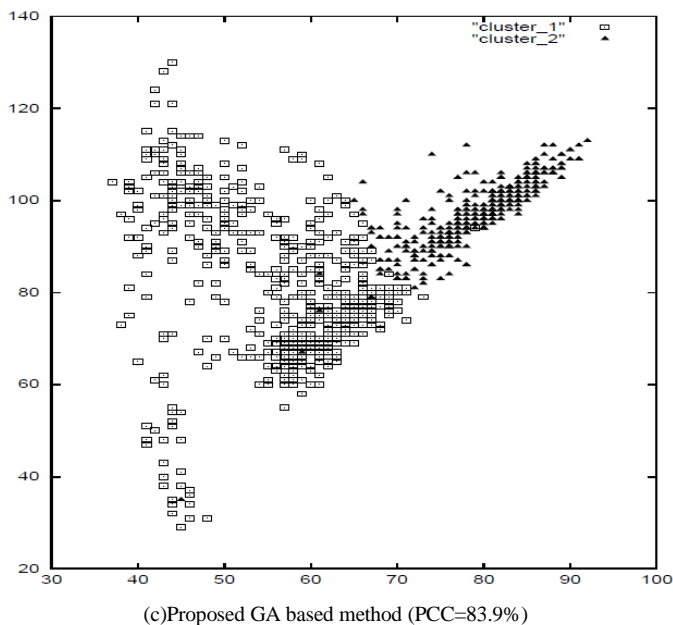


Fig. 17. Clustering results of data distribution on feature plane

For the proposed GA based method, between cluster variance depends on iteration number, obviously. Figure 18 (a) and (b) shows the between cluster variances for the original image #1 and #2, respectively.

### C. Comparison with Geographical Map

Comparison between geographical map and the clustered resultant images is conducted. Figure 19 (a) shows the geographical map while Figure 19 (b) shows Landsat-5 TM image. Figure 20 shows the clustered images by the proposed method with and without merge and split processes. The clustered image by the proposed method with merge and split is much similar to the geographical map data than that by the proposed method without merge and split processes. Therefore, it is said that the proposed GA based clustering method is superior to the other conventional clustering methods, k-means and ISODATA as well as the proposed GA based clustering method without merge and split processes.

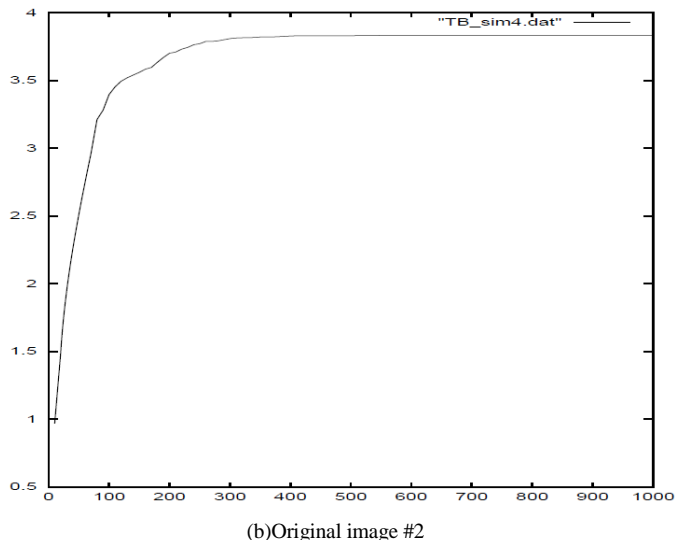
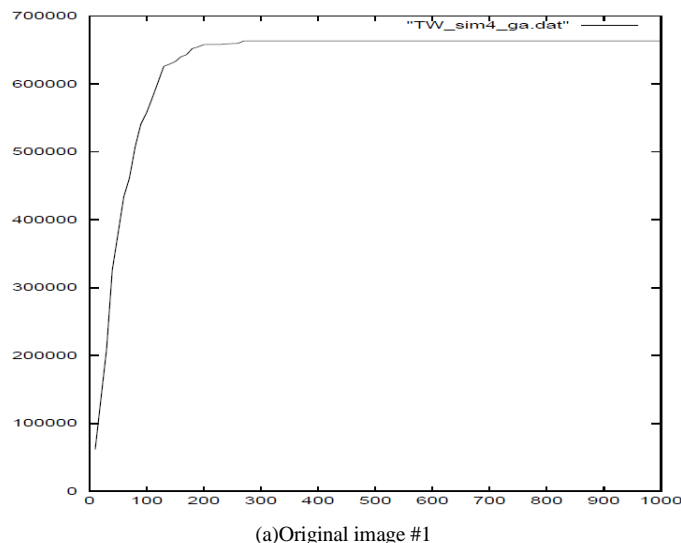


Fig. 18. Between cluster variances for the original images 1 and 2

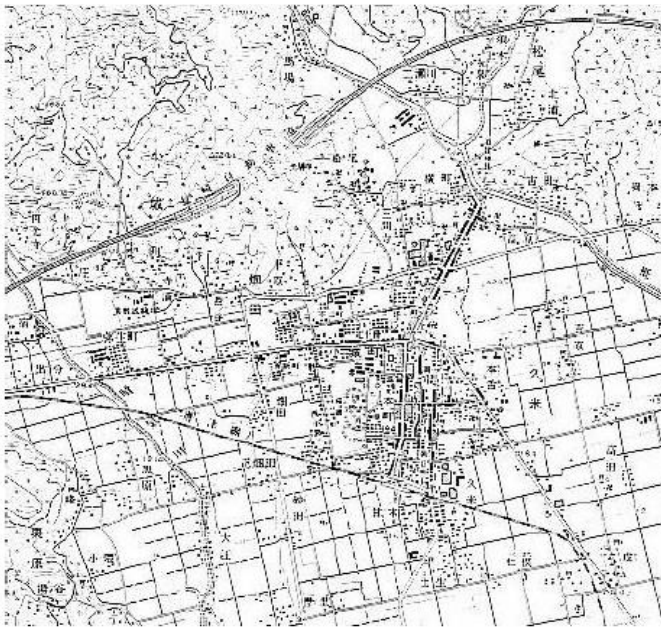


(a) Geographical map of Saga city, Japan



(b) Landsat-5 TM image of Saga city, Japan

Fig. 19. Comparison between Landsat-5 TM image and the corresponding geographical map



(a)Portion of geographical map



(b)Without merge and split

(c)With merge and split

Fig. 20. Clustered images by the proposed method with and without merge and split processes

#### IV. CONCLUSION

Genetic algorithm utilizing image clustering with merge and split processes which allows minimizing Fisher distance between clusters is proposed. Through experiments with simulation and real remote sensing satellite imagery data, it is found that the proposed clustering method is superior to the

conventional k-means and ISODATA clustering methods in comparison to the geographic maps and classification results from Maximum Likelihood classification method.

The clustered image by the proposed method with merge and split is much similar to the geographical map data than that by the proposed method without merge and split processes. Therefore, it is said that the proposed GA based clustering method is superior to the other conventional clustering methods, k-means and ISODATA as well as the proposed GA based clustering method without merge and split processes.

#### ACKNOWLEDGMENT

The author would like to thank Ms. Shuko Yoshimura for her effort to conduct the experiments.

#### REFERENCES

- [1] G. Eason, B. Noble, and I. N. Sneddon, "On certain integrals of Lipschitz-Hankel type involving products of Bessel functions," *Phil. Trans. Roy. Soc. London*, vol. A247, pp. 529–551, April 1955. (references)
- [2] J. Clerk Maxwell, *A Treatise on Electricity and Magnetism*, 3rd ed., vol. 2. Oxford: Clarendon, 1892, pp.68–73.
- [3] I. S. Jacobs and C. P. Bean, "Fine particles, thin films and exchange anisotropy," in *Magnetism*, vol. III, G. T. Rado and H. Suhl, Eds. New York: Academic, 1963, pp. 271–350.
- [4] K. Elissa, "Title of paper if known," unpublished.
- [5] R. Nicole, "Title of paper with only first word capitalized," *J. Name Stand. Abbrev.*, in press.
- [6] Y. Yorozu, M. Hirano, K. Oka, and Y. Tagawa, "Electron spectroscopy studies on magneto-optical media and plastic substrate interface," *IEEE Transl. J. Magn. Japan*, vol. 2, pp. 740–741, August 1987 [Digests 9th Annual Conf. Magnetics Japan, p. 301, 1982].
- [7] M. Young, *The Technical Writer's Handbook*. Mill Valley, CA: University Science, 1989.

#### AUTHORS PROFILE

Kohei Arai, He received BS, MS and PhD degrees in 1972, 1974 and 1982, respectively. He was with The Institute for Industrial Science and Technology of the University of Tokyo from April 1974 to December 1978 and also was with National Space Development Agency of Japan from January, 1979 to March, 1990. During from 1985 to 1987, he was with Canada Centre for Remote Sensing as a Post Doctoral Fellow of National Science and Engineering Research Council of Canada. He moved to Saga University as a Professor in Department of Information Science on April 1990. He was a councilor for the Aeronautics and Space related to the Technology Committee of the Ministry of Science and Technology during from 1998 to 2000. He was a councilor of Saga University for 2002 and 2003. He also was an executive councilor for the Remote Sensing Society of Japan for 2003 to 2005. He is an Adjunct Professor of University of Arizona, USA since 1998. He also is Vice Chairman of the Commission A of ICSU/COSPAR since 2008. He wrote 30 books and published 332 journal papers.

# Secure Copier Which Allows Reuse Copied Documents with Sorting Capability in Accordance with Document Types

Kohei Arai <sup>1</sup>

Graduate School of Science and Engineering  
Saga University  
Saga City, Japan

**Abstract**—Secure copy machine which allows reuse copied documents with sorting capability in accordance with the document types. Through experiments with a variety of document types, it is found that copied documents can be shared and stored in database in accordance with automatically classified document types securely. The copied documents are protected by data hiding based on wavelet Multi Resolution Analysis: MRA.

**Keywords**—data hiding; MPA; wavelet; secure copy

## I. INTRODUCTION

The conventional copy machines can make a copy. Also the conventional secure copiers erase copied documents immediately after the documents are copied. The secure copy machine proposed here has the following functionalities,

- 1) Make a copy
- 2) Save the copied documents in database of classified document types after applying data hiding
- 3) Copied documents can be reused by among the authenticated users

Because the proposed copy machine is secure enough with data hiding, copied documents are protected from outsiders without authentication even if outsiders break network security and database security. Therefore, there is no need to erase the copied documents. Thus the proposed copy machine allows reuse the copied documents. Therefore, the copied documents have to classify by the document types for convenience of reuse. Key methods of the proposed secure copy machine are as follows,

- 1) Data hiding
- 2) Classification of copied documents

Data hiding method based on wavelet Multi Resolution Analysis: MRA has been proposed already [1]-[3]. Also the method for keyword extraction from the original documents based on Analytic Hierarchical Process: AHP <sup>1</sup> has been proposed already [4]. Invisibility of hidden documents has also been improved by means of random scanning [5].

The following section describes the proposed secure copy machine together with the key methods of data hiding and classification methods. Then experiments on data hiding and classification performance will be followed. Finally, conclusion with some discussions is described.

## II. PROPOSED METHOD

The proposed secure copy machine is not only for making copy of original documents but also for making the copied documents available to use again for authenticated users. In this section, system configuration is, at first, described followed by process flow. Then the key components of the system, steganography and watermarking <sup>2</sup> for the copied documents, keyword extraction from the copied documents, classification of the copied documents are described.

### A. System Configuration and Process Flow

System configuration of the proposed document server which allows reuse previously acquired documents which are protected with steganography and watermarking and watermarking is shown in Figure 1.

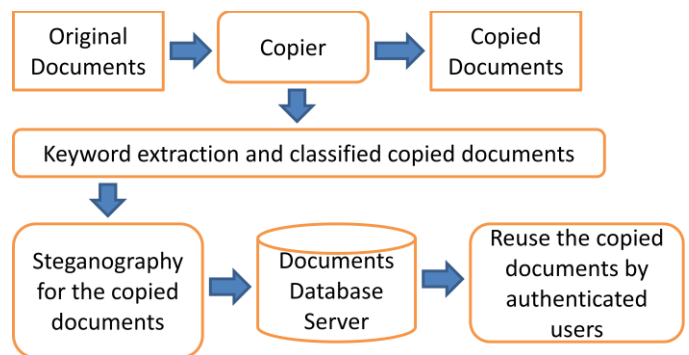


Fig. 1. System configuration of the proposed document server which allows reuse previously acquired documents which are protected with steganography and watermarking and watermarking

Original documents can be copied and use the copied documents for general users. Once the original documents are copied, keyword of the documents is extracted from the copied documents automatically and then classified the copied

<sup>1</sup> <http://ja.wikipedia.org/wiki/%E9%9A%8E%E5%B1%A4%E5%88%86%E6%9E%90%E6%B3%95>

<sup>2</sup> <http://www.jjtc.com/Steganography/>

documents based on the extracted keyword. After that, steganography and watermarking is applied to the copied documents and stored in the documents database server. Therefore, the copied documents can be reused by authenticated users who know the way to decryption of the steganography and watermarking of reusable copied documents.

**B. Steganography and Watermarking**

The copied documents are to be stored in the appropriate subject holder in the documents database server through steganography and watermarking. Even if the general users who do not authenticated at all access to the documents database server and acquire the copied documents, such users could not decryption the original documents at all because such users do not know the way for decryption of the documents which are protected by steganography and watermarking.

Original image can be decomposed with horizontally and vertically low as well as high wavelet frequency components based on wavelet Multi Resolution Analysis: MRA which is expressed in equation (1).

$$F=C_n\eta \tag{1}$$

Where  $F$ ,  $C_n$ , and  $\eta$  is wavelet frequency component, wavelet transformation matrix, and input data in time and/or space domain. Because  $C_n^t=C_n^{-1}$ ,  $\eta$  can be easily reconstructed with wavelet frequency component,  $F$ . Equation (1) is one dimensional wavelet transformation and is easily expanded to multi dimensional wavelet transformation.

$$F=(C_n (C_m (C_l \eta)^5)^t)^t... \tag{2}$$

In the case of wavelet transformation of images, two dimensional wavelet transformations is defined as follows. Horizontally low wavelet frequency component and vertically low frequency component is called  $LL_1$  component at the first stage. Horizontally low wavelet frequency component and vertically high frequency component is called  $LH_1$  component at the first stage. Horizontally high wavelet frequency component and vertically low frequency component is called  $HL_1$  component at the first stage. Horizontally high wavelet frequency component and vertically high frequency component is called  $HH_1$  component at the first stage. Then  $LL_1$  component can be decomposed with  $LL_2$ ,  $LH_2$ ,  $HL_2$ , and  $HH_2$  components at the second stage. Also  $LL_2$  component is decomposed with  $LL_3$ ,  $LH_3$ ,  $HL_3$ , and  $HH_3$  components at the third stage as shown in Figure 2.

Thus Laplacian pyramid<sup>3</sup> which is shown in Figure 3 is created. If these four decomposed components,  $LL_n$ ,  $LH_n$ ,  $HL_n$ , and  $HH_n$  are given, then  $LL_{n-1}$  is reconstructed. Therefore, the original image can be reconstructed with all the wavelet frequency components perfectly.

The copied documents can be replaced into the designated portion of wavelet frequency component. Furthermore, the Least Significant Bit: LSB is also replaced to the encrypted location of wavelet frequency component in which the copied documents are replaced. Moreover, the encrypted location is

randomly scanned with Mersenne Twister<sup>4</sup> of random number generator. Therefore, only the authenticated users who know the parameters of the random number generator can decode the location of the wavelet frequency component.

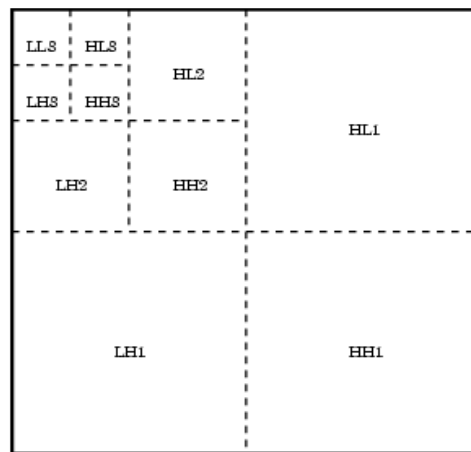


Fig. 2. Two dimensional wavelet transformation

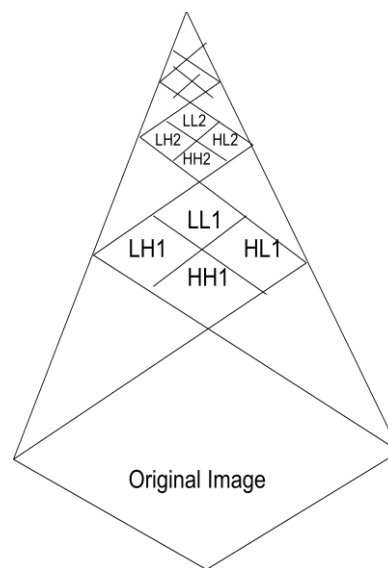


Fig. 3. Laplacian pyramid of wavelet Multi Resolution Analysis: MRA

**C. Keyword Extraction**

Documents can be classified into three categories, (1) figures which include photos, diagrams, drawings, illustrates, etc., (2) documents, and (3) tables. One of the examples of the figures is shown in Figure 4. These categories of documents have keywords in the documents. For instance, the example has its keywords which are located at "A" in the figure.

Based on the knowledge on the location, font size, frequency for keywords, the keywords can be extracted. For example, keywords are located at the top left, center, and right corners as well as the bottom left, center, and right corners. The

<sup>3</sup> [http://en.wikipedia.org/wiki/Laplacian\\_pyramid](http://en.wikipedia.org/wiki/Laplacian_pyramid)

<sup>4</sup> <http://www.math.sci.hiroshima-u.ac.jp/~m-mat/MT/mt.html>

font size of the keywords is relatively large in comparison to the other. The keywords are used to be appeared frequently. These features of keywords are common to the all kinds of documents types.

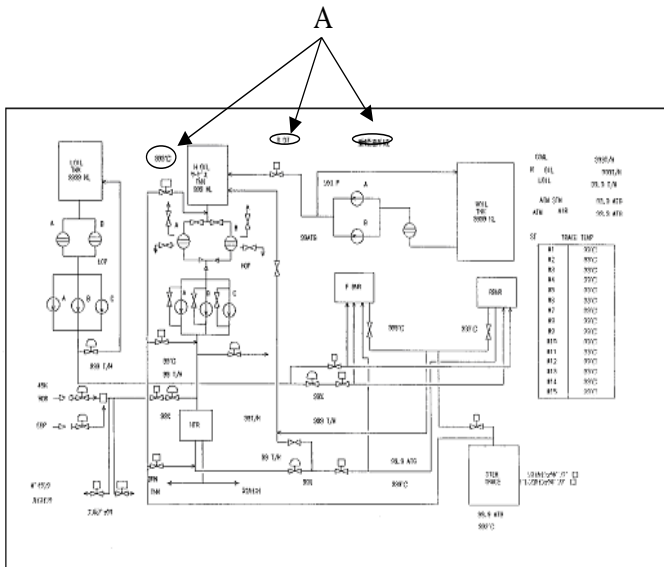


Fig. 4. Example of the documents of figures category

#### D. Classification of the Copied Documents

The extracted keywords are categorized through Morphological Analysis<sup>5</sup> using “ChaSen”<sup>6</sup> through the URL : <http://chasen.aist-nara.ac.jp>.

Then the keywords are decomposed with Morpheme<sup>7</sup>. After that, lexical conceptual structure is checked for classify the copied documents. Thus the copied documents are categorized into the appropriate subjects and stored in the documents database server for reuse of the copied documents.

### III. EXPERIMENTS

#### A. Steganography and watermarking

Using the fourth order of Daubechies wavelet<sup>8</sup> base function of MRA, copied document (image) (see Appendix) is hidden (steganography and watermarking). One of the example images is shown in Figure 5. “Lena” (one of the standard image for data compression performance evaluation, SIDBA<sup>9</sup>) of Figure 5 (a) is decomposed with Figure 5 (b) and (c).

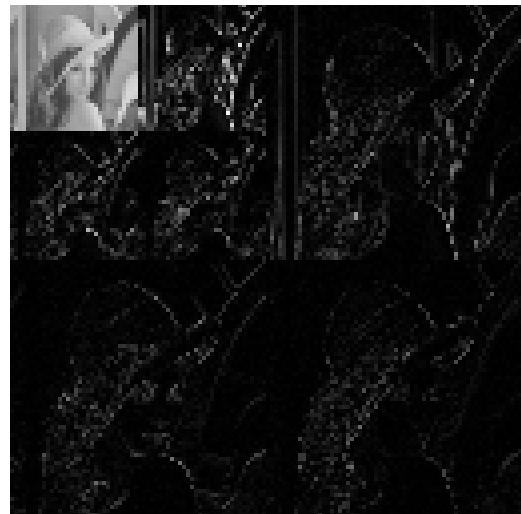
Figure 6 shows the example of which the copied document of “CRAMPS” is hidden in LH<sub>1</sub> wavelet frequency component. Also, Figure 7 shows the example of reconstructed image which contains the copied document of “CRAMPS”.



(a)Lena image



(b)First stage of the decomposed image



(c)Second stage of the decomposed image

Fig. 5. Example of decomposed images

<sup>5</sup> [http://en.wikipedia.org/wiki/Morphological\\_analysis](http://en.wikipedia.org/wiki/Morphological_analysis)

<sup>6</sup> <http://ja.wikipedia.org/wiki/ChaSen>

<sup>7</sup> <http://en.wikipedia.org/wiki/Morpheme>

<sup>8</sup> [http://en.wikipedia.org/wiki/Daubechies\\_wavelet](http://en.wikipedia.org/wiki/Daubechies_wavelet)

<sup>9</sup> <http://imagingolution.blog107.fc2.com/blog-entry-180.html>



Fig. 6. Example of which the copied document of “CRAMPS” is hidden in LH1 wavelet frequency component

The users who are not authenticated can get only the image of Figure 7. The copied document, “CRAMPS” cannot be gotten by such users. On the other hand, the authenticated users may get the copied document, “CRAMPS” because they know the parameters of random number generator, the location of wavelet frequency component, how to decryption of the code.



Fig. 7. Example of reconstructed image which contains the copied document of “CRAMPS”.

#### IV. CONCLUSION

Secure copy machine which allows reuse copied documents with sorting capability in accordance with the document types. Through experiments with a variety of document types, it is found that copied documents can be shared and stored in database in accordance with automatically classified document types securely. The copied documents are protected by data hiding based on wavelet Multi Resolution Analysis: MRA.

Through the experiments with SIDBA image database, it is found that the proposed secure copier ensure that original image can be protected from unauthenticated users and can be accessible from authenticated user who knows initial parameter of the random number generator.

#### APPENDIX

Daubechies wavelet base function utilized wavelet transformation (or decomposition) is defined as follows,

$$C_n \begin{bmatrix} \eta_1 \\ \eta_2 \\ \vdots \\ \eta_n \end{bmatrix} \quad (A1)$$

Where  $\eta$  denotes input data while  $C_n$  denotes wavelet transformation matrix which is represented as follows,

$$C_8^{[2]} = \begin{bmatrix} p_0 & p_1 \\ q_0 & q_1 & & & & & & \\ & & p_0 & p_1 & & & & \\ & & q_0 & q_1 & & & & \\ & & & & p_0 & p_1 & & \\ & & & & q_0 & q_1 & & \\ & & & & & & p_0 & p_1 \\ & & & & & & q_0 & q_1 \end{bmatrix} \begin{bmatrix} \eta_1 \\ \eta_2 \\ \eta_3 \\ \eta_4 \\ \eta_5 \\ \eta_6 \\ \eta_7 \\ \eta_8 \end{bmatrix} = \begin{bmatrix} p_0x_1 + p_1x_2 \\ q_0\eta_1 + q_1\eta_2 \\ p_0\eta_3 + p_1\eta_4 \\ q_0\eta_3 + q_1\eta_4 \\ p_0\eta_5 + p_1\eta_6 \\ q_0\eta_5 + q_1\eta_6 \\ p_0\eta_7 + p_1\eta_8 \\ q_0\eta_7 + q_1\eta_8 \end{bmatrix} \quad (A2)$$

Where n denotes input data size (or order) while  $p$  and  $q$  are determined with the following equation (A3),

$$\begin{aligned}
 (C_n^{[2]})^T C_n^{[2]} &= I_n \\
 p_0 + p_1 &= \sqrt{2} \\
 q_0 &= p_1 \\
 q_1 &= -p_0 \\
 0^0 q_0 + 1^0 q_1 &= 0
 \end{aligned} \tag{A3}$$

Equation (A2) is for the support length of two of wavelet transformation matrix while the support length of four of wavelet transformation matrix is expressed as follows,

$$\begin{aligned}
 C_8^{[4]} &= \begin{bmatrix} \eta_1 \\ \eta_2 \\ \eta_3 \\ \eta_4 \\ \eta_5 \\ \eta_6 \\ \eta_7 \\ \eta_8 \end{bmatrix} = \begin{bmatrix} p_0 & p_1 & p_2 & p_3 & & & & \\ q_0 & q_1 & q_2 & q_3 & & & & \\ & & p_0 & p_1 & p_2 & p_3 & & \\ & & q_0 & q_1 & q_2 & q_3 & & \\ & & & p_0 & p_1 & p_2 & p_3 & \\ & & & q_0 & q_1 & q_2 & q_3 & \\ p_2 & p_3 & & & p_0 & p_1 & & \\ q_2 & q_3 & & & q_0 & q_1 & & \end{bmatrix} \begin{bmatrix} \eta_1 \\ \eta_2 \\ \eta_3 \\ \eta_4 \\ \eta_5 \\ \eta_6 \\ \eta_7 \\ \eta_8 \end{bmatrix} \\
 &= \begin{bmatrix} p_0\eta_1 + p_1\eta_2 + p_2\eta_3 + p_3\eta_4 \\ q_0\eta_1 + q_1\eta_2 + q_2\eta_3 + q_3\eta_4 \\ p_0\eta_3 + p_1\eta_4 + p_2\eta_5 + p_3\eta_6 \\ q_0\eta_3 + q_1\eta_4 + q_2\eta_5 + q_3\eta_6 \\ p_0\eta_5 + p_1\eta_6 + p_2\eta_7 + p_3\eta_8 \\ q_0\eta_5 + q_1\eta_6 + q_2\eta_7 + q_3\eta_8 \\ p_0\eta_7 + p_1\eta_8 + p_2\eta_1 + p_3\eta_2 \\ q_0\eta_7 + q_1\eta_8 + q_2\eta_1 + q_3\eta_2 \end{bmatrix}
 \end{aligned} \tag{A4}$$

Where  $p$  and  $q$  are determined as follows,

$$\begin{aligned}
 (C_n^{[4]})^T C_n^{[4]} &= I_n \\
 p_0 + p_1 + p_2 + p_3 &= \sqrt{2} \\
 q_0 &= p_3 \\
 q_1 &= -p_2 \\
 q_2 &= p_1 \\
 q_3 &= -p_0 \\
 0^0 q_0 + 1^0 q_1 + 2^0 q_2 + 3^0 q_3 &= 0 \\
 0^1 q_0 + 1^1 q_1 + 2^1 q_2 + 3^1 q_3 &= 0
 \end{aligned} \tag{A5}$$

In accordance with this manner, support length of "sup" of wavelet transformation matrix as well as any data size of wavelet transformation matrix can be determined as follows,

$$\begin{aligned}
 (C_n^{[sup]})^T C_n^{[sup]} &= I_n \\
 \sum_{j=0}^{sup-1} p_j &= \sqrt{2} \\
 q_j &= (-1)^j p_{(sup-1-j)} \quad (j = 0, 1, 2, \dots, (sup-1)) \\
 \sum_{j=0}^{sup-1} j^r q_j &= 0 \quad \left( r = 0, 1, 2, \dots, \left( \frac{sup}{2} - 1 \right) \right)
 \end{aligned} \tag{A6}$$

#### ACKNOWLEDGMENT

The author would like to thank Dr. Kaname Seto for his effort to conduct the experiments of data hiding.

#### REFERENCES

- [1] K.Arai and K.Seto, Data hiding method based on wavelet Multi Resolution Analysis: MRA, Journal of Visualization Society of Japan, Vol.22, Suppl.No.1, 229-232, 2002.
- [2] K.Arai and K.Seto, Data hiding method based on wavelet Multi Resolution Analysis: MRA utilizing eigen value decomposition, Journal of Visualization Society of Japan, Vol.23, No.8, pp.72-79,2003.
- [3] K.Arai and K.Seto, Data hiding method based on wavelet Multi Resolution Analysis: MRA utilizing image space coordinate conversion, Journal of Visualization Society of Japan, 25, Suppl.No.1, 55-58,(2005)
- [4] K.Arai, Keyword extraction method from paper based documents, drawings, based on knowledge importance evaluation with Analytic Hierarchy Process: AHP method, Journal of Image and Electronic Engineering Society of Japan, 34, 5, 636-644, (2005)
- [5] K.Arai and K.Seto, Data hiding method based on wavelet Multi Resolution Analysis: MRA utilizing random scanning for improving invisibility of the secret image, Journal of Visualization Society of Japan, 29, Suppl.1, 167-170, 2009.

#### AUTHORS PROFILE

**Kohei Arai**, He received BS, MS and PhD degrees in 1972, 1974 and 1982, respectively. He was with The Institute for Industrial Science, and Technology of the University of Tokyo from 1974 to 1978 also was with National Space Development Agency of Japan (current JAXA) from 1979 to 1990. During from 1985 to 1987, he was with Canada Centre for Remote Sensing as a Post Doctoral Fellow of National Science and Engineering Research Council of Canada. He was appointed professor at Department of Information Science, Saga University in 1990. He was appointed councilor for the Aeronautics and Space related to the Technology Committee of the Ministry of Science and Technology during from 1998 to 2000. He was also appointed councilor of Saga University from 2002 and 2003 followed by an executive councilor of the Remote Sensing Society of Japan for 2003 to 2005. He is an adjunct professor of University of Arizona, USA since 1998. He also was appointed vice chairman of the Commission "A" of ICSU/COSPAR in 2008. He wrote 30 books and published 332 journal papers.

# Bi-Directional Reflectance Distribution Function: BRDF Effect on Un-mixing, Category Decomposition of the Mixed Pixel (MIXEL) of Remote Sensing Satellite Imagery Data

Kohei Arai <sup>1</sup>

Graduate School of Science and Engineering  
Saga University  
Saga City, Japan

**Abstract**—Method for unmixing, category decomposition of the mixed pixel (MIXEL) of remote sensing satellite imagery data taking into account the effect due to Bi-Directional Reflectance Distribution Function: BRDF is proposed. Although there is not so small BRDF effect on estimation mixing ratios, conventional unmixing methods do not take into account the effect. Through experiments, the effect is clarified. Also the proposed unmixing method with consideration of BRDF effect is validated.

**Keywords**—Unmixing; BRDF; Mixel; Lambertian surface; Category decomposition

## I. INTRODUCTION

The pixels in earth observed images which are acquired with Visible to Near Infrared: VNIR sensors onboard remote sensing satellites are, essentially mixed pixels (mixels) which consists of several ground cover materials [1]. Some mixel model is required for analysis such as un-mixing of the mixel in concern [2],[3]. Typical mixel is linear mixing model which is represented by linear combination of several ground cover materials with mixing ratio for each material [4]. It is not always true that the linear mixel model is appropriate [5]. Due to the influences from multiple reflections between the atmosphere and ground, multiple scattering in the atmosphere on the observed radiance from the ground surface, pixel mixture model is essentially non-linear rather than linear. These influences are interpreted as adjacency effect [6], [7].

Although there is not so small BRDF effect on estimation mixing ratios, conventional unmixing methods do not take into account the effect. Method for unmixing, category decomposition of the mixed pixel (MIXEL) of remote sensing satellite imagery data taking into account the effect due to Bi-Directional Reflectance Distribution Function: BRDF is proposed. In order to take into account BRDF effect, Minneart Reflectance Model: MRM is utilized for representation of BRDF. Through experiments, the effect is clarified. Also the proposed unmixing method with consideration of BRDF effect is validated.

The following section, the proposed method is described followed by the experiments. Then conclusion is described together with some discussions.

## II. PROPOSED METHOD

### A. Surface Reflectance Models

BRDF is defined in equation (1).

$$dL_i(\theta_i, \phi_i, \theta_r, \phi_r, E_i) / dE_i(\theta_i, \phi_i) \quad (1)$$

Where  $dL_i(\theta_i, \phi_i, \theta_r, \phi_r, E_i)$  and  $dE_i(\theta_i, \phi_i)$  denotes reflected radiance and incident irradiance, reflectively.

Lambertian surface, on the other hand, is defined in equation (2).

$$I_\theta = I_n \cos \theta \quad (2)$$

Where  $I_n$  denote incident irradiance in the normal direction while  $I_\theta$  denotes reflected radiance in direction of  $\theta$ . Therefore, the Lambertian surface reflectance is constant at all direction, for entire hemisphere.

Minneart reflection is defined in equation (3).

$$B(\gamma, \nu) = \frac{k+1}{2\pi} (\gamma\nu)^{k-1} \quad (3)$$

Where  $\gamma, \nu$  denotes solar zenith angle and observation angle, respectively while  $k$  denotes Minneart coefficient. If  $k=1$ , it is totally equation to Lambertian surface.

### B. Unmixing, Category Decomposition Method

One single pixel of remote sensing satellite imagery data,  $P$  can be represented as combination of weighted spectral characteristics,  $H_j$  of the considerable ground cover targets included in the Instantaneous Field of View: IFOV with their mixing ratios,  $a_j$  as is shown in equation (4).

$$P = \sum_{j=1}^k a_j H_j$$
$$\sum_{j=1}^k a_j = 1$$
$$a_j \geq 0 \quad (4)$$

This is rewritten in the following vector representation,

$$P = HA \tag{5}$$

where

$$P = [p_1, p_2, \dots, p_n]^t$$

$$H = \begin{bmatrix} h_{11} & h_{12} & \dots & h_{1k} \\ h_{21} & h_{22} & \dots & h_{2k} \\ \vdots & \vdots & \ddots & \vdots \\ h_{n1} & h_{n2} & \dots & h_{nk} \end{bmatrix}$$

$$A = [a_1, a_2, \dots, a_k]^t \tag{6}$$

In general, H is rectangle matrix. Therefore, Moore-Penrose generalized inverse matrix is needed to estimate mixing ratio vector A as shown in equation (7).

$$A = (H^t H)^{-1} H^t P$$

$$= H^+ P$$

$$H^+ = (H^t H)^{-1} H^t \tag{7}$$

C. Monte Carlo Ray Tracing Simulation

In order to show a validity of the proposed non-linear mixel model, MCRT simulation study and field experimental study is conducted. MCRT allows simulation of polarization characteristics of sea surface with designated parameters of the atmospheric conditions and sea surface and sea water conditions. Illustrative view of MCRT is shown in Figure 1.

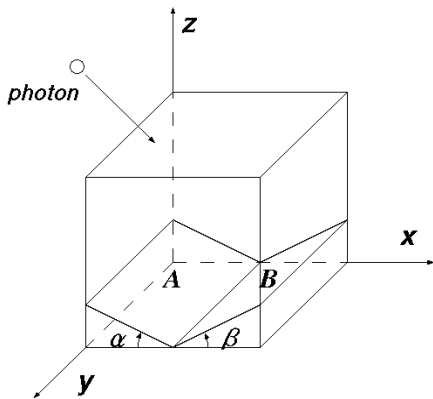


Fig. 1. Illustrative view of MCRT for the atmosphere and sea water

Photon from the sun is input from the top of the atmosphere (the top of the simulation cell). Travel length of the photon is calculated with optical depth of the atmospheric molecule and that of aerosol. There are two components in the atmosphere; molecule and aerosol particles while three are also two components, water and particles; suspended solid and phytoplankton in the ocean.

When the photon meets molecule or aerosol (the meeting probability with molecule and aerosol depends on their optical depth), then the photon scattered in accordance with scattering properties of molecule and aerosol. The scattering property is called as phase function<sup>1</sup>. In the visible to near infrared wavelength region, the scattering by molecule is followed by Rayleigh scattering law [8] while that by aerosol is followed by Mie scattering law [8]. Example of phase function of Mie scattering is shown in Figure 2 (a) while that of Rayleigh scattering is shown in Figure 2 (b).

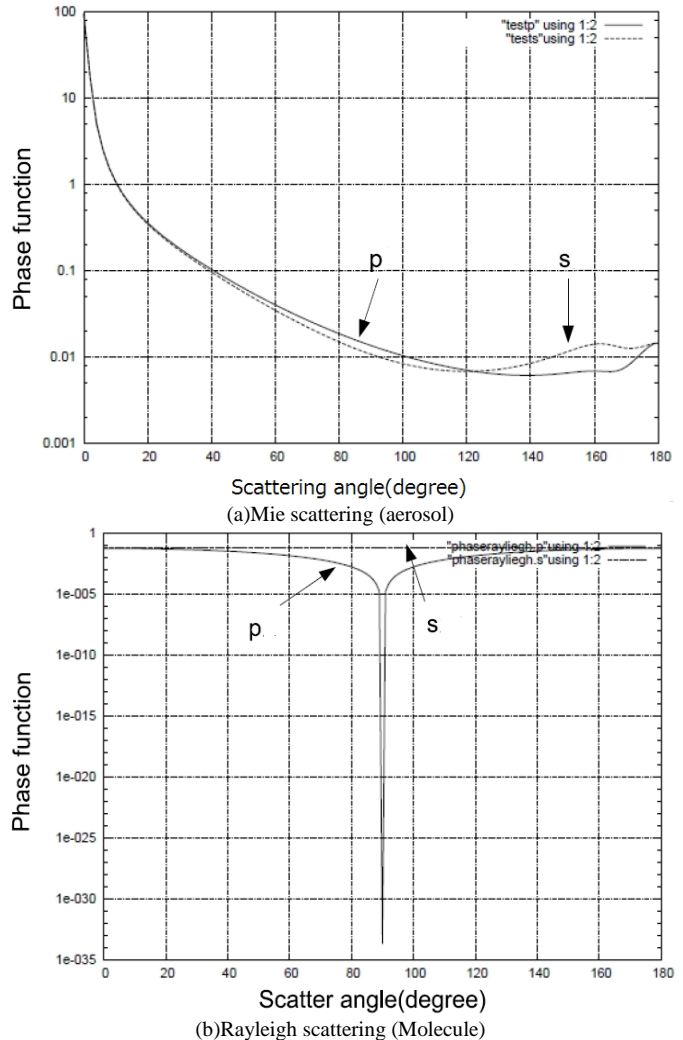


Fig. 2. Phase functions for Mie and Rayleigh scattering

In the atmosphere, there are absorption due to water vapor, ozone and aerosols together with scattering due to the atmospheric molecules, aerosols. Atmospheric Optical Depth: AOD (optical thickness) in total, Optical Depth: OD due to water vapor (H<sub>2</sub>O), ozone (O<sub>3</sub>), molecules (MOL), aerosols (AER), and real observed OD (OBS) are plotted in Figure 3 as an example.

<sup>1</sup> <http://ejje.weblio.jp/content/phase+function>

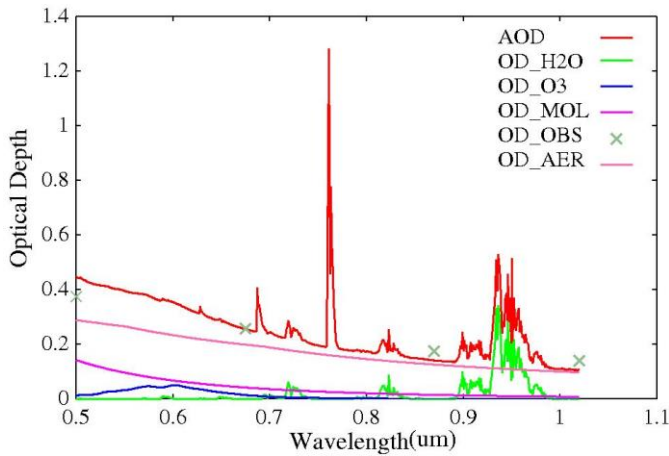


Fig. 3. Example of observed atmospheric optical depth in total and the best fit curves of optical depth due to water vapor, ozone, molecules, and aerosols calculated with MODTRAN of atmospheric radiative transfer software code..

For simplifying the calculations of the atmospheric influences, it is assumed that the atmosphere containing only molecules and aerosols. As shown in Figure 3, this assumption is not so bad. Thus the travel length of the photon at once,  $L$  is expressed with equation (8).

$$L=L_0 \text{RND}(i) \quad (8)$$

$$L_0=Z_{max}/\tau \quad (9)$$

Where  $Z_{max}$ ,  $\tau$ ,  $\text{RND}(i)$  are maximum length, altitude of the atmosphere, optical depth, and  $i$ -th random number, respectively. In this equation,  $\tau$  is optical depth of molecule or aerosol. The photon meets molecule when the random number is greater than  $\tau$ . Meanwhile, if the random number is less than  $\tau$ , then the photon meets aerosol. The photon is scattered at the molecule or aerosol to the direction which is determined with the aforementioned phase function and with the rest of the travel length of the photon.

### III. SIMULATION STUDIES AND THE EXPERIMENTS

#### A. Preliminary Simulation Studies

A mixed pixel model which consists of two categories is created. Also two different surface reflectance models, Minneart and Lambertian surface models are assumed as shown in Figure 4.

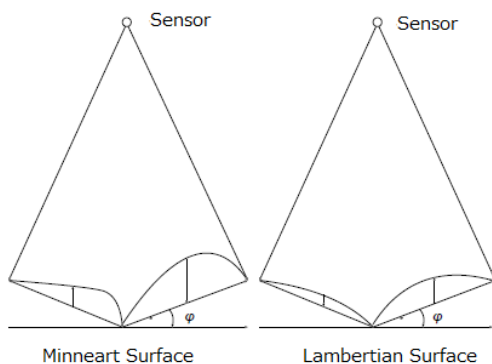


Fig. 4. Assumed surface models for simulation study

Alunite and Cheat grass are selected for the categories. These spectral characteristics are given by USGS spectral library. Mixel with 50% of Alunite and 50% of Cheat grass is created with the surface slope of 20 degree. Observed radiance from the mixel is derived from MCRT at wavelength of 550 and 650 nm. Unmixing is attempted with Minneart and Lambertian surface models. Spectral characteristics of Alunite and Cheat grass are shown in Figure 5 (a) and (b). Also angle distribution of Minneart surface with Minneart coefficients of 0.3, 0.8 and 1.0 (Lambertian surface) is shown in Figure 6. Due to the fact that the surface slope angle is set at 20 degree, reflectance between Lambertian and Minneart reflection models show no difference at 20 and 110 degree of observation angles. Also Figure 7 shows reflectance as a function of slope. Figure 7 (a) shows the calculated reflectance of Alunite as a function of slope angle with the different parameters of Minneart coefficients, 0.3, 0.8, and 1.0 while Figure 7 (b) shows that of Cheat grass as a function of slope angle with the different parameters of Minneart coefficients, 0.3, 0.8, and 1.0 at the wavelength of 550 nm. Therefore, slope effect is quite dependent on Minneart coefficients. Unmixing results based on Minneart reflectance model show correct mixing ratio of 50 versus 50% while those based on Lambert reflectance model show 52.25 versus 47.75%.

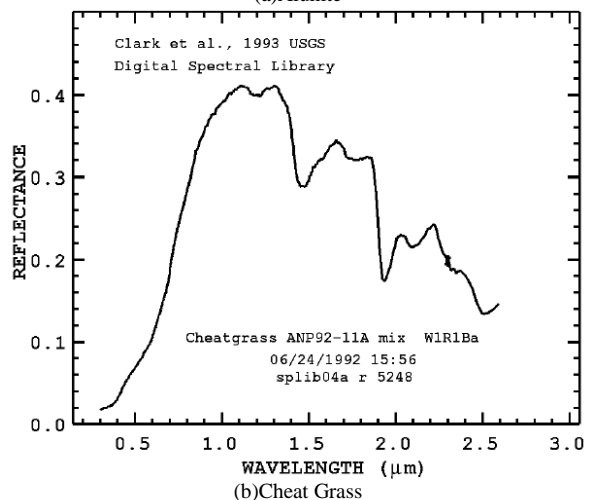
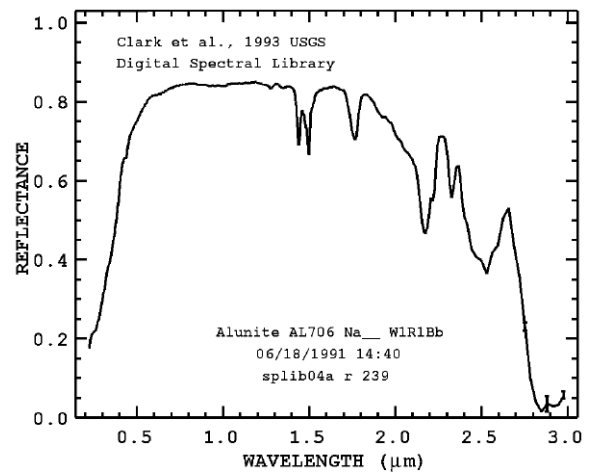


Fig. 5. Spectral characteristics of Alunite and Cheat grass derived from USGS spectral library

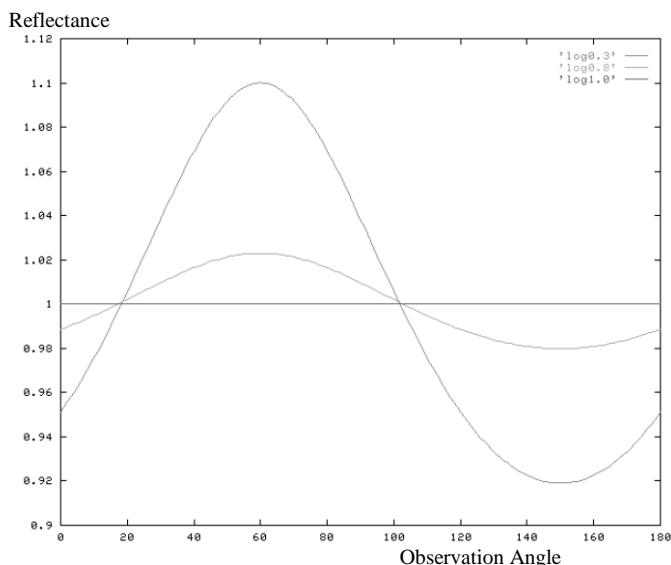
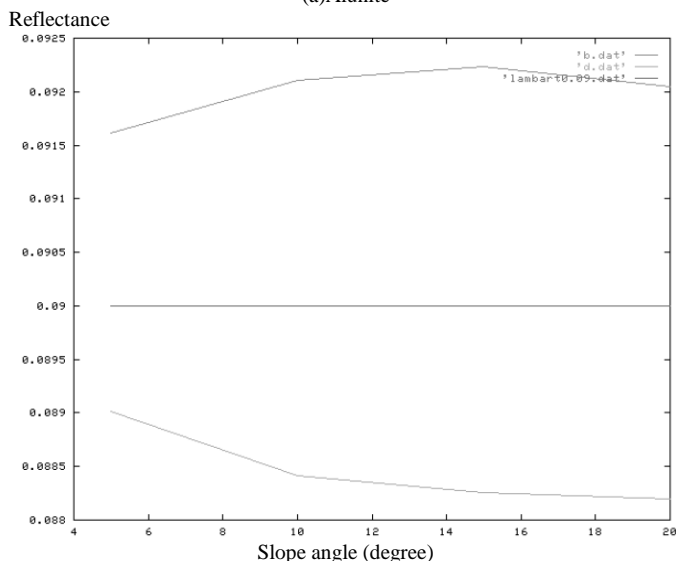
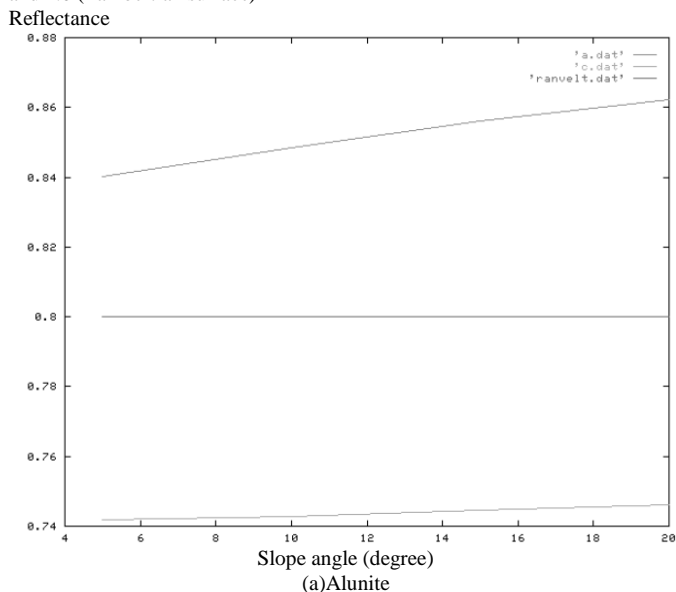


Fig. 6. Angle distribution of reflectance at Minneart coefficients, 0.3, 0.8, and 1.0 (Lambertian surface)



(b)Cheat grass

Fig. 7. Slope effect on the calculated surface reflectance

Therefore, 2.25% of estimation error is observed for the mixing ratio for the Lambertian surface model. The results show that there is significant error on mixing ratio estimation when BRDF is not taken into account.

**B. Simulation Studies**

Visible to Near Infrared: VNIR radiometer onboard remote sensing satellite is simulated with MCRT. VNIR consists of three bands, 400, 700, and 900nm with IFOV of 15m. Observation angle is set at zero zenith angle (nadir view) while solar zenith angle is set at 20 degree.

Ground surface is assumed to be covered with soil) default materials of MODTRAN. Within a IFOV, there are three soils with the different reflectance, 0.1, 0.3, and 0.5 of Lambertian and Minneart surfaces. Minneart coefficients are 1.0 for Lambertian surface and 0.8 for Minneart surface, respectively.

Mid. Latitude Summer of the atmospheric model is selected from MODTRAN. Optical depth of atmospheric molecule is set at 0.0003 while that of aerosol particle is set at 0.2 at 700 nm. Refractive index of aerosol particle is set at 1.44 - i 0.005. Junge size distribution of aerosol particle is assumed with Junge parameter of 3.0. Then phase function (scattering characteristic) can be derived from Mie code which is included in MODTRAN. Top of the Atmosphere: TOA radiance, then calculated for pixel by pixel basis. Table 1 shows the TOA radiance in unit of mW/cm<sup>2</sup>/str. Also the TOA radiance of the assumed mixels with the different mixing ratio is calculated. Mixing ratio of 0.1, 0.3, and 0.5 of reflectance soils is 0.5, 0.3, and 0.2, The results are 0.295 (@400nm), 0.222 (@700nm), and 0.185 (@900nm), respectively for Lambertian surface while those for Mineart surface are 0.262 (@400nm), 0.201 (@700nm), and 0.175 (@900nm), respectively.

Using the aforementioned TOA radiance of the assumed mixels for both Lambertian and Minneart surfaces, mixing ratio of the different reflectance of soils are estimated based on the proposed unmixing method of category decomposition. The result is as follows,

6.65% (soil #1), 82.74% (soil #2), 10.61% (soil #3) for Lambertian surface while

49.95% (soil #1), 27.59% (soil #2), 22.46% (soil #3) for Minneart surface.

TABLE I. TOA RADIANCE

(a) Lambertian Surface			
Reflectance	TOA radiance (mW/cm <sup>2</sup> /str)		
	@400nm	@700nm	@900nm
0.1	0.240	0.189	0.166
0.3	0.322	0.236	0.196
0.5	0.441	0.291	0.234

(b)Minneart Surface			
Reflectance	TOA radiance (mW/cm <sup>2</sup> /str)		
	@400nm	@700nm	@900nm
0.1	0.226	0.183	0.162
0.3	0.277	0.210	0.185
0.5	0.350	0.247	0.209

This implies that the estimated mixing ratios are appropriate when BRDF is taken into account (Minneart surface) while the estimated mixing ratios have significant errors if BRDF is not taken into account (Lambertian surface).

#### IV. CONCLUSION

Method for unmixing, category decomposition of the mixed pixel (MIXEL) of remote sensing satellite imagery data taking into account the effect due to Bi-Directional Reflectance Distribution Function: BRDF is proposed. Although there is not so small BRDF effect on estimation mixing ratios, conventional unmixing methods do not take into account the effect. Through experiments, the effect is clarified. Also the proposed unmixing method with consideration of BRDF effect is validated.

The estimated mixing ratios are appropriate when BRDF is taken into account (Minneart surface) while the estimated mixing ratios have significant errors if BRDF is not taken into account (Lambertian surface).

#### ACKNOWLEDGMENT

The author would like to thank Ms. Chiaki Sakai for his efforts through experiments and simulations.

#### REFERENCES

- [1] Masao Matsumoto, Hiroki Fujiku, Kiyoshi Tsuchiya, Kohei Arai, Category decomposition in the maximum likelihood classification, Journal of Japan Society of Phtogrammetro and Remote Sensing, 30, 2, 25-34, 1991.
- [2] Masao Moriyama, Yasunori Terayama, Kohei Arai, Claffication method based on the mixing ratio by means of category decomposition, Journal of Remote Sensing Society of Japan, 13, 3, 23-32, 1993.

- [3] Kohei Arai and H.Chen, Unmixing method for hyperspectral data based on subspace method with learning process, Techninical Notes of the Science and Engineering Faculty of Saga University,, 35, 1, 41-46, 2006.
- [4] Kohei Arai and Y.Terayama, Label Relaxation Using a Linear Mixture Model, International Journal of Remote Sensing, 13, 16, 3217-3227, 1992.
- [5] Kohei Arai, Yasunori Terayama, Yoko Ueda, Masao Moriyama, Cloud coverage ratio estimations within a pixel by means of category decomposition, Journal of Japan Society of Phtogrammetro and Remote Sensing, 31, 5, 4-10, 1992.
- [6] Kohei Arai, Non-linear mixture model of mixed pixels in remote sensing satellite images based on Monte Carlo simulation, Advances in Space Research, 41, 11, 1715-1723, 2008.
- [7] Kohei Arai, Kakei Chen, Category decomposition of hyper spectral data analysis based on sub-space method with learning processes, Journal of Japan Society of Phtogrammetro and Remote Sensing, 45, 5, 23-31, 2006.
- [8] Arai, K, Lecture Notes on Remote Sensing, Morikita-Shuppan, Co.Ltd., 2005

#### AUTHORS PROFILE

**Kohei Arai**, He received BS, MS and PhD degrees in 1972, 1974 and 1982, respectively. He was with The Institute for Industrial Science and Technology of the University of Tokyo from April 1974 to December 1978 also was with National Space Development Agency of Japan from January, 1979 to March, 1990. During from 1985 to 1987, he was with Canada Centre for Remote Sensing as a Post Doctoral Fellow of National Science and Engineering Research Council of Canada. He moved to Saga University as a Professor in Department of Information Science on April 1990. He was a councilor for the Aeronautics and Space related to the Technology Committee of the Ministry of Science and Technology during from 1998 to 2000. He was a councilor of Saga University for 2002 and 2003. He also was an executive councilor for the Remote Sensing Society of Japan for 2003 to 2005. He is an Adjunct Professor of University of Arizona, USA since 1998. He also is Vice Chairman of the Commission "A" of ICSU/COSPAR since 2008. He wrote 30 books and published 322 journal papers

# Visualization of 5D Assimilation Data for Meteorological Forecasting and Its Related Disaster Mitigations Utilizing Vis5D of Software Tool

Kohei Arai <sup>1</sup>

Graduate School of Science and Engineering  
Saga University  
Saga City, Japan

**Abstract**—Method for visualization of 5D assimilation data for meteorological forecasting and its related disaster mitigations utilizing Vis5D of software tool is proposed. In order to mitigate severe weather related disaster, meteorological forecasting and prediction is needed. There are some numerical weather forecasting data, in particular, assimilation data. Time series of three dimensional geophysical parameters have to be represented visually onto computer display in a comprehensive manner. On the other hand, there are some visualization software tools. In particular, Vis5D of software tool for animation of three dimensional imagery data can be displayed. Through experiments with NCEP/GDAS assimilation data, it is found that the proposed method is appropriate for representation of 5D assimilation data in a comprehensive manner.

**Keywords**—animation; assimilation data; weather related disaster; Vis5D; NCEP/GDAS

## I. INTRODUCTION

In order to mitigate severe weather related disaster, meteorological forecasting and prediction is needed. There are some numerical weather forecasting data, in particular, assimilation data. Time series of three dimensional geophysical parameters have to be represented visually onto computer display in a comprehensive manner. On the other hand, there are some visualization software tools. In particular, Vis5D of software tool for animation of three dimensional imagery data can be displayed.

Method for visualization of 5D assimilation data for meteorological forecasting and its related disaster mitigations utilizing Vis5D of software tool is proposed. Through experiments with NCEP/GDAS assimilation data, it is found that the proposed method is appropriate for representation of 5D assimilation data in a comprehensive manner.

The following section, the proposed method is described followed by the experiments. Then conclusion is described together with some discussions.

## II. PROPOSED METHOD

### A. Vis5D Outline

Vis5D software tool allows display five dimensional imagery data, three dimensional location data (x, y, z), time, and geophysical parameters.

The number of lattice points, the name of geographical map, the name of variables (geophysical parameters), the acquisition time, etc. are attributes of the five dimensional data. Vis5D supports two types of data format, v5d and comp5d formats. Comp5d format is old format so that v5d format is popular and default format at this time.

Figure 1 shows control panel of Vis5D while Figure 2 shows manipulating images.

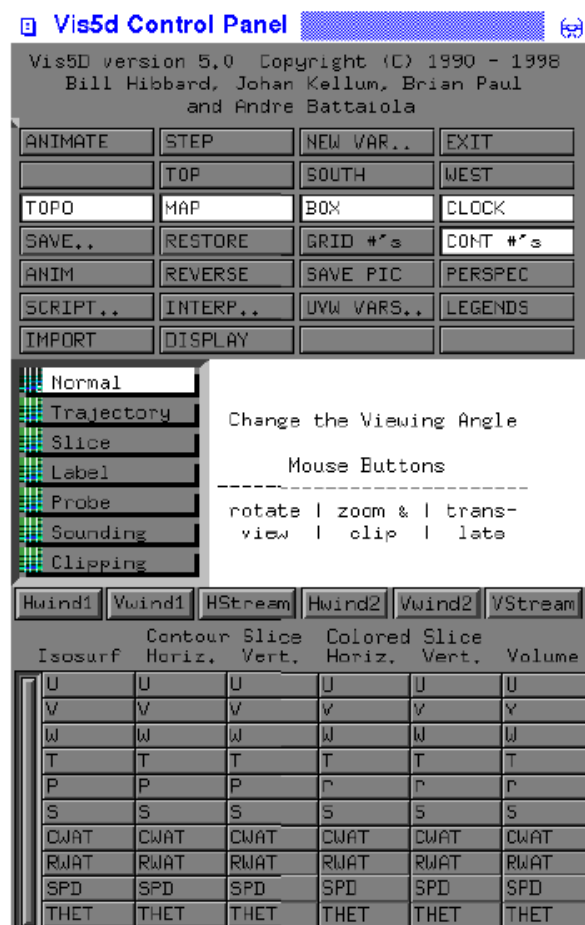


Fig. 1. Control panel for Vis5D

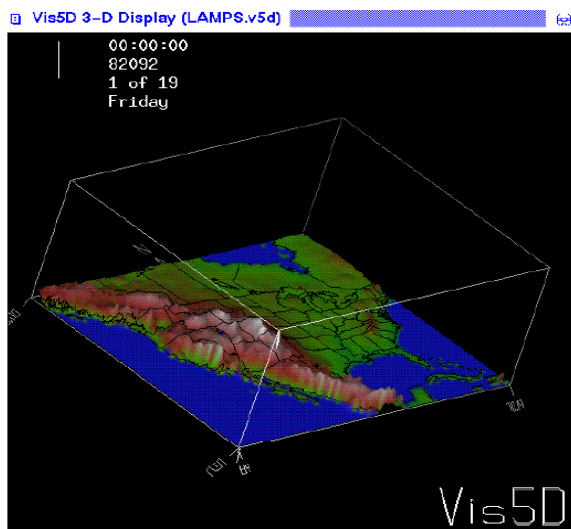


Fig. 2. Displayed image

**B. Vis5D Functions**

Process menus and parameters can be selected from the control panel. Input images as well as manipulating and resultant images are displayed on the right hand of control parameter. Therefore, image manipulation can be done interactively with the menu as shown in Table 1. Animation can be done by ANIMATION function with mouse operations together with STEP function. 3D display is available with Vis5D as shown in Figure 3.

TABLE I. MENU OF VIS5D

Normal
Trajectory
Slice
Label
Probe
Sounding
Clipping

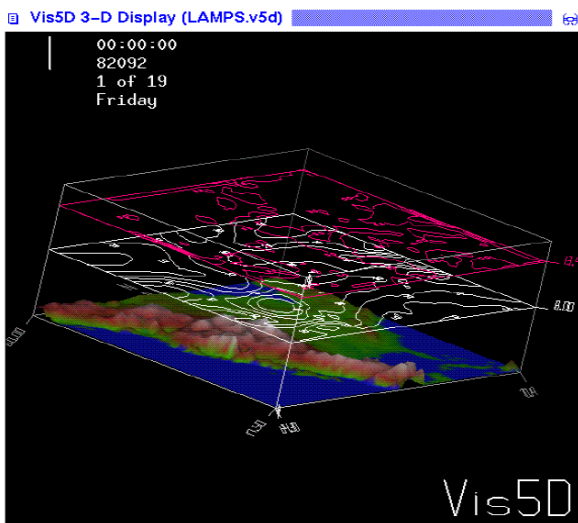


Fig. 3. Example of 3D display with Vis5D

The menu “Normal” has geometric conversion of the displayed manipulation images such as magnification rotation, translation, etc. By using the menu “Trajectory”, object tracking result of trajectory can be displayed. “Slice” allows horizontal and vertical line features location identification. 3D displayed image label can be process with “Label” while meshed grid data can be checked with “Probe”. Using “Sound”, vertical profile can be retrieved while “Clip” allows clipping 3D objects.

**C. Geographical Map Format Conversion**

Input data format of geographical data provided by Japanese Survey Geography is shown in Figure 4. It is quite simple format, starting from header record followed by line by line data. This type of map data can be treated by Vis5D.

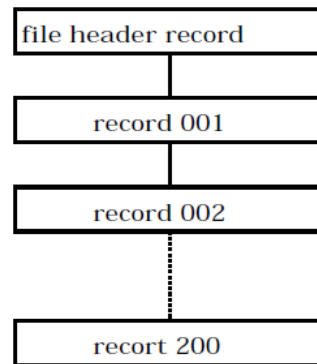


Fig. 4. Data format treated by Vis5D

Geographic map of meshed data such as geographical data can be treated with Vis5D as well. Data format for meshed data is shown in Table 2. There are sets of combined data of mesh code, record number and elevation data. Figure 5 shows the example of Shimonoseki, Japan. It can be transformed to ASCII code by using geographical map data conversion software tool developed as shown in Figure 6.

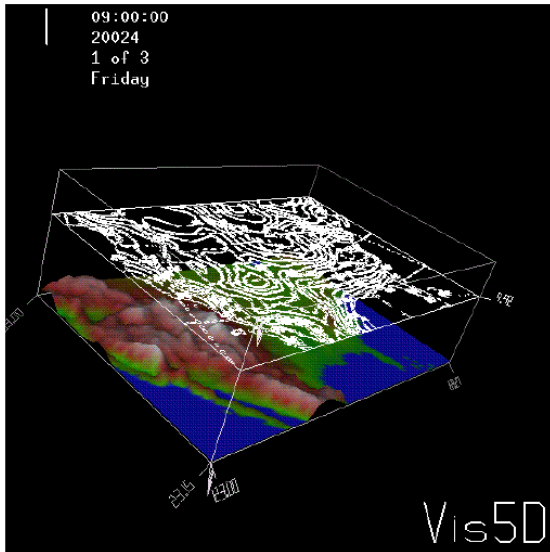
TABLE II. GEOGRAPHICAL MAP OF MESHED DATA

Mesh Code	Record No.	Elevation Data
??????	001	1 2 3 4 ... 199 200
??????	002	1 2 3 4 ... 199 200
??????	003	1 2 3 4 ... 199 200
.	.	.
.	.	.
.	.	.
??????	199	1 2 3 4 ... 199 200
??????	200	1 2 3 4 ... 199 200

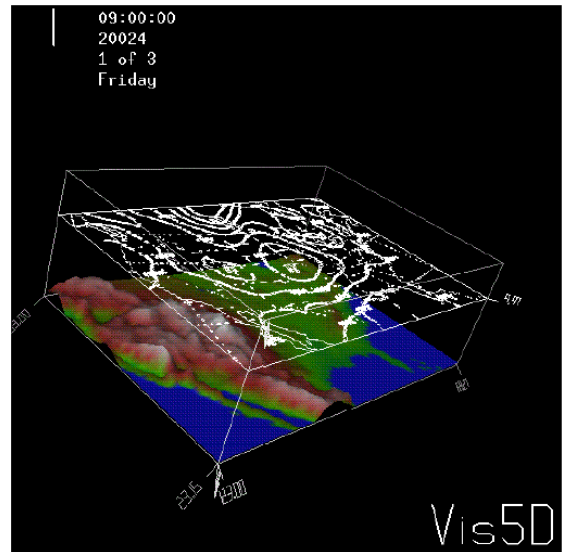
**D. Vis5D Examples**

Figure 7 shows examples of the GIF formatted meteorological assimilation data of Dew point (a), Air temperature (b), and Atmospheric pressure (c) downloaded from Illinois University site. Format conversion can be done with xv of software tool, from GIF to pgm format, in this case.

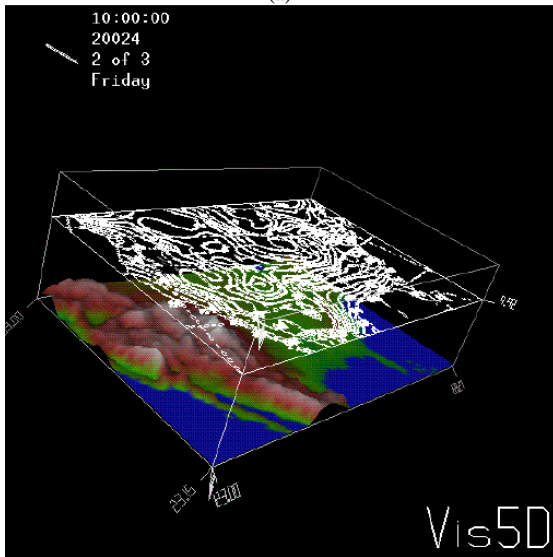




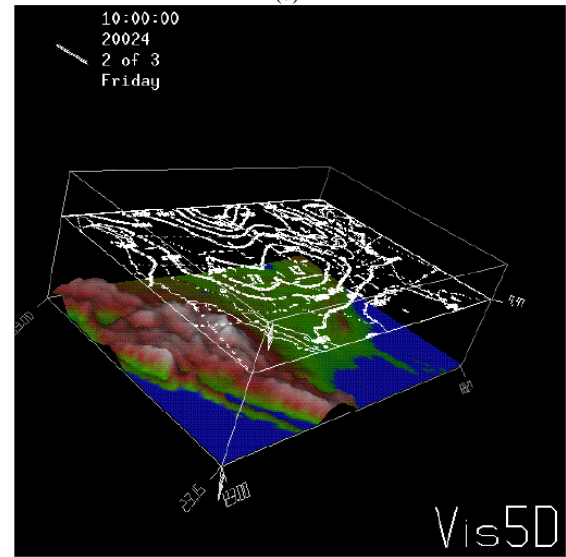
(a)



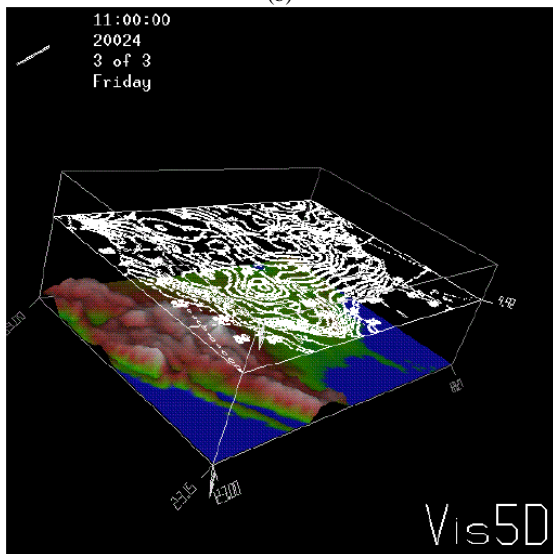
(d)



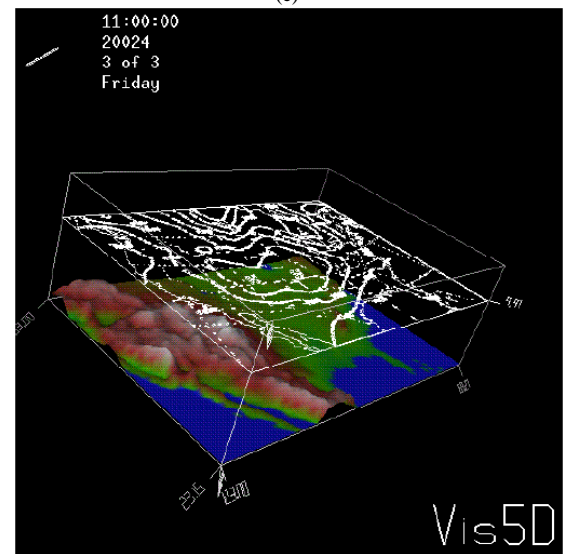
(b)



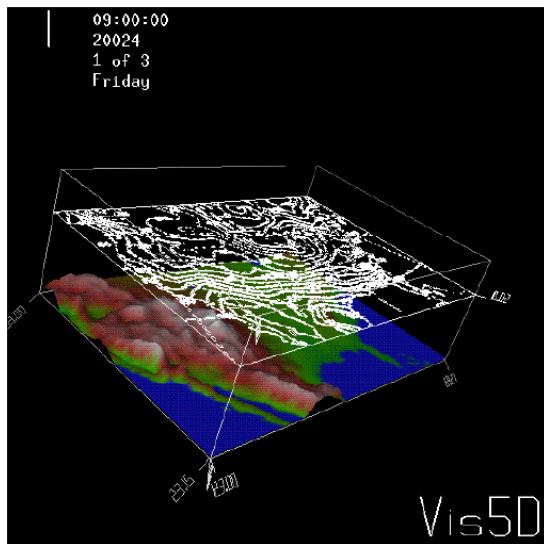
(e)



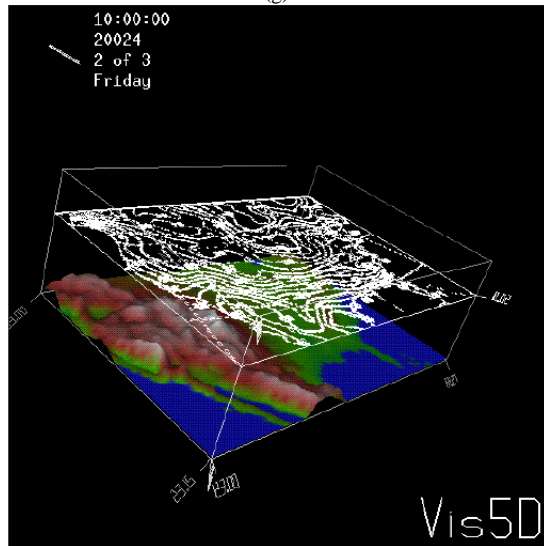
(c)



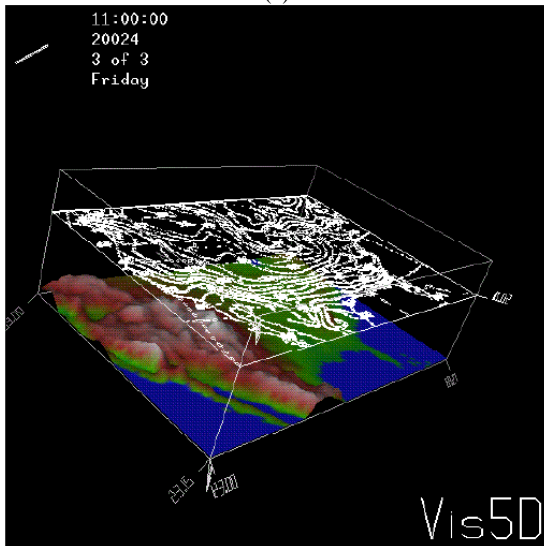
(f)



(g)



(h)



(i)

Fig. 8. Example of time series data display by time by time

The second representation method is to display the time series of data by using different colors. Namely, different color is assigned to the specific geophysical parameter. Then these colored geophysical parameters are superimposed and displayed onto screen as shown in Figure 9. Time series of geophysical parameters can be displayed with animations. It, however, is hard to see. In particular for layered geophysical parameters, it cannot be displayed.

The third representation method is to display the time series of three layered geophysical parameters with different color assignment as shown in Figure 10. It can be displayed with animation as shown in Figure 11. Figure 11 (a), (b), and (c) shows time series of three layered geophysical parameters of relative humidity, air temperature, and atmospheric pressure at the three altitudes. These can be animated with Vis5D.

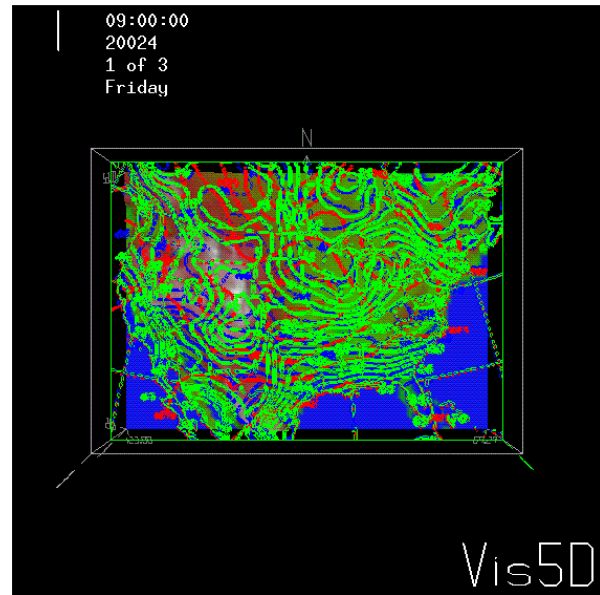


Fig. 9. Example of geophysical parameter display with the different colors

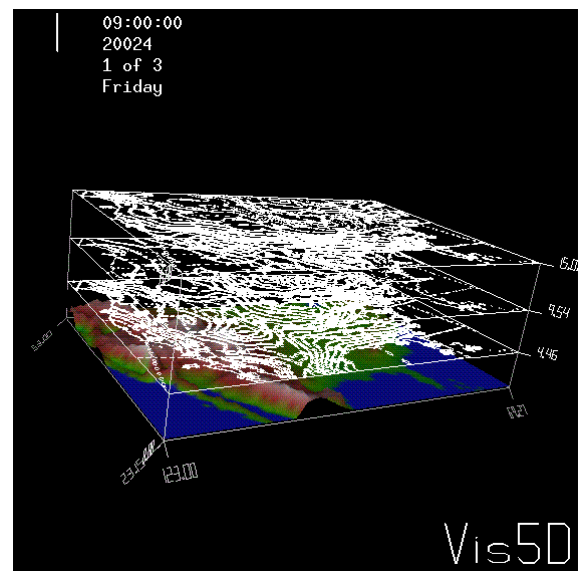
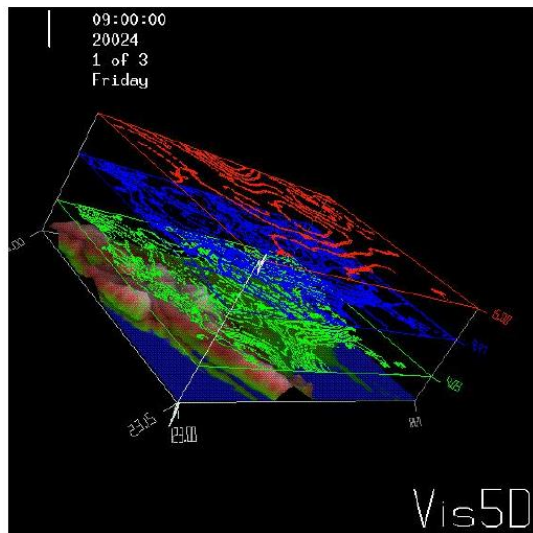
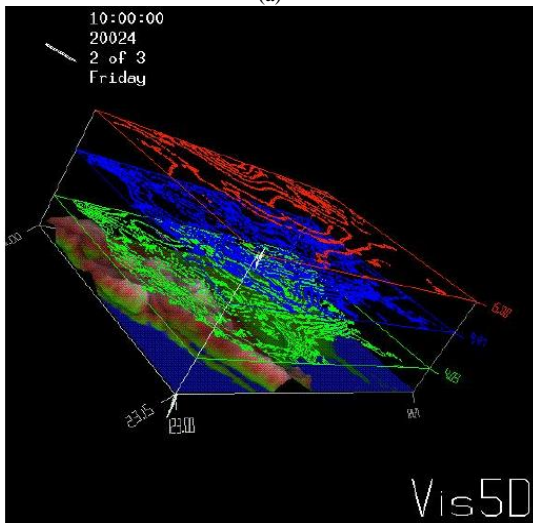


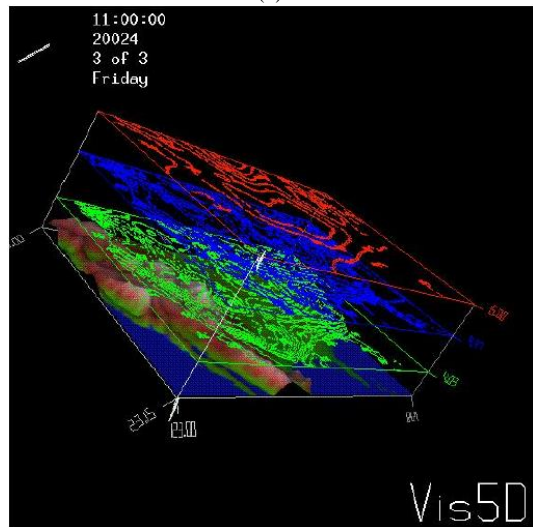
Fig. 10. Example of three layered geophysical parameter display



(a)



(b)



(c)

Fig. 11. Example of display the time series of three layered geophysical parameters with different color assignments

### III. CONCLUSION

Method for visualization of 5D assimilation data for meteorological forecasting and its related disaster mitigations utilizing Vis5D of software tool is proposed. In order to mitigate severe weather related disaster, meteorological forecasting and prediction is needed. There are some numerical weather forecasting data, in particular, assimilation data.

Time series of three dimensional geophysical parameters have to be represented visually onto computer display in a comprehensive manner. On the other hand, there are some visualization software tools. In particular, Vis5D of software tool for animation of three dimensional imagery data can be displayed.

Through experiments with NCEP/GDAS assimilation data, it is found that the proposed method is appropriate for representation of 5D assimilation data in a comprehensive manner.

It is found that the most appropriate method for displaying time series of three layered geophysical parameter data is to use Vis5D with animation with different colors. It can be used for meteorological forecasting and prediction as well as disaster mitigations.

### ACKNOWLEDGMENT

The author would like to thank Mr. Yatsushige for his efforts through experiments and simulations.

### REFERENCES

- [1] Masao Matsumoto, Hiroki Fujiku, Kiyoshi Tsuchiya, Kohei Arai, Category decomposition in the maximum likelihood classification, Journal of Japan Society of Photogrammetry and Remote Sensing, 30, 2, 25-34, 1991.

### AUTHORS PROFILE

**Kohei Arai**, He received BS, MS and PhD degrees in 1972, 1974 and 1982, respectively. He was with The Institute for Industrial Science and Technology of the University of Tokyo from April 1974 to December 1978 also was with National Space Development Agency of Japan from January, 1979 to March, 1990. During from 1985 to 1987, he was with Canada Centre for Remote Sensing as a Post Doctoral Fellow of National Science and Engineering Research Council of Canada. He moved to Saga University as a Professor in Department of Information Science on April 1990. He was a councilor for the Aeronautics and Space related to the Technology Committee of the Ministry of Science and Technology during from 1998 to 2000. He was a councilor of Saga University for 2002 and 2003. He also was an executive councilor for the Remote Sensing Society of Japan for 2003 to 2005. He is an Adjunct Professor of University of Arizona, USA since 1998. He also is Vice Chairman of the Commission "A" of ICSU/COSPAR since 2008. He wrote 30 books and published 322 journal papers.

# Comparative Study Among Least Square Method, Steepest Descent Method, and Conjugate Gradient Method for Atmospheric Sounder Data Analysis

Kohei Arai <sup>1</sup>

Graduate School of Science and Engineering  
Saga University  
Saga City, Japan

**Abstract**—Comparative study among Least Square Method: LSM, Steepest Descent Method: SDM, and Conjugate Gradient Method: CGM for atmospheric sounder data analysis (estimation of vertical profiles for water vapor) is conducted. Through simulation studies, it is found that CGM shows the best estimation accuracy followed by SDM and LSM. Method dependency on atmospheric models is also clarified.

**Keywords**—nonlinear optimization theory; solution space; atmospheric sounder

## I. INTRODUCTION

Air-temperature and water vapor profiles are used to be estimated with Infrared Sounder data [1]. One of the problems on retrieving vertical profiles is its retrieving accuracy. In particular, estimation accuracy of air-temperature and water vapor at tropopause<sup>1</sup> altitude is not good enough because there are gradient changes of air-temperature and water vapor profile in the tropopause so that observed radiance at the specific channels are not changed for the altitude.

In order to estimate air-temperature and water vapor, least square based method is typically used. In the process, Root Mean Square: RMS difference between observed radiance and calculated radiance with the designated physical parameters are minimized. Then the designated physical parameters including air-temperature and water vapor at the minimum RMS difference are solutions.

Typically, Newton-Raphson method<sup>2</sup> which gives one of local minima is used for minimization of RMS difference. Newton-Raphson needs first and second order derivatives, Jacobean and Hessian at around the current solution. It is not easy to formularize these derivatives analytically. The proposed method is based on Levenberg Marquardt: LM of non-linear least square method<sup>3</sup>. It uses numerically calculated first and second order derivatives instead of analytical based derivatives. Namely, these derivatives can be calculated with radiative transfer model based radiance calculations. At

around the current solution in the solution space, directional derivatives are calculated with the radiative transfer model.

The proposed method is validated for air-temperature and water vapor profile retrievals with Infrared: IR sounder<sup>4</sup> data derived from Atmospheric Infrared Sounder:/AIRS onboard AQUA satellite [2]-[7]. A comparison of retrieving accuracy between Newton-Raphson method and the proposed method based on LM method [8] is made in order to demonstrate an effectiveness of the proposed method in terms of estimation accuracy in particular for the altitude of tropopause [9]. Global Data Assimilation System: GDAS<sup>5</sup> data of assimilation model derived 1 degree mesh data is used as truth data of air-temperature and water vapor profiles. The experimental data show that the proposed method is superior to the conventional Newton-Raphson method.

The following section describes proposed method for water vapor profile retrievals followed by experiments. Then finally, conclusion and some discussions are described.

## II. THEORETICAL BACKGROUND AND SIMULATION METHOD

### A. Radiative Transfer Equation

Radiative transfer equation is expressed with equation (1).

$$R_{\nu} = (I_0)_{\nu} \tau_{\nu}(z_0) + \int_{z_0}^{\infty} B_{\nu}\{T(z)\}K_{\nu}(z)dz \quad (1)$$

where  $\nu$  denotes wave number (cm-1), and  
 $R_{\nu}$ : at sensor brightness temperature  
 $(I_0)_{\nu}$ : brightness temperature of ground surface  
 $\tau_{\nu}(z_0)$ : total column atmospheric transmittance  
 $B_{\nu}\{T(z)\}$ : Planckian function of air temperature at the altitude of  $z$   
 $K_{\nu}(z)$ : atmospheric transmittance at the altitude of  $z$

This equation (1) can be linearized as follows,

$$R=BK \quad (2)$$

<sup>1</sup> <http://en.wikipedia.org/wiki/Tropopause>

<sup>2</sup> [http://en.wikipedia.org/wiki/Newton's\\_method](http://en.wikipedia.org/wiki/Newton's_method)

<sup>3</sup>

[http://en.wikipedia.org/wiki/Levenberg%E2%80%93Marquardt\\_algorithm](http://en.wikipedia.org/wiki/Levenberg%E2%80%93Marquardt_algorithm)

<sup>4</sup> [http://en.wikipedia.org/wiki/Atmospheric\\_Infrared\\_Sounder](http://en.wikipedia.org/wiki/Atmospheric_Infrared_Sounder)

<sup>5</sup> <http://www.mmm.ucar.edu/mm5/mm5v3/data/gdas.html>

Where the number of unknown variables and the number of given equations are same. Therefore, it can be solved relatively easily. This solution from linear inversion provides initial value of the steepest descent method. Without this initial value, steepest descent method falls in one of local minima easily.

### B. Water Vapor Profile Retrieval Method

For instance, it can be solved based on steepest descent method as shown in equation (3)

$$R - R_0 = \frac{\partial R}{\partial q} (q - q_0) \quad (3)$$

Also, it is possible to estimate water vapor profile to minimize the following covariance matrix of error,

$$\hat{x} = x_a + (A^T S_\varepsilon^{-1} A + S_a^{-1})^{-1} A^T S_\varepsilon^{-1} (R - R_a) \quad (4)$$

Where

$x_a$ : Designated variable matrix

$\hat{x}$ : Variable matrix for estimation

A: Jacobian Matrix

S: Covariance matrix for measurement error

R: Observed brightness temperature

$R_a$ : Estimated brightness temperature

Covariance matrix can be defined as equation (5).

$$S_{ij} = \varepsilon (x_i - \hat{x}_i)(x_j - \hat{x}_j)^T \quad (5)$$

Jacobian Matrix can be expressed in equation (6).

$$A = \begin{pmatrix} \frac{\partial R_1}{\partial q_1} & \frac{\partial R_1}{\partial q_2} & \dots & \frac{\partial R_1}{\partial q_n} \\ \frac{\partial R_2}{\partial q_1} & \frac{\partial R_2}{\partial q_2} & \dots & \frac{\partial R_2}{\partial q_n} \\ \vdots & \vdots & \ddots & \vdots \\ \frac{\partial R_n}{\partial q_1} & \frac{\partial R_n}{\partial q_2} & \dots & \frac{\partial R_n}{\partial q_n} \end{pmatrix} \quad (6)$$

### C. Steepest Descent Method (Non-linear optimization method)

Steepest descent method can be represented in equation (7).

$$q_k = q_{k-1} + \alpha_k g_k \quad (7)$$

Where

$q_k$ : estimated value at the iteration number k

g: updating vector

$\alpha$ : step width

Estimated value can be updated with the direction of g and

with step size of  $\alpha$ . Then estimation process is converged at one of local minima, not global optimum solution. This learning or updating process can be illustrated as shown in Figure 1. Initial value is derived from the linear inversion,  $K=B^{-1}R$ .

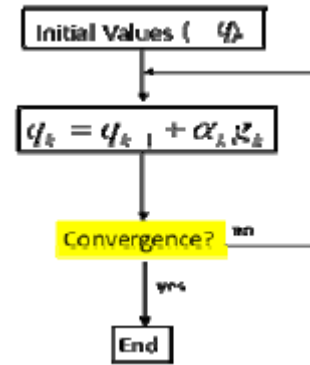


Fig. 1. Process flow of steepest descent method

### D. Simulation Method

From equation (1), observed brightness temperature of atmospheric sounder can be expressed as follows,

$$R_w = \alpha + \beta e^{-(\gamma w + \phi)} \quad (8)$$

Where  $w$  denotes water vapor content in the atmosphere while  $\alpha$ ,  $\beta$ ,  $\gamma$ ,  $\phi$  denotes coefficients. Using MODTRAN of radiative transfer software code including six atmospheric models, Tropic: TRP, Mid. Latitude Summer: MLS, Mid. Latitude Winter: MLW, Sub-Arctic Summer: SAS, Sub-Arctic Winter: SAW, and 1976 US Standard atmosphere: USS, observed brightness temperature at certain wavelength can be calculated. With the reference to AIRS observation wavelength, the following three wavelength are selected for simulation study, 6.7, 7.3, and 7.5  $\mu\text{m}$ . Therefore, coefficients in equation (8) can be estimated for each observation wavelength together with Root Mean Square Error: RMSE of water vapor retrieval error.

## III. SIMULATION RESULTS

### A. Water Vapor Profile

Figure 2 to 8 shows water vapor profiles for 6 different atmospheric models with default relative humidity, and its plus minus 10%, 20%, and 30% while Figure 9 to 15 shows accumulated water vapor profiles for 6 different atmospheric models with default relative humidity, and its plus minus 10%, 20%, and 30% derived from MODTRAN 4.3, respectively. These water vapor profiles and accumulated water vapor profiles are totally dependent on relative humidity, obviously. It is also obvious that water vapor and accumulated water vapor of the Tropic atmosphere is greatest followed by Mid. Latitude Summer, 1976 U.S. Standard, Mid. Latitude Winter, Sub Arctic Summer, and Sub Arctic Winter.

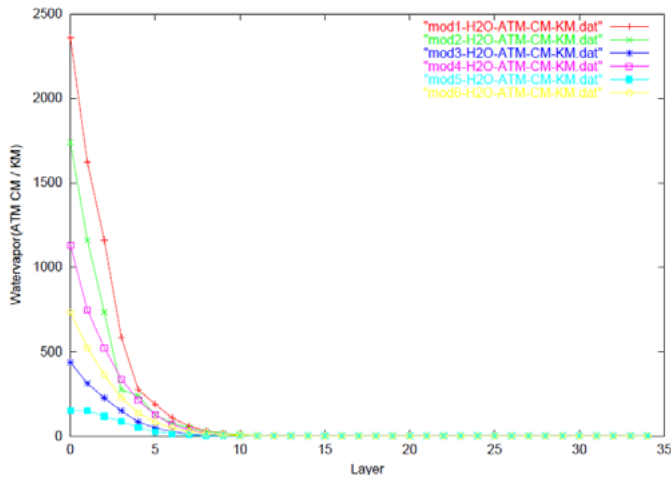


Fig. 2. Water vapor profiles for 6 atmospheric models with default relative Humidity

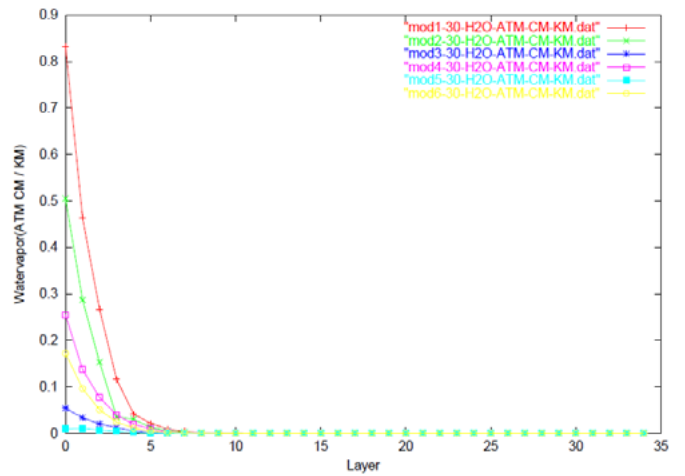


Fig. 5. Water vapor profiles for 6 atmospheric models with default relative humidity minus 30%

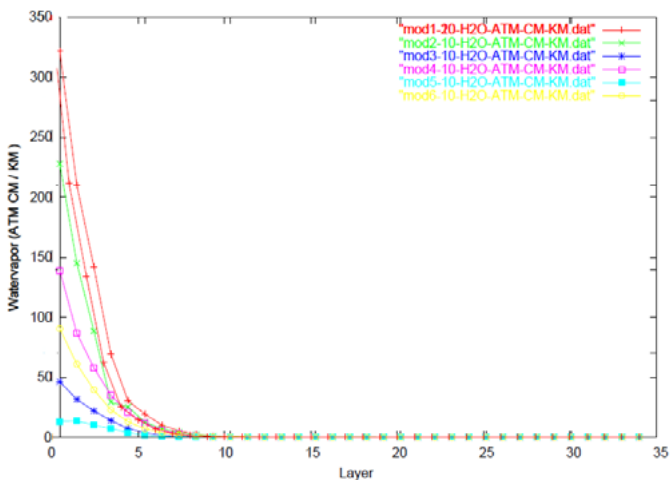


Fig. 3. Water vapor profiles for 6 atmospheric models with default relative humidity minus 10%

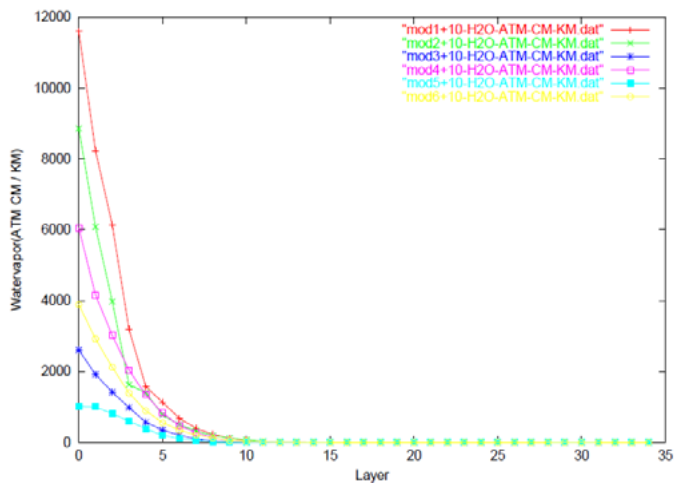


Fig. 6. Water vapor profiles for 6 atmospheric models with default relative humidity plus 10%

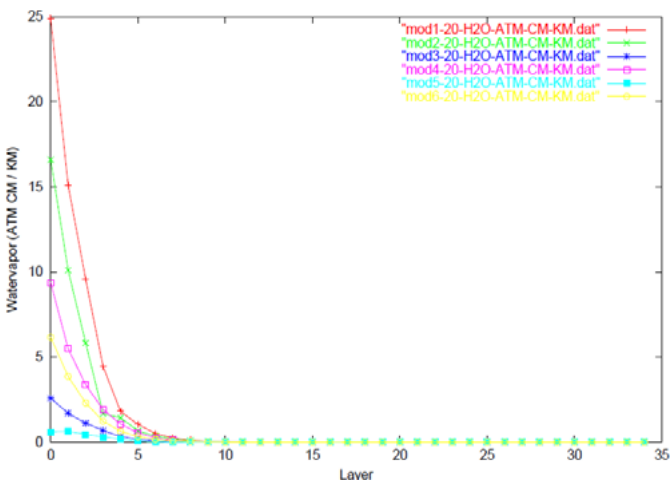


Fig. 4. Water vapor profiles for 6 atmospheric models with default relative humidity minus 20%

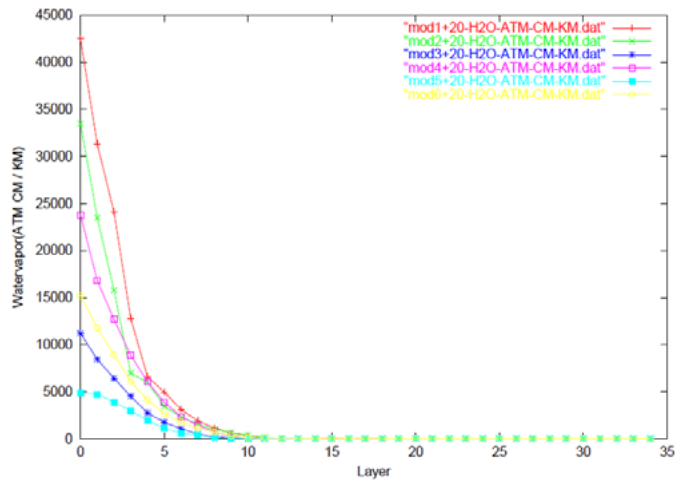


Fig. 7. Water vapor profiles for 6 atmospheric models with default relative humidity plus 20%

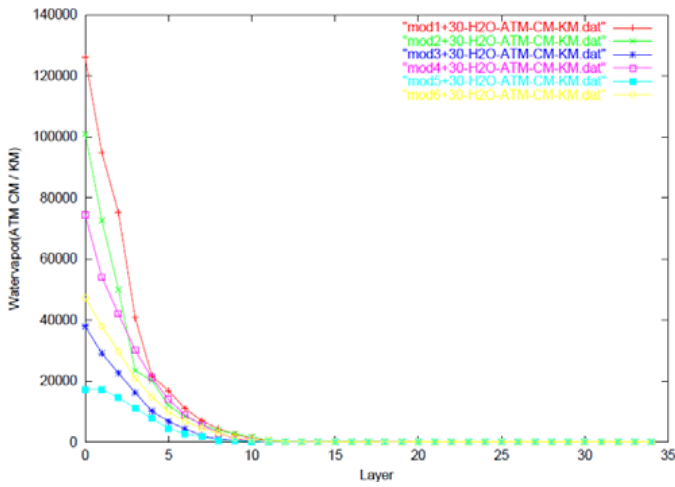


Fig. 8. Water vapor profiles for 6 atmospheric models with default relative humidity plus 30%

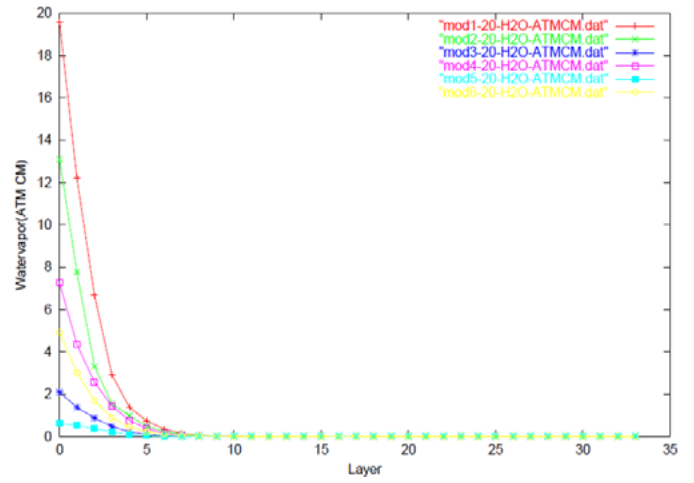


Fig. 11. Accumulative water vapor profiles for 6 atmospheric models with default relative humidity minus 20%

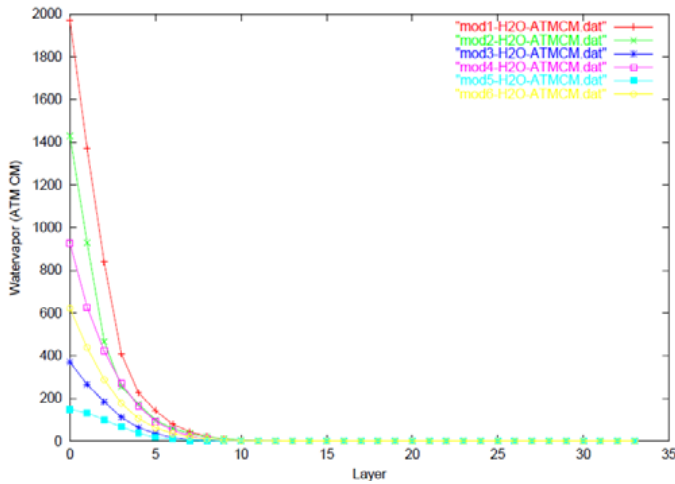


Fig. 9. Accumulative water vapor profiles for 6 atmospheric models with default relative humidity

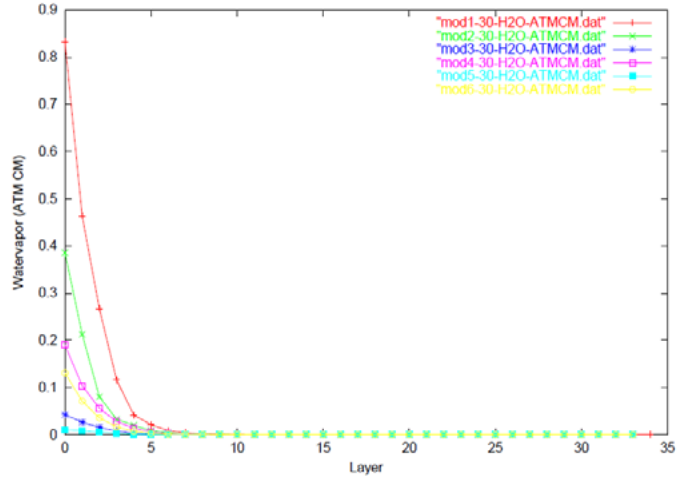


Fig. 12. Accumulative water vapor profiles for 6 atmospheric models with default relative humidity minus 30%

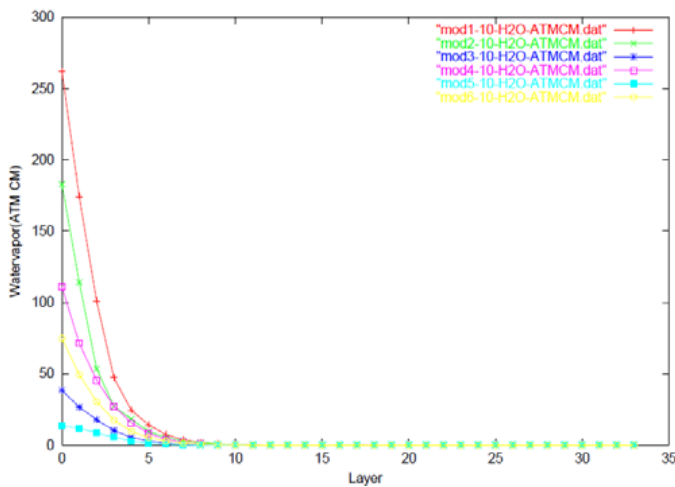


Fig. 10. Accumulative water vapor profiles for 6 atmospheric models with default relative humidity minus 10%

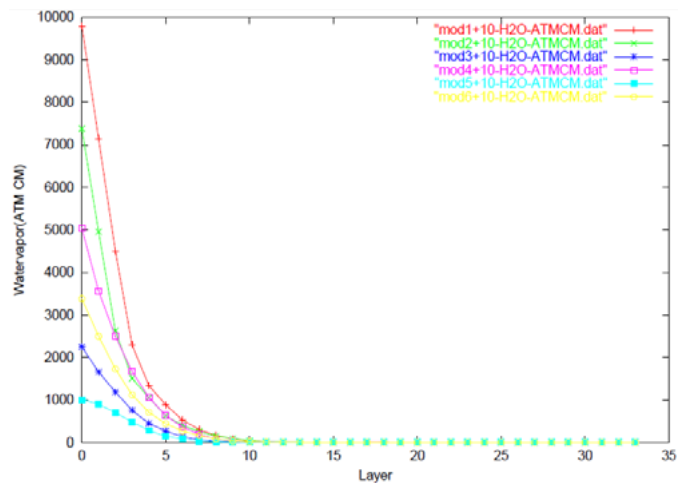


Fig. 13. Accumulative water vapor profiles for 6 atmospheric models with default relative humidity plus 10%

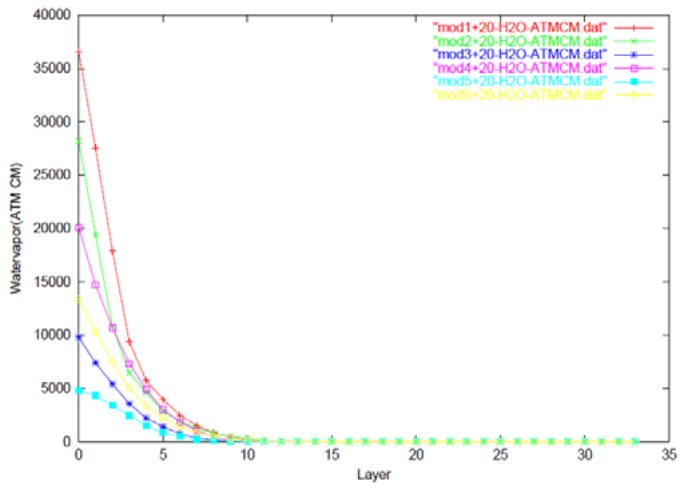


Fig. 14. Accumulative water vapor profiles for 6 atmospheric models with default relative humidity plus 20%

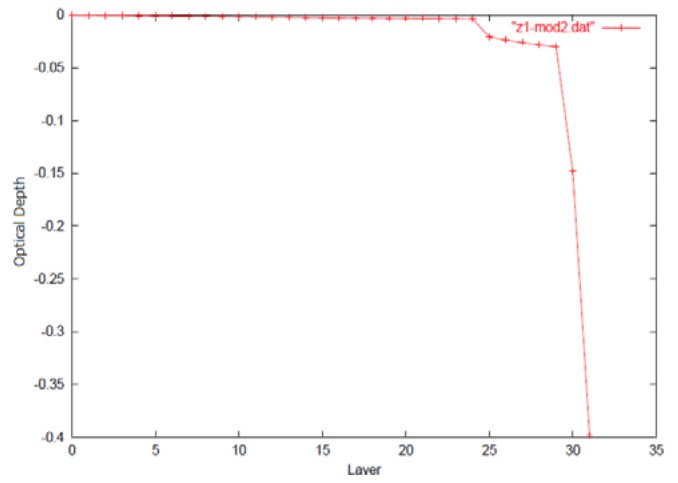


Fig. 17. Optical depth profile for the Mid. Latitude Summer atmospheric Model

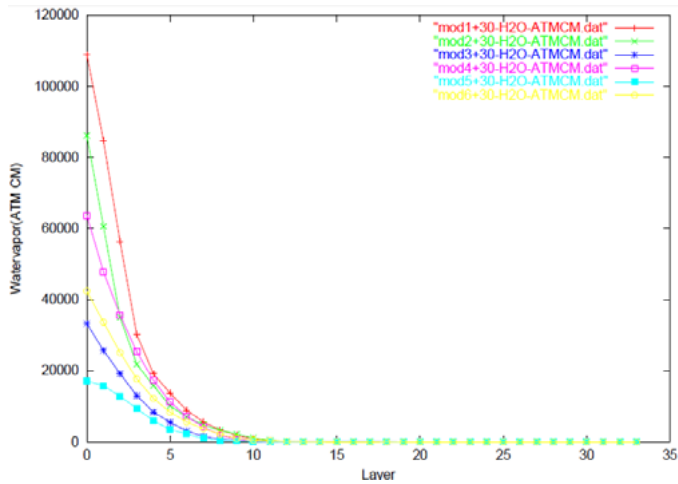


Fig. 15. Accumulative water vapor profiles for 6 atmospheric models with default relative humidity plus 30%

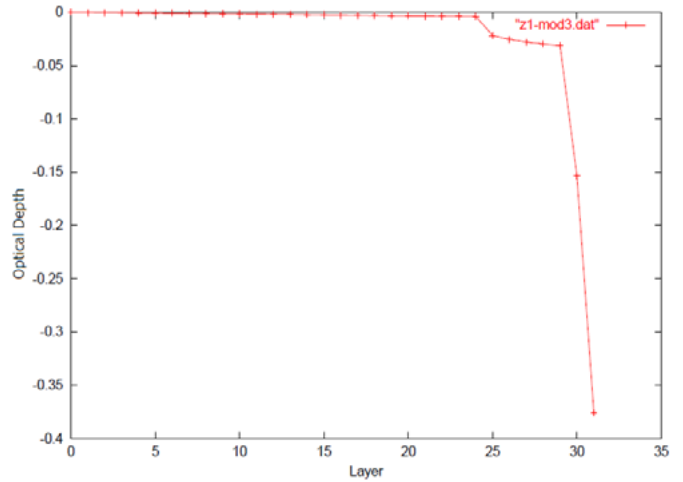


Fig. 18. Optical depth profile for the Mid. Latitude Winter atmospheric model

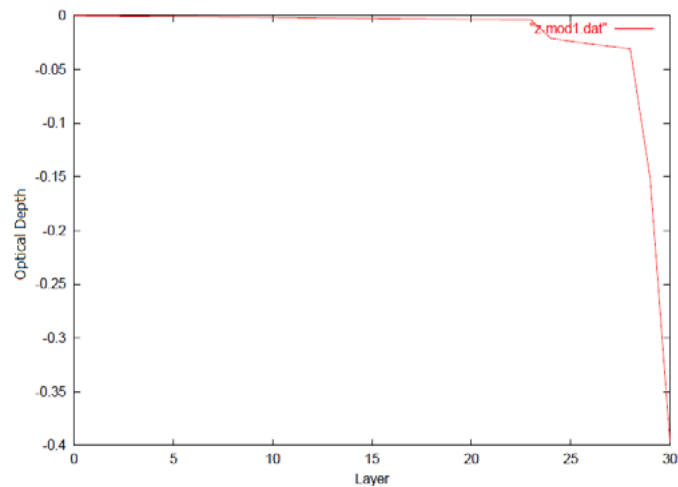


Fig. 16. Optical depth profile for the tropic atmospheric model

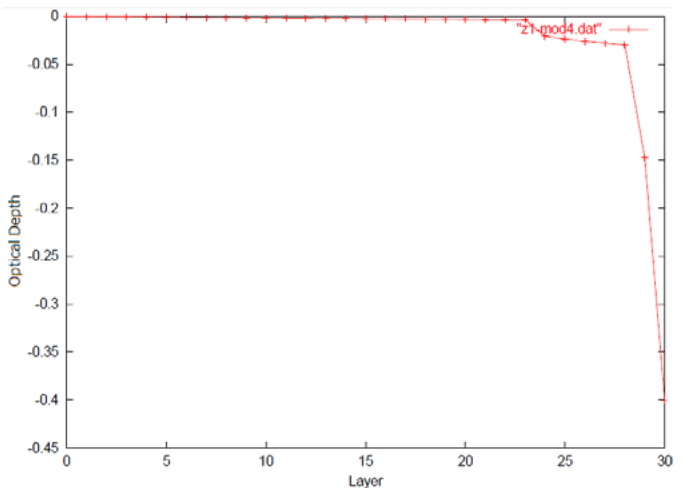


Fig. 19. Optical depth profile for the Sub Arctic Summer atmospheric model

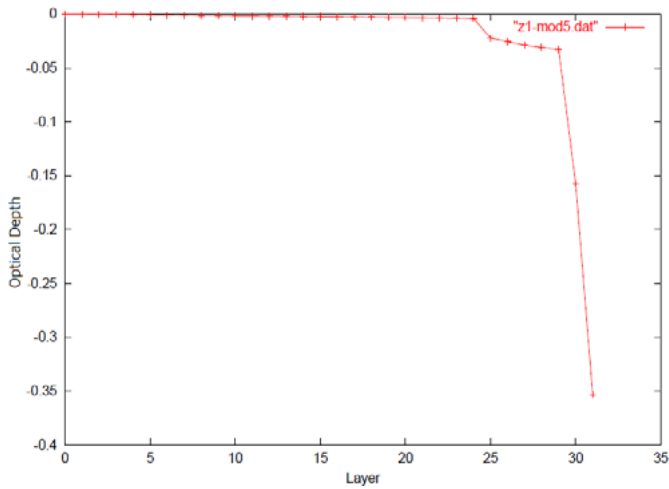


Fig. 20. Optical depth profile for the Sub Arctic Winter atmospheric model

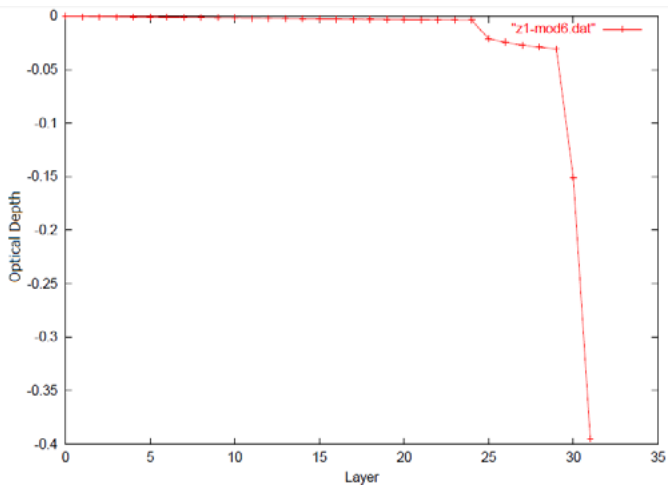


Fig. 21. Optical depth profile for the 1976 U.S. Standard atmospheric model

### B. Optical Depth Profile

Figure 16 to 21 shows optical depth profiles for 6 different atmospheric models. It is also obvious that optical depth of the Tropic atmosphere is greatest followed by Mid. Latitude Summer, 1976 U.S. Standard, Mid. Latitude Winter, Sub Arctic Summer, and Sub Arctic Winter.

### C. Up-welling Radiance Profile

Figure 22 to 26 shows up-welling radiance profiles for 6 different atmospheric models. It is also obvious that upwelling radiance of the Tropic atmosphere is greatest followed by Mid. Latitude Summer, 1976 U.S. Standard, Mid. Latitude Winter, Sub Arctic Summer, and Sub Arctic Winter.

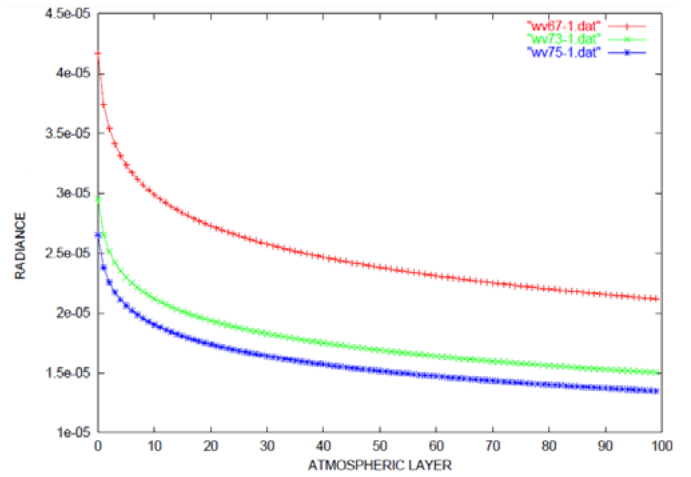


Fig. 22. Up-welling radiance profiles for the Tropic atmospheric model

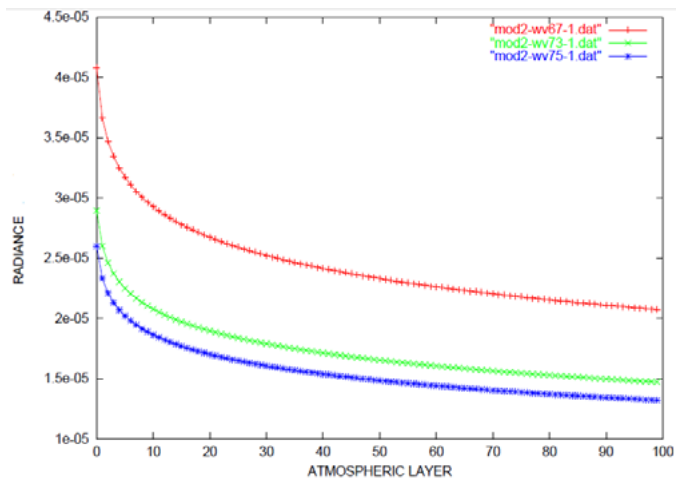


Fig. 23. Up-welling radiance profiles for the Mid. Latitude Summer atmospheric model

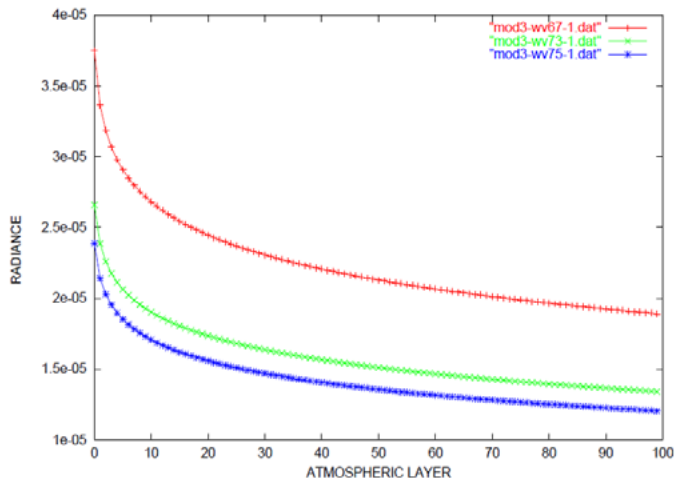


Fig. 24. Up-welling radiance profiles for the Mid. Latitude Winter atmospheric model

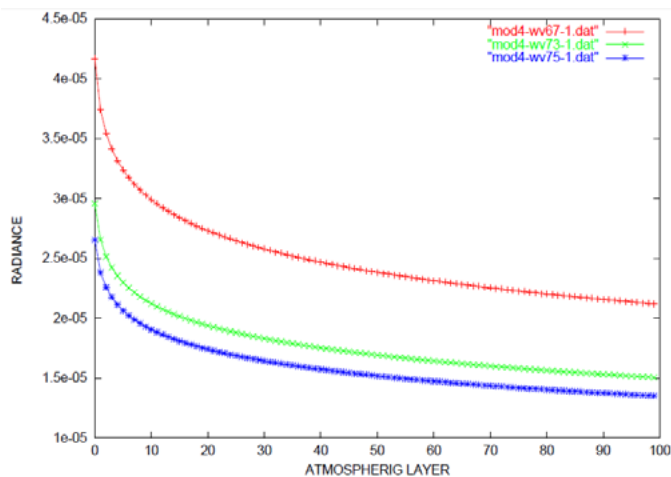


Fig. 25. Up-welling radiance profiles for the Sub Arctic Summer atmospheric model

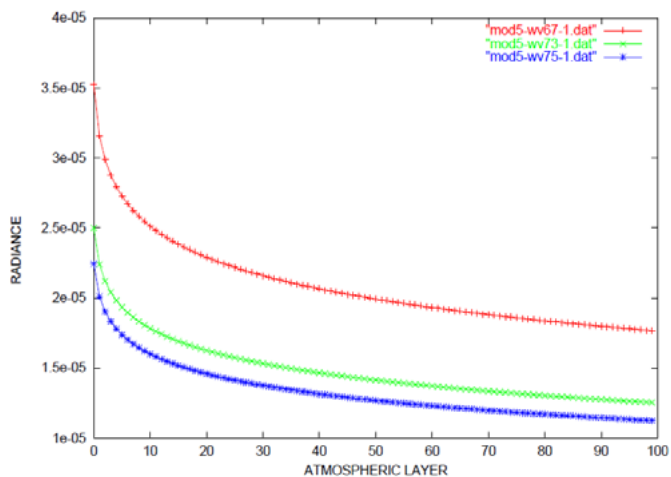


Fig. 26. Up-welling radiance profiles for the Sub Arctic Winter atmospheric Model

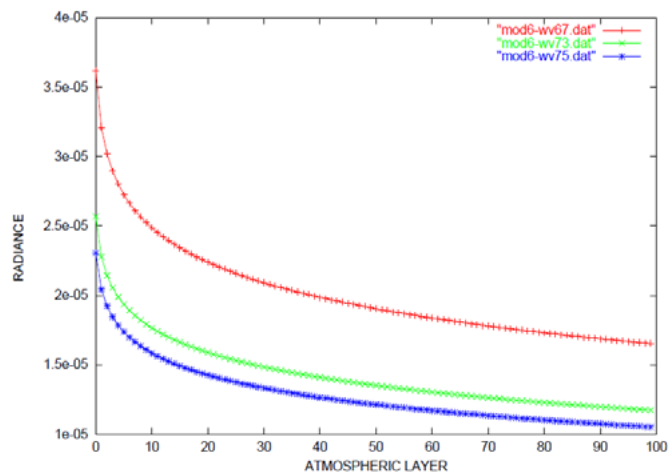


Fig. 27. Up-welling radiance profiles for the 1976 U.S. Standard atmospheric model

#### D. RMSE for Three Different Methods for Water Vapor Profile Estimation

Root Mean Square Error: RMSE of three different water vapor estimation methods are evaluated. Using spectral upwelling radiance, it is possible to estimate water vapor profile. With the reference to AIRS observation wavelength, the following three wavelengths are selected for simulation study, 6.7, 7.3, and 7.5  $\mu\text{m}$ . Up-welling radiance at the wavelength is calculated for 6 different atmospheric models with MODTRAN 4.3, then water vapor profile is estimated with the Least Square Method, Steepest Descent Method, and Conjugate Gradient Method. True water vapor profiles are given by MODTRAN 4.3. Therefore, RMSE can be evaluated.

Table 1 to 3 shows RMSE. It is found that RMSE of the Conjugate Gradient Method is smallest followed by Steepest Descent Method and Least Square Method. Least Square Method is totally equal to Linear Regression. Because water vapor profile estimation is not linear problem solving, RMSE of the Least Square Method is not so good. Meanwhile, both Conjugate Gradient and Steepest Descent Methods find one of local minima. Steepest Descent Method often output trivial solution due to algorithm nature. Therefore, Conjugate Gradient Method is better than Steepest Descent Method mostly.

TABLE I. RMSE FOR STEEPEST DESCENT METHOD FOR 6 ATMOSPHERIC MODELS

$\lambda(\mu\text{m})$	6.7	7.3	7.5
$\alpha$	-9.9042927e-01	-9.8428169e-01	-9.8428161e-01
$\beta$	-5.8044111e-01	-1.2968778e+00	-2.0132363e+00
$\gamma$	6.1027836e-01	1.2968778e+00	2.0132363e+00
$\psi$	2.1518239e-02	2.3999963e-02	2.3999963e-02
RMSE(atom-cm)	1.286716e-02	1.283178e-02	1.283175e-02

TABLE II. RMSE FOR CONJUGATE GRADIENT METHOD FOR 6 ATMOSPHERIC MODELS

$\lambda(\mu\text{m})$	6.7	7.3	7.5
$\alpha$	-9.9469977e-01	-1.0010890e+00	-9.9546792e-01
$\beta$	1.0482258e-01	-4.8530780e-02	3.9825363e-02
$\gamma$	2.2675326e-01	3.0309994e-01	2.7884224e-01
$\psi$	2.2841551e-01	1.2047212e-01	3.2866798e-02
RMSE(atom-cm)	3.711227e-03	3.818651e-03	3.711227e-03

TABLE III. RMSE FOR LEAST SQUARE METHOD FOR 6 ATMOSPHERIC MODELS

$\lambda(\mu\text{m})$	6.7	7.3	7.5
$\alpha$	-4.6402598e+00	-1.4154191e+01	-1.4366376e+01
$\beta$	1.3551852e+00	-9.7287497e-05	1.0303786e-01
$\gamma$	-3.1595048e-04	2.4652031e+00	-1.9849016e-03
$\psi$	7.4871903e+00	-2.6431300e+03	1.5466422e+00
RMSE(atom-cm)	1.946242e+01	8.258933e-01	7.951221e-01

#### IV. CONCLUSION

Comparative study among Least Square Method: LSM, Steepest Descent Method: SDM and Conjugate Gradient Method: CGM for atmospheric sounder data analysis (estimation of vertical profiles for water vapor) is conducted. Three retrieval methods, SDM, LSM, and CGM are compared in terms of Root Mean Square Error: RMSE. In particular, atmospheric model dependency on RMSE is to be clarified. Thus it becomes possible to use the most appropriate method for each atmospheric model. Through simulation studies, it is found that CGM shows the best estimation accuracy followed by SDM and LSM. Method dependency on atmospheric models is also clarified.

#### ACKNOWLEDGMENT

The author would like to thank Mr. Chen Ding for his effort to conduct simulation studies.

#### REFERENCES

- [1] Kohei Arai, Lecture Note on Remote Sensing, Morikita-Shuppan publishing Co. Ltd, 2004.
- [2] NASA/JPL, "AIRS Overview".  
NASA/JPL.<http://airs.jpl.nasa.gov/overview/overview/>.
- [3] NASA "Aqua and the A-Train".  
NASA.[http://www.nasa.gov/mission\\_pages/aqua/](http://www.nasa.gov/mission_pages/aqua/).

- [4] NASA/GSFC "NASA Goddard Earth Sciences Data and Information Services Center".  
NASA/GSFC.[http://disc.gsfc.nasa.gov/AIRS/data\\_products.shtml](http://disc.gsfc.nasa.gov/AIRS/data_products.shtml).
- [5] NASA/JPL "How AIRS Works".  
NASA/JPL.[http://airs.jpl.nasa.gov/technology/how\\_AIRS\\_works](http://airs.jpl.nasa.gov/technology/how_AIRS_works).
- [6] NASA/JPL "NASA/NOAA Announce Major Weather Forecasting Advancement".  
NASA/JPL.<http://jpl.nasa.gov/news/news.cfm?release=2005-137>.
- [7] NASA/JPL "New NASA AIRS Data to Aid Weather, Climate Research".  
NASA/JPL. <http://www.jpl.nasa.gov/news/features.cfm?feature=1424>.

#### AUTHORS PROFILE

Kohei Arai He received BS, MS and PhD degrees in 1972, 1974 and 1982, respectively. He was with The Institute for Industrial Science and Technology of the University of Tokyo from April 1974 to December 1978 and also was with National Space Development Agency of Japan from January, 1979 to March, 1990. During from 1985 to 1987, he was with Canada Centre for Remote Sensing as a Post Doctoral Fellow of National Science and Engineering Research Council of Canada. He moved to Saga University as a Professor in Department of Information Science on April 1990. He was a councilor for the Aeronautics and Space related to the Technology Committee of the Ministry of Science and Technology during from 1998 to 2000. He was a councilor of Saga University for 2002 and 2003. He also was an executive councilor for the Remote Sensing Society of Japan for 2003 to 2005. He is an Adjunct Professor of University of Arizona, USA since 1998. He also is Vice Chairman of the Commission-A of ICSU/COSPAR since 2008. He wrote 30 books and published 332 journal papers.

# An Approach with Support Vector Machine using Variable Features Selection on Breast Cancer Prognosis

Sandeep Chaurasia

Department of Computer Science & Engineering,  
Sir Padampat Singhanian University,  
Udaipur, India

Dr. P Chakrabarti

Department of Computer Science & Engineering,  
Sir Padampat Singhanian University,  
Udaipur, India

**Abstract**—Cancer diagnosis and clinical outcome prediction are among the most important emerging applications of machine learning. In this paper we have used an approach by using support vector machine classifier to construct a model that is useful for the breast cancer survivability prediction. We have used both 5 cross and 10 cross validation of variable selection on input feature vectors and the performance measurement through bio-learning class performance while measuring AUC, specificity and sensitivity. The performance of the SVM is much better than the other machine learning classifier.

**Keywords**—Breast cancer; feature selection; Support vectors; Support Vector Machine; Wisconsin Breast Cancer Dataset.

## I. INTRODUCTION

A major category of problems in medical science deals with the diagnosis of disease, based upon various tests performed upon the patient. For this reason the use of classifier systems in medical diagnosis is gradually increasing. There is no doubt that evaluation of data taken from patients and decisions of experts are the most important factors in diagnosis. But the different artificial intelligence techniques for classification also help experts a great deal. Classification systems, minimizing possible errors that might be made because of fatigued or inexperienced experts, provide more detailed medical data for examination in a shorter time.

The importance of patterns classification of breast cancer is a major real world medical problem. Breast cancer has become one of the major causes of mortality around the world and research into cancer diagnosis and treatment has become an important issue for the scientific community. The etiologist of breast cancer remain unclear and no single dominant cause has emerged. [2][3]

Prevention is still a mystery and the only way to help patients survive is by early detection. If the cancerous cells are detected before spreading to other organs, the survival rate for patients is more than 97%. [4]

## II. BACKGROUND MATERIAL

There are many applications for Machine Learning (ML) of which the most significant is data mining and pattern classification. Major areas of ML where it can often be successfully applied for classification and regression problems by improving the efficiency and design of the systems. Every

instance or attribute in any of the dataset used by the machine learning algorithms is represented using the same set of features. The features may be of different dimension, if instances are given with known labels with corresponding correct outputs then this type of learning is called supervised learning, where as unsupervised learning, the instances are unlabeled or the outputs are unknown. Another kind of machine learning is reinforcement learning where the training information is provided to the learning system by the external teacher is in the form of a scalar reinforcement signal that constitutes a measure of how well the system operates. The learner is not instructed to take any desired actions, but rather discovering which actions yield the best solution, by continuously trying each action to improve the efficiency.

### A. Supervised Learning Algorithms

Machine learning is the process of learning a set of rules from instance from a training set, or more generalizing, creating a classifier that can be used to generalize from new instances. The procedures or learning is as follow; the first step is to collect the dataset, if a dataset collected by any of the arbitrary method is not directly suitable for induction. It may contain noisy and missing data values, and therefore requires significant pre-processing [5]. The second step is the data preparation and data pre-processing and the feature subset selection is the process of identifying and removing as many irrelevant and redundant features as possible [6]. This reduces the dimension of the data and allowing algorithms to perform faster and more efficiently. But many features depend on one another and may influence the accuracy of supervised Machine Learning classification models.

### B. Algorithm selection

Specifically the selection of learning algorithm is a critical procedure. Once at preliminary stage when testing is judged and it comes out satisfactory, then the classifier is generalized [11]. The accuracy of the classifier's evaluation is typically often based on prediction (the ratio of correct prediction over the total number of predictions). There are many techniques are available to calculate the classifier's accuracy. One way is to split the training set by dividing the two-thirds for training and rest for estimating performance. Another method is known as cross-validation in which the training set is divided into mutually exclusively equally-sized subsets and for every subset the classifier is trained on the union of remaining

subsets. The average error rate of each subset results an estimate of the error rate for the classifier. If the error (%) is not tolerable then the algorithm go back to the previous stage of the supervised ML process. There has been research on medical diagnosis of breast cancer with WBCD using Artificial Neural Networks (ANNs) in literature, and most has reported high classification accuracy.

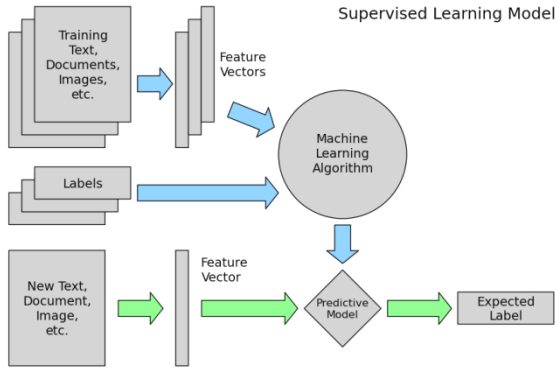


Fig. 1. Supervised learning model

The support vector machine (SVM) algorithm [8] is a classification algorithm that provides the best performance in various application domains such as object recognition, speaker identification, face detection and other classifications problems. Two main motivations to use SVMs in the field of computational biology first, many problems have high dimensional as well as noisy data, for which SVM are known to perform well as compared to other statistical or machine learning methods. Second, in contrast to most machine learning methods, kernel methods like the SVM can easily handle non-vector inputs, such as variable length sequences or graphs. These types of data are common in biology applications.

### III. METHODOLOGY

#### A. Support vector machines

The support vector machine is originally a binary classification method developed by Vapnik et.al at Bell laboratories [9]. For a binary problem, we have training data points:  $\{x_i, y_i\}, i = 1 \dots l, y_i \in \{-1, 1\}, x_i \in \mathbb{R}^d$ . Suppose we have some hyperplane that separates or classify the positive label from the negative labels with a separating hyperplane. The points  $x$  which is on the hyperplane satisfy  $w \cdot x + b = 0$ , where  $w$  is normal to the hyperplane,  $|b|/\|w\|$  is the perpendicular distance from the hyperplane to the origin, and  $\|w\|$  is the Euclidean norm of  $w$ . Let  $d_+$   $d_-$  be the shortest distance from the separating hyperplane to the closest positive or negative points. Define the margin of a separating hyperplane to be  $d_+ + d_-$ . For the linearly separable classes, the support vector algorithm simply looks for the separating hyperplane with the biggest margin. This can be mathematically stated as follows: assume that all the training data satisfy the following constraints:

$$x_i \cdot w + b \geq +1 \text{ for } y_i = +1, \quad (1)$$

$$x_i \cdot w + b \leq -1 \text{ for } y_i = -1, \quad (2)$$

Combining (1) and (2) into one set of inequalities results:

$$y_i(x_i \cdot w + b) - 1 \geq 0 \quad \forall i \quad (3)$$

TABLE I. CONTRIBUTION IN MACHINE LEARNING

Researcher (Years)	Accuracy	Method
Quinlan (1996)	94.74%	C4.5 decision tree method
Hamiton, Shan, and Cercone (1996)	94.99%	RIAC method
Ster and Dobnikar (1996)	96.8%	linear discreet analysis method
Nauck and Kruse (1999)	95.06%	neuron-fuzzy techniques
Pena-Reyes and Sipper (1999)	97.36%	fuzzy-GA method
In Setiono (2000)	98.10%	Feed forward neural network rule extraction algorithm.
Albrecht, Lappas, Vinterbo, Wong, and Ohno-Machado (2002)	98.8%	Logarithmic simulated annealing with the perceptron algorithm
Abonyi and Szeifert (2003)	95.57%	supervised fuzzy clustering technique

Now considering the equality in equation (1) holds that require that there exist a point which is equivalent to choosing a value for  $w$  and  $b$ . These points are on the hyperplane  $H_1: x_i \cdot w + b = 1$  with normal  $w$  and perpendicular distance from the origin  $|1 - b|/\|w\|$ . Similarly the points for the equality in equation (2) holds to lie on the hyperplane  $H_2: x_i \cdot w + b = -1$ , with normal again  $w$  and perpendicular distance from the origin  $|-1 - b|/\|w\|$ . Hence  $d_+ = d_- = 1/\|w\|$  and the margin  $2/\|w\|$

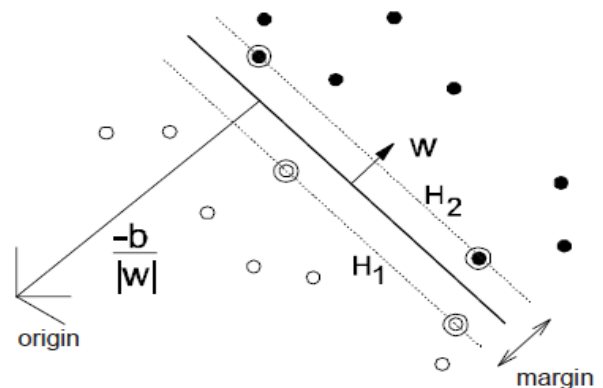


Fig. 2. Linear separating hyperplanes for the separable case. The support vectors are circled.

From Fig 2 it has observed that  $H_1$  and  $H_2$  are parallel they have the same normal vector and that no training points fall between  $H_1$  and  $H_2$ . So we can find the pair of hyperplanes which maximize the margin by minimizing  $\|w\|^2$ , subject to constraints defined in equation (3). Thus to find the solution for a typical two dimensional case to have the form shown on Fig.2. We have to introduce non-negative Lagrange multipliers  $\alpha_i$ , where  $i = 1, \dots, l$  for each one of the inequality

constraints in equation (3). As defined above the rule is that for constraints of the form  $c_i \geq 0$ , the constraint equations are multiply by the non-negative Lagrange multipliers and get subtracted by the objective function, to form the Lagrangian. For equality constraints, the Lagrange multipliers are unconstrained [12]. This gives Lagrangian:

$$L_p \equiv \frac{1}{2} \|w\|^2 - \sum_{i=1}^l \alpha_i y_i (x_i \cdot w + b) + \sum_{i=1}^l \alpha_i, \quad (4)$$

We must now minimize  $L_p$  with respect to  $w$  and  $b$ , and maximize with respect to all  $\alpha_i$  simultaneously, all are subject to the constraints  $\alpha_i \geq 0$  as set of constraints named C1. We get a convex quadratic programming problem, as the objective function is also convex, and that points which are satisfying the constraints also generate a convex set. This concludes that we can also solve the following dual problem to maximize  $L_p$ , subject to the constraints that the gradient of  $L_p$  with respect to  $w$  and  $b$  vanish, and subject to the constraints that the  $\alpha_i \geq 0$  as a set of constraints named C2. This particular dual formulation of the problem is called the Wolfe dual [10]. It has the property that the maximize  $L_p$ , subject to constraints C2, occurs for the same values of the  $w$ ,  $b$  and  $\alpha$ , as the minimize  $L_p$ , subject to constraints C1. Requiring that the gradient of  $L_p$  with respect to  $w$  and  $b$  vanish gives the conditions:

$$\begin{aligned} w &= \sum_i \alpha_i y_i x_i, & (5) \\ \sum_i \alpha_i y_i &= 0. & (6) \end{aligned}$$

As these are the equality constraints in the dual formulation, we can substitute them into equation (4) to give

$$L_D \equiv \sum_i \alpha_i - \frac{1}{2} \sum_{i,j} \alpha_i \alpha_j \cdot y_i y_j x_i \cdot x_j \quad (7)$$

Now we have provided the Lagrangian with different labels P for primal and D for dual to emphasize that the two formulations are different:  $L_p$  and  $L_D$  generated from the same objective function but with different constraints, and the solution is obtained by minimizing  $L_p$  or by maximizing  $L_D$  respectively. Also note that if we formulate the problem with  $b = 0$ , which constitute that all hyperplanes passes through the origin, the constraint defined in equation 6 does not needed. This is a soft restriction for high dimensional spaces, and therefore it amounts to reduce the number of degrees of freedom by one.

Support vector training (linearly separable) therefore amounts to maximizing  $L_D$  with respect to the  $\alpha_i$ , subject to the constraints defined in equation (6) and positivity to the  $\alpha_i$ , with solution given by given in equation (5). Now we have Lagrange multiplier  $\alpha_i$  for the every training point. Those points from solution set where  $\alpha_i > 0$  are known as support vectors and therefore lying on any of the hyperplanes H1, H2. All other training points have  $\alpha_i = 0$  and lie either on H1 or H2 as earlier defined in the equality in equation (3) holds, or on other side of H1 or H2 such that it is defined inequality in equation (3) holds.

For these kind models the support vectors are major component of the training set. They are located nearest to the decision boundary, if we remove all the remaining training points or moved them around subjected to a condition that

they do not cross H1 or H2, and training has repeated and consequently the same hyperplane is generated then the above algorithm for linearly separable data when applied for the non-separable data does not guarantee a feasible solution.

This will justify that using the objective function as dual Lagrangian that grows arbitrarily large. How we classify the non-separable data. To achieve this first we have to relax the constrained defined in equation (1) and equation (2) and for this we have to introduce positive slack variables  $e_i$ ;  $i = 1, \dots, l$ , in the constraints, which then become:

$$x_i \cdot w + b \geq +1 - e_i \text{ for } y_i = +1, \quad (8)$$

$$x_i \cdot w + b \leq -1 + e_i \text{ for } y_i = -1, \quad (9)$$

$$e_i \geq 0 \forall i \quad (10)$$

If an error is occur then the corresponding  $e_i$  must exceed unity, so  $\sum_i e_i$  is an upper bound on the number of training errors. So to assign an extra cost for the errors is to change the objective function, it should be minimized from  $\|w\|^2/2$  to  $\|w\|^2/2 + C(\sum_i e_i)$ , where  $C$  is a parameter that has decided by the user for the large value of  $C$  correspond to high rate to errors. We have to generalized the above method to the case where  $\text{sign}(f(x))$  represents the class ( $f(x)$  is a decision function) assigned to data point  $x$  is not a linear function of the data. The only approach is that we need to assure that the data appears in the training problem, is in the form of dot products of  $x_i \cdot x_j$ . Now we first mapped the data to some other dimension such as Euclidean space  $H$ , using a mapping here we call as  $\Phi$ :

$$\Phi: R^d \rightarrow H, \quad (11)$$

Then consequently the training algorithm would only depend on the data through dot products in  $H$ , i.e. on functions of the form  $\Phi(x_i) \cdot \Phi(x_j)$ . Now introducing the concept of the kernel function  $K$  such that  $K(x_i, x_j) = \Phi(x_i) \cdot \Phi(x_j)$ , then only  $K$  is used in the training algorithm and we are not considering the value what  $\Phi$  is. The kernel function has to satisfy Mercer's condition. One example for this function is Gaussian:

$$K(x_i, x_j) = \exp\left(-\frac{\|x_i - x_j\|^2}{2\sigma^2}\right), \quad (12)$$

In this particular example,  $H$  is infinite dimensional (Euclidean space), so it is not easy to work with  $\Phi$  explicitly. However, if one replaces  $x_i \cdot x_j$  by  $K(x_i, x_j)$  everywhere in the training algorithm, the algorithm will generate a support vector machine which lives in an infinite dimension space.

Now considering all of the previous section, since we are doing a linear separation, but in a different plane. To implement this model we need  $w$ , and that reside in  $H$  and in test phase an SVM is used by computing dot products of a given test point  $x$  with  $w$ , or more specifically by computing the sign of equation as stated below

$$f(x) \equiv \sum_{i=1}^{N_s} \alpha_i y_i \Phi(s_i) \cdot \Phi(x) + b = \sum_{i=1}^{N_s} \alpha_i y_i K(s_i, x) + b, \quad (13)$$

Where  $s_i$  are the support vectors and we can avoid computing  $\Phi(x)$  by the use of  $K(s_i, x) = \Phi(s_i) \cdot \Phi(x)$ .

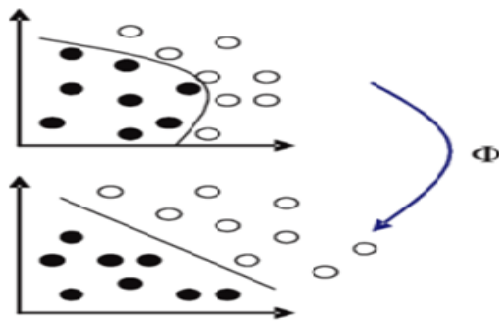


Fig. 3. General principle of SVM: projection of data in an optimal dimensional space.

#### IV. EXPERIMENTAL SETUP

##### A. Breast Cancer Dataset

In this study, the Wisconsin Breast Cancer Database an UCI Machine Learning Repository was analysed. The WBCD dataset consists of 699 instances taken from Fine Needle Aspirates (FNA) of human breast tissue. Each record in the database has nine attribute.

TABLE II. ATTRIBUTES OF THE SIMPLE DATASET

Attribute	Domain
1. Sample code number	id number
2. Clump Thickness	1 – 10
3. Uniformity of Cell Size	1 – 10
4. Uniformity of Cell Shape	1 – 10
5. Marginal Adhesion	1 – 10
6. Single Epithelial Cell Size	1 – 10
7. Bare Nuclei	1 – 10
8. Bland Chromatin	1 – 10
9. Normal Nucleoli	1 – 10
10. Mitoses	1 – 10
11. Class:	2 - benign, 4- malignant

Attributes 2 through 10 have been used to represent instance. The nine attributes are detailed in Table 2. The measurements are assigned an integer value between 1 and 10, with 1 being the closest to benign and 10 to malignant. Associated with each sample is its class label, which is either benign or malignant. This dataset contains 16 instances with missing attribute values. Since many classification algorithms have discarded these data samples, for the ease of comparison, the same method is followed and the remaining 683 samples are taken for use. Therefore, the class has a distribution of 444 (65.0%) benign samples and 239 (35.0%) malignant samples.

##### B. Experimental Setup

The original data is present in the form of analogue values with values ranging from 0-10 [13]. The data are converted to their equivalent integer form. Scaling is required to map the dataset into desired range of variable ranging between minimum and maximum range of network input. Based on total number of attribute (assume N). N-1 will be numeric

feature and 1 is class category. The numerical attributes are ranging in between 0 and 1 the new value obtained are converted into binary form by the following scaling grouping is done on the basis of range  $[0, x) = '0'$  and  $[x, 10] = '1'$

These attributes are fed into the variable feature selection for training and testing to obtain the result for 10 and 5 cross fold validation to compute the performance of the support vector machine classifier. We have simulated the result using the kernel function as the radial basis function (rbf kernel).

TABLE III. PERFORMANCE FOR THE SVM CLASSIFIER USING VARIABLE FEATURE SELECTION WITH 10 AND 5 CROSS VALIDATION

Attribute	Sensitivity	Specificity	ErrorRate	AUC
[2,3]	0.945945	0.945606	0.054172	0.956400
[2,3,4]	0.959459	0.949791	0.043924	0.988900
[2,3,4,5]	0.952703	0.966527	0.042460	0.955500
[2,3,4,5,6]	0.950451	0.966527	0.043924	0.955600
[2,3,4,5,6,7]	0.954954	0.987447	0.033675	0.988600
[2,3,4,5,6,7,8]	0.941441	0.987948	0.042460	0.955600
[2,3,4,5,6,7,8,9]	0.936937	0.991631	0.043400	0.966700
[2,3,4,5,6,7,8,9,10]	0.930180	0.987447	0.049700	0.945833
<b>10 cross validation</b>				
Attribute	Sensitivity	Specificity	ErrorRate	AUC
[2,3]	0.959641	0.941176	0.046783	0.966700
[2,3,4]	0.954954	0.932773	0.052780	0.977300
[2,3,4,5]	0.954751	0.983193	0.035294	0.965900
[2,3,4,5,6]	0.936937	0.983333	0.046780	0.977800
[2,3,4,5,6,7]	0.959641	0.991667	0.029155	0.988900
[2,3,4,5,6,7,8]	0.932126	0.975000	0.052786	0.955600
[2,3,4,5,6,7,8,9]	0.940909	1.000000	0.038340	0.965900
[2,3,4,5,6,7,8,9,10]	0.919280	1.000000	0.052631	0.977800
<b>5 cross validation</b>				

##### C. Result

The result obtained using the support vector machine classifier by selecting variable attribute selection. As shown in table 3 the classifier gives the best sensitivity with 0.9886 0.9889 with attribute A [2, 3, 4, 5, 6, 7] are selected for training and testing the machine for each 10 and 5 cross validation respectively. The best specificity is achieved when attribute A [2, 3, 4, 5, 6, 7, 8, 9] are selected for training and testing with 0.99163 and 1.00 respectively. The lowest error rate and the best AUC are obtained with A [2, 3, 4, 5, 6, 7]. The accuracy is the proportion of the total number of predictions that were correct. The best accuracy is evaluated when we considered the attribute A [2, 3, 4, 5, 6, 7] is 96.4%

and for the remaining selection of attributes the accuracy lies between in a range of 95.09 to 95.7.

## V. CONCLUSION

This paper describes the potency of SVMs in the field of computational biology for which SVM are known to perform well as compared to other statistical or machine learning methods. After a better understating of the strengths of each method it has been observed that the results are generated on the basis of AUC, sensitivity and specificity. The accuracy of support vector machine is far better as compared with other machine learning classifier. The result may be much better for the larger set of real data.

## REFERENCES

- [1] T. S. Subashini, Vennila Ramalingam, S. Palanivel Breast mass classification based on cytological patterns using RBFNN and SVM Expert Syst. Appl. 36(3): 5284-5290 (2009).
- [2] Ioanna Christoyianni, Evangelos Dermatas, George K. Kokkinakis Automatic detection of abnormal tissue in mammography ICIP (2) 2001: 877-880
- [3] P.S. Rodrigues, R. Chang, and J.S. Suri, "Non-Extensive Entropy for CAD Systems of Breast Cancer Images", in Proc. SIBGRAPI, 2006, pp.121-128.
- [4] American Cancer Society Homepage, <http://www.cancer.org/> 2008
- [5] Zhang Z, Schwartz S, Wagner L, Miller W. A greedy algorithm for aligning DNA sequences J Comput Biol. 2000 Feb-Apr;7(1-2):203-14.
- [6] Lei Yu, Huan Liu Efficient Feature Selection via Analysis of Relevance and Redundancy The Journal of Machine Learning Research Volume 5, 12/1/2004 Pages 1205-1224
- [7] AstroML: Machine Learning and Data Mining for Astronomy <http://www.astroml.org/>
- [8] Boser, B. E., Guyon, I. M., and Vapnik, V. A training algorithm for optimum margin classifiers. In Fifth Annual Workshop on Computational Learning Theory, Pittsburgh. ACM. 1992
- [9] V. Vapnik. The nature of statistical learning Theory, 2nd Ed. Springer, NewYork, 1999.][C. J. C. Burges. A tutorial on support vector machines for pattern recognition. Data Min. Knowledge Disc. 2 (1998) 121.
- [10] R. Fletcher. Practical methods of optimization. 2nd Ed. Wiley & Sons. Chichester (1987)
- [11] Marcano-Cedeño J, Quintanilla-Domínguez, D. Andina WBCD breast cancer database classification applying artificial metaplasticity neural network Expert Systems with Applications 38 (2011) 9573–9579
- [12] Gjorgji Madzarov, Dejan Gjorgjevikj and Ivan Chorbev A Multi-class SVM Classifier Utilizing Binary Decision Tree. Informatica 33 (2009) 233-241 233
- [13] Sandeep Chaurasia, Prasun Chakrabarti, Neha Chourasia An Application of Classification Techniques on Breast Cancer Prognosis"International Journal of Computer Applications (0975 – 8887) Volume 59– No.3, page 6-10, December 2012.

# A Discrete Mechanics Approach to Gait Generation on Periodically Unlevel Grounds for the Compass-type Biped Robot

Tatsuya Kai

Department of Applied Electronics  
Faculty of Industrial Science and Technology  
Tokyo University of Science

6-3-1 Niijuku, Katsushika-ku, Tokyo 125-8585 JAPAN  
Email: kai@rs.tus.ac.jp

Takeshi Shintani

Kyocera Corporation

6 Takeda Tobadono-cho, Fushimi-ku, Kyoto 612-8501, JAPAN

**Abstract**—This paper addresses a gait generation problem for the compass-type biped robot on periodically unlevel grounds. We first derive the continuous/discrete compass-type biped robots (CCBR/DCBR) via continuous/discrete mechanics, respectively. Next, we formulate a optimal gait generation problem on periodically unlevel grounds for the DCBR as a finite dimensional nonlinear optimization problem, and show that a discrete control input can be obtained by solving the optimization problem with the sequential quadratic programming. Then, we develop a transformation method from a discrete control input into a continuous zero-order hold input based on the discrete Lagrange-d’Alembert principle. Finally, we show numerical simulations, and it turns out that our new method can generate a stable gaits on a periodically unlevel ground for the CCBR.

## I. INTRODUCTION

Numerous work on humanoid robots have been done via various approaches in the fields of robotics and control theory until now. For instance, there are the following approaches: theoretical analysis of passive walking [1], [2], [3], [4], researches associated with nonlinear dynamical theory such as Poincaré sections and limit cycles [5], [6], [7], [8], [9], [10], [11], gait pattern generation based on CPG (central pattern generation) and ZMP (zero-moment point) [12], [13], [14], [15], and self-motivating acquirement of gaits by learning theory and evolutionary computing [16], [17], [18], [19]. Especially, as one of the simplest models of humanoid robots, the compass-type biped robot has been mainly studied by a lot of researchers. In general, it is quite difficult to realize stable gaits for humanoid robots in terms of nonlinear control problems, and hence there are still a lot of problems left to solve.

In almost every work on humanoid robots, models derived by normal continuous-time mechanics are used. On the other hand, *discrete mechanics*, which is a new discretizing tool for nonlinear mechanical systems and is derived by discretization of basic principles and equations of classical mechanics, has been focused on [20], [21], [22], [23], [24], [25]. a discrete model (the discrete Euler-Lagrange equations) in discrete mechanics has some interesting characteristics; (i) less numerical error in comparison with other numerical solutions such as Euler method and Runge-Kutta method, (ii) it can describe energies for both conservative and dissipative systems with less

errors, (iii) some laws of physics such as Noether’s theorem are satisfied. (iv) simulations can be performed for large sampling times. Hence, discrete mechanics has a possibility of analysis and controller synthesis with high compatibility with computers.

We have focused on discrete mechanics and considered its applications to control theory. In [26], [27], [28], we applied discrete mechanics to control problems for the cart-pendulum system, and confirmed the application potentiality to control theory. Moreover, in [29], [30], [31], [32], we have considered a gait generation problem for the compass-type biped robot and confirmed that the proposed method can generate stable gaits on flats and slopes. However, the method cannot be applied to gait generation problems on more complex grounds.

Therefore, this paper aims at gait generation for the compass-type biped robot on periodically unlevel grounds which are more complex than flats and slopes from the standpoint of discrete mechanics. This paper is organized as follows. In Section II, a brief summary on discrete mechanics is presented. Next, in section III, we derive the continuous and discrete compass-type biped robots by using continuous and discrete mechanics, respectively. In Section IV, we then formulate a gait generation problem for the discrete compass-type biped robot and propose a solving method of it by the sequential quadratic programming to calculate a discrete control input. In addition, we also introduce a transformation method from a discrete control input into a continuous zero-order hold input based on discrete Lagrange-d’Alembert principle. Finally, we show some numerical simulations on gait generation on a periodically unlevel ground for the continuous compass-type biped robot in order to confirm the effectiveness of our method in Section V.

## II. DISCRETE MECHANICS

In this section, some basic concepts in discrete mechanics are summarized. See [20], [21], [22], [23] for more details on discrete mechanics.

Let  $Q$  be an  $n$ -dimensional configuration manifold and  $q \in \mathbf{R}^n$  be a generalized coordinate of  $Q$ . We also refer to  $T_q Q$  as the tangent space of  $Q$  at a point  $q \in Q$  and  $\dot{q} \in T_q Q$  denotes

a generalized velocity. Moreover, we consider a time-invariant Lagrangian as  $L^c(q, \dot{q}) : TQ \rightarrow \mathbf{R}$ . We first explain about the discretization method. The time variable  $t \in \mathbf{R}$  is discretized as  $t = kh$  ( $k = 0, 1, 2, \dots$ ) by using a sampling interval  $h > 0$ . We denote  $q_k$  as a point of  $Q$  at the time step  $k$ , that is, a curve on  $Q$  in the continuous setting is represented as a sequence of points  $q^d := \{q_k\}_{k=1}^N$  in the discrete setting. The transformation method of discrete mechanics is carried out by the replacement:

$$q \approx (1 - \alpha)q_k + \alpha q_{k+1}, \quad \dot{q} \approx \frac{q_{k+1} - q_k}{h}, \quad (1)$$

where  $q$  is expressed as a internally dividing point of  $q_k$  and  $q_{k+1}$  with an internal division ratio  $\alpha$  ( $0 < \alpha < 1$ ) We then define a *discrete Lagrangian*:

$$L_\alpha^d(q_k, q_{k+1}) := hL \left( (1 - \alpha)q_k + \alpha q_{k+1}, \frac{q_{k+1} - q_k}{h} \right), \quad (2)$$

and a *discrete action sum*:

$$S_\alpha^d(q_0, q_1, \dots, q_N) = \sum_{k=0}^{N-1} L_\alpha^d(q_k, q_{k+1}). \quad (3)$$

We next summarize the discrete equations of motion. Consider a variation of points on  $Q$  as  $\delta q_k \in T_{q_k}Q$  ( $k = 0, 1, \dots, N$ ) with the fixed condition  $\delta q_0 = \delta q_N = 0$ . In analogy with the continuous setting, we define a variation of the discrete action sum (3) as

$$\delta S_\alpha^d(q_0, q_1, \dots, q_N) = \sum_{k=0}^{N-1} \delta L_\alpha^d(q_k, q_{k+1}) \quad (4)$$

as shown in Fig. 1. The discrete Hamilton's principle states that *only a motion which makes the discrete action sum (3) stationary is realized*. Calculating (4), we have

$$\delta S_\alpha^d = \sum_{k=1}^{N-1} \{D_1 L_\alpha^d(q_k, q_{k+1}) \delta q_k + D_2 L_\alpha^d(q_{k-1}, q_k)\} \delta q_k, \quad (5)$$

where  $D_1$  and  $D_2$  denotes the partial differential operators with respect to the first and second arguments, respectively. Consequently, from the discrete Hamilton's principle and (5), we obtain *the discrete Euler-Lagrange equations*:

$$D_1 L_\alpha^d(q_k, q_{k+1}) + D_2 L_\alpha^d(q_{k-1}, q_k) = 0, \quad k = 1, \dots, N-1 \quad (6)$$

with the initial and terminal equations:

$$D_2 L^c(q_0, \dot{q}_0) + D_1 L_\alpha^d(q_0, q_1) = 0 \\ - D_2 L^c(q_N, \dot{q}_N) + D_2 L_\alpha^d(q_{N-1}, q_N) = 0. \quad (7)$$

It turns out that (6) is represented as difference equations which contains three points  $q_{k-1}, q_k, q_{k+1}$ , and we need  $q_0, q_1$  as initial conditions when we simulate (6).

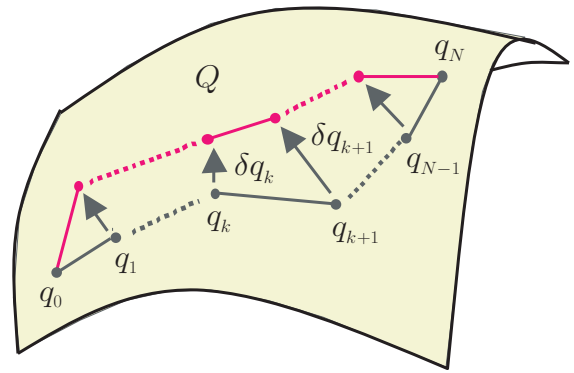


Figure 1 : Discrete Hamilton's principle

Then, we consider a method to add external forces to the discrete Euler-Lagrange equations. By an analogy of continuous mechanics, we denote discrete external forces by  $F_\alpha^d : Q \times Q \rightarrow T^*(Q \times Q)$ , and discretize continuous Lagrange-d'Alembert's principle as

$$\delta \sum_{k=0}^{N-1} L_\alpha^d(q_k, q_{k+1}) + \sum_{k=0}^{N-1} F_\alpha^d(q_k, q_{k+1}) \cdot (\delta q_k, \delta q_{k+1}) = 0, \quad (8)$$

where we define *right/left discrete external forces*:  $F_\alpha^{d+}, F_\alpha^{d-} : Q \times Q \rightarrow T^*Q$  as

$$F_\alpha^{d+}(q_k, q_{k+1}) \delta q_k = F_\alpha^d(q_k, q_{k+1}) \cdot (\delta q_k, 0), \quad (9) \\ F_\alpha^{d-}(q_k, q_{k+1}) \delta q_{k+1} = F_\alpha^d(q_k, q_{k+1}) \cdot (0, \delta q_{k+1}),$$

respectively. By right/left discrete external forces, a continuous external force  $F^c : TQ \rightarrow T^*Q$  can be discretized as

$$F_\alpha^{d+}(q_k, q_{k+1}) = (1 - \alpha)hF^c \left( (1 - \alpha)q_k + \alpha q_{k+1}, \frac{q_{k+1} - q_k}{h} \right), \\ F_\alpha^{d-}(q_k, q_{k+1}) = \alpha hF^c \left( (1 - \alpha)q_k + \alpha q_{k+1}, \frac{q_{k+1} - q_k}{h} \right). \quad (10)$$

Therefore, by calculating variations for (8), we obtain *the discrete Euler-Lagrange equations with discrete external forces*:

$$D_1 L^d(q_k, q_{k+1}) + D_2 L^d(q_{k-1}, q_k) \\ + F_\alpha^{d+}(q_k, q_{k+1}) + F_\alpha^{d-}(q_{k-1}, q_k) = 0, \quad k = 1, \dots, N-1, \quad (11)$$

with the initial and terminal equations:

$$D_2 L^c(q_0, \dot{q}_0) + D_1 L_\alpha^d(q_0, q_1) + F_\alpha^{d+}(q_0, q_1) = 0 \\ - D_2 L^c(q_N, \dot{q}_N) + D_2 L_\alpha^d(q_{N-1}, q_N) + F_\alpha^{d-}(q_{N-1}, q_N) = 0. \quad (12)$$

### III. CONTINUOUS AND DISCRETE COMPASS-TYPE BIPED ROBOTS

#### A. Setting of compass-type biped robot

In this subsection, we first give a problem setting of the compass-type biped robot. In this paper, we consider a simple compass-type biped robot which consists of two rigid bars (Leg 1 and 2) and a joint without rotational friction (Waist) as shown in Fig. 2. In Fig. 2, Leg 1 is called *the supporting leg* which connects to ground and Leg 2 is called *the swing leg* which is

ungrounded. Moreover, for the sake of simplicity, we give the following assumptions; (i) the supporting leg does not slip at the contact point with the ground, (ii) the swing leg hits the ground with completely inelastic collision, (iii) the compass-type biped robot is supported by two legs for just a moment, (iv) the length of the swing leg gets smaller by infinitely small when the swing leg and the supporting leg pass each other.

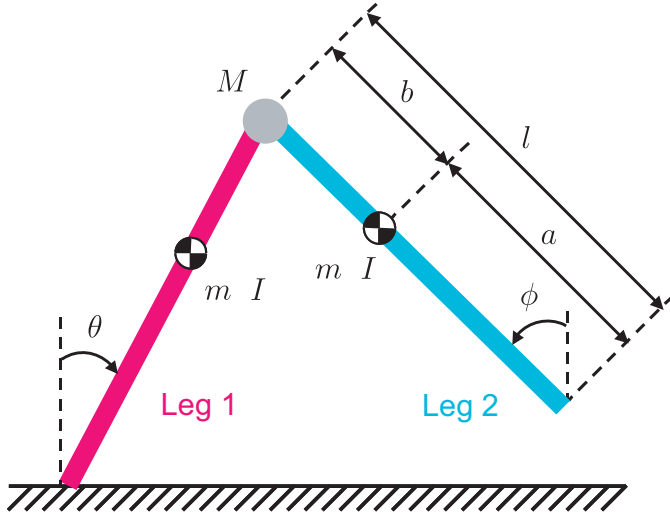


Figure 2 : Compass-type biped robot

Let  $\theta$  and  $\phi$  be the angles of Leg 1 and 2, respectively. We also use the notations:  $m$ : the mass of the legs,  $M$ : the mass of the waist,  $I$ : the inertia moment of the legs,  $a$ : the length between the waist and the center of gravity,  $b$ : the length between the center of gravity and the toe of the leg,  $l (= a + b)$ : the length between the waist and the toe of the leg.

In the walking process of the compass-type biped robot, there exist two modes: *the swing phase* and *the impact phase*. In the swing phase the swing leg is ungrounded, and in the impact phase the toe of the swing leg hit the ground. As shown in Fig. 3, it is noted that the swing phase and the impact phase occur alternately and the swing leg and the supporting leg switch positions with each other with respect to each collision. We denote the order of the swing phase and the impact phase by  $i = 1, 2, \dots, L$  and  $i = 1, 2, \dots, L - 1$ , respectively. In addition, we assume that Leg 1 is the swing leg and Leg 2 is the supporting leg in odd-numbered swing phases, and Leg 1 is the supporting leg and Leg 2 is the swing leg in even-numbered swing phases.

### B. Continuous compass-type biped robot (CCBR)

In this subsection, we derive a model of *continuous compass-type biped robot (CCBR)* via usual continuous mechanics. We denote the angles of Leg 1 and 2 in the  $i$ -th swing phase by  $\theta^{(i)}$ ,  $\phi^{(i)}$ , respectively. In addition,  $\dot{\theta}^{(i)}$ ,  $\dot{\phi}^{(i)}$  denote their angular velocities.

First, we consider a model of the CCBR in the  $i$ -th swing phase where Leg 1 is the supporting leg and Leg 2 is the swing leg. We assume that the torque at the waist can be controlled, and denote it by  $v^{(i)} \in \mathbf{R}$ . The Lagrangian of this system  $L^c$  is given by (13). Substituting the Lagrangian (13) into the Euler-Lagrange equations and adding the control

input to the right-hand sides of them, we have the model of the CCBR in the  $i$ -th swing phase as (14), (15). We then derive a model of the CCBR in the  $i$ -th impact phase. It is assumed that the swing leg hits the ground with completely inelastic collision, and  $\theta^{(i)} = \theta^{(i+1)}$ ,  $\phi^{(i)} = \phi^{(i+1)}$  holds because of an instantaneous impact. Hence, calculating the principle of conservation of angular momentum for the CCBR, we obtain the model of the CCBR in the  $i$ -th impact phase as (16), where  $a^-, a^+ \in \mathbf{R}^{2 \times 2}$  are the coefficient matrices defined by (17) and (18).

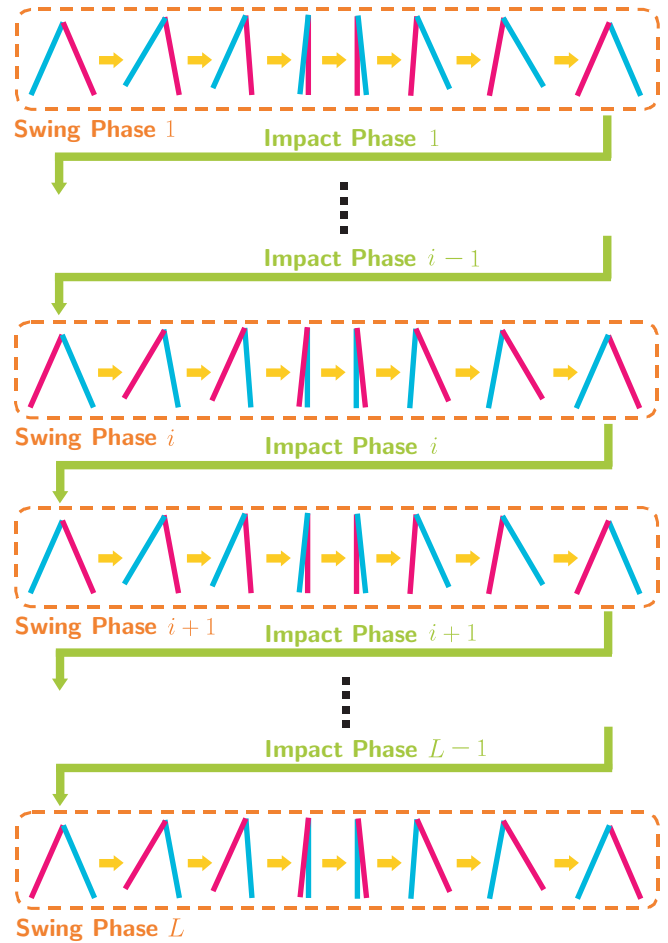


Figure 3 : Gait of compass-type biped robot

### C. Discrete compass-type biped robot (DCBR)

Next, we derive a model of *discrete compass-type biped robot (DCBR)* by discrete mechanics in this subsection. We here use the notations;  $h$ : the sampling time,  $k = 1, 2, \dots, N$ : the time step,  $i = 1, \dots, L$ : the order of the swing phases,  $\alpha = 1/2$ : the internal division ratio in discrete mechanics,  $\theta_k^{(i)}$ ,  $\phi_k^{(i)}$ : the angles of Leg 1 and 2 at the  $k$ -th step in the  $i$ -th swing phase.

In this paper, we use only the model of the DCBR in the swing phases, and hence we will derive it. By using the transformation law from a continuous Lagrangian into a discrete Lagrangian (2), we obtain the discrete Lagrangian as (19) from (13). Since the left and right discrete external forces (9) satisfy  $F^{d+}(q_k, q_{k+1}) = F^{d-}(q_k, q_{k+1})$  for  $\alpha = 1/2$ , we

$$L^c(\theta^{(i)}, \dot{\theta}^{(i)}, \phi^{(i)}, \dot{\phi}^{(i)}) = \frac{1}{2}(I + ma^2 + Ml^2 + ml^2)(\dot{\theta}^{(i)})^2 + \frac{1}{2}(I + mb^2)(\dot{\phi}^{(i)})^2 - mbl \cos(\theta^{(i)} - \phi^{(i)})\dot{\theta}^{(i)}\dot{\phi}^{(i)} - (ma + mg + Ml)g \cos \phi^{(i)} + mgb \cos \phi^{(i)} \quad (13)$$

$$\frac{d}{dt} \left( \frac{\partial L^c(\theta^{(i)}, \dot{\theta}^{(i)}, \phi^{(i)}, \dot{\phi}^{(i)})}{\partial \dot{\theta}^{(i)}} \right) - \frac{\partial L^c(\theta^{(i)}, \dot{\theta}^{(i)}, \phi^{(i)}, \dot{\phi}^{(i)})}{\partial \theta^{(i)}} = v^{(i)} \quad (14)$$

$$\frac{d}{dt} \left( \frac{\partial L^c(\theta^{(i)}, \dot{\theta}^{(i)}, \phi^{(i)}, \dot{\phi}^{(i)})}{\partial \dot{\phi}^{(i)}} \right) - \frac{\partial L^c(\theta^{(i)}, \dot{\theta}^{(i)}, \phi^{(i)}, \dot{\phi}^{(i)})}{\partial \phi^{(i)}} = -v^{(i)} \quad (15)$$

$$a^-(\theta^{(i)}, \phi^{(i)}) \begin{bmatrix} \dot{\theta}^{(i)} \\ \dot{\phi}^{(i)} \end{bmatrix} = a^+(\theta^{(i)}, \phi^{(i)}) \begin{bmatrix} \dot{\theta}^{(i+1)} \\ \dot{\phi}^{(i+1)} \end{bmatrix} \quad (16)$$

$$a^- := \begin{bmatrix} -(2mal + Ml^2) \cos(\theta^{(i)} - \phi^{(i)}) + mbl - I & mab - I \\ mab - I & 0 \end{bmatrix}, \quad (17)$$

$$a^+ := \begin{bmatrix} -mb^2 + mbl \cos(\theta^{(i+1)} - \phi^{(i+1)}) - I & -(2ma^2 + Ml^2) + mbl \cos(\theta^{(i+1)} - \phi^{(i+1)}) - I \\ -mb^2 - I & mbl \cos(\theta^{(i+1)} - \phi^{(i+1)}) \end{bmatrix}. \quad (18)$$

$$L^d(\theta_k^{(i)}, \theta_{k+1}^{(i)}, \phi_k^{(i)}, \phi_{k+1}^{(i)}) = \frac{1}{2}(I + ma^2 + Ml^2 + ml^2) \left( \frac{\theta_{k+1}^{(i)} - \theta_k^{(i)}}{h} \right)^2 + \frac{1}{2}(I + mb^2) \left( \frac{\phi_{k+1}^{(i)} - \phi_k^{(i)}}{h} \right)^2 - mbl \cos \left( \frac{\theta_k^{(i)} + \theta_{k+1}^{(i)}}{2} - \frac{\phi_k^{(i)} + \phi_{k+1}^{(i)}}{2} \right) \frac{\theta_{k+1}^{(i)} - \theta_k^{(i)}}{h} \frac{\phi_{k+1}^{(i)} - \phi_k^{(i)}}{h} - (ma + mg + Ml)g \cos \left( \frac{\phi_k^{(i)} + \phi_{k+1}^{(i)}}{2} \right) + mgb \cos \left( \frac{\phi_k^{(i)} + \phi_{k+1}^{(i)}}{2} \right) \quad (19)$$

$$D_2 L^d(\theta_{k-1}^{(i)}, \theta_k^{(i)}, \phi_{k-1}^{(i)}, \phi_k^{(i)}) - D_1 L^d(\theta_k^{(i)}, \theta_{k+1}^{(i)}, \phi_k^{(i)}, \phi_{k+1}^{(i)}) + u_{k-1}^{(i)} + u_k^{(i)} = 0 \quad (k = 2, \dots, N) \quad (21)$$

$$D_4 L^d(\theta_{k-1}^{(i)}, \theta_k^{(i)}, \phi_{k-1}^{(i)}, \phi_k^{(i)}) - D_3 L^d(\theta_k^{(i)}, \theta_{k+1}^{(i)}, \phi_k^{(i)}, \phi_{k+1}^{(i)}) - u_{k-1}^{(i)} - u_k^{(i)} = 0 \quad (k = 2, \dots, N) \quad (22)$$

$$D_2 L^c(\theta_1^{(i)}, \dot{\theta}_1^{(i)}, \phi_1^{(i)}, \dot{\phi}_1^{(i)}) + D_1 L^d(\theta_1^{(i)}, \theta_2^{(i)}, \phi_1^{(i)}, \phi_2^{(i)}) + u_1^{(i)} = 0 \quad (k = 2, \dots, N) \quad (23)$$

$$D_4 L^c(\theta_1^{(i)}, \dot{\theta}_1^{(i)}, \phi_1^{(i)}, \dot{\phi}_1^{(i)}) + D_3 L^d(\theta_1^{(i)}, \theta_2^{(i)}, \phi_1^{(i)}, \phi_2^{(i)}) - u_1^{(i)} = 0 \quad (k = 2, \dots, N) \quad (24)$$

$$-D_2 L^c(\theta_N^{(i)}, \dot{\theta}_N^{(i)}, \phi_N^{(i)}, \dot{\phi}_N^{(i)}) + D_1 L^d(\theta_{N-1}^{(i)}, \theta_N^{(i)}, \phi_{N-1}^{(i)}, \phi_N^{(i)}) + u_{N-1}^{(i)} = 0 \quad (25)$$

$$-D_4 L^c(\theta_N^{(i)}, \dot{\theta}_N^{(i)}, \phi_N^{(i)}, \dot{\phi}_N^{(i)}) + D_3 L^d(\theta_{N-1}^{(i)}, \theta_N^{(i)}, \phi_{N-1}^{(i)}, \phi_N^{(i)}) - u_{N-1}^{(i)} = 0 \quad (26)$$

$$a^-(\theta_N^{(i)}, \phi_N^{(i)}) \begin{bmatrix} \dot{\theta}_N^{(i)} \\ \dot{\phi}_N^{(i)} \end{bmatrix} = a^+(\theta_N^{(i)}, \phi_N^{(i)}) \begin{bmatrix} \dot{\theta}_1^{(i+1)} \\ \dot{\phi}_1^{(i+1)} \end{bmatrix}, \quad (27)$$

set a discrete control input that consists of only the left discrete external force  $F^{d-}$  as

$$u_k^{(i)} := F^{d-}(q_k, q_{k+1}), \quad k = 1, \dots, N - 1. \quad (20)$$

Then, substituting (19) into the discrete Euler-Lagrange equations (11), (12) and using the discrete control input (20), we have the model of the DCBR in the  $i$ -th swing phase as (21)–(26).

For the impact phases, we use the model of the CCBP (16), and we rewrite it with the terminal variables of the  $i$ -th swing phase  $\theta_N^{(i)}, \phi_N^{(i)}, \dot{\theta}_N^{(i)}, \dot{\phi}_N^{(i)}$  and the initial variables of the  $(i + 1)$ -th swing phase  $\theta_1^{(i+1)}, \phi_1^{(i+1)}, \dot{\theta}_1^{(i+1)}, \dot{\phi}_1^{(i+1)}$  as (27). This representation (27) will be utilized in the next section.

#### IV. GAIT GENERATION METHOD ON PERIODICALLY UNLEVEL GROUNDS

##### A. Setting of periodically unlevel grounds

First, this subsection formulates the problem setting of grounds on which the compass-type biped robot walks. As shown in Fig. 4, set the  $x$  and  $z$  axes to the horizontal and vertical directions, respectively, and  $P_0$  denotes the origin of the  $xz$ -plane. We also set  $L$  points:  $P_1, P_2, \dots, P_L$  in the  $xz$ -plane, and represent  $P_i$  as  $P_i = (r_i, \rho_i)$  by using the polar

coordinate with reference to  $P_{i-1}$  as illustrated in Fig. 5. Note that  $r_i > 0, -\pi/2 < \rho_i < \pi/2$  are assumed. The sequence of points  $P_1, P_2, \dots, P_L$  are reference grounding points for the compass-type biped robot as shown in Fig. 6.

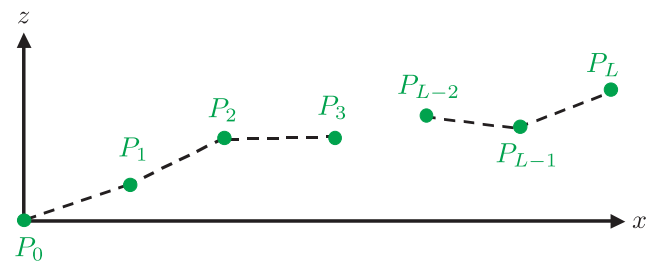


Figure 4 : Reference grounding points in  $xz$ -plane

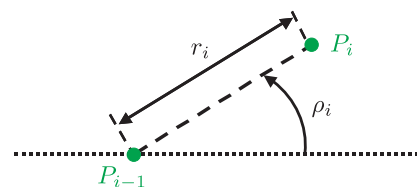


Figure 5 :  $r_i$  and  $\rho_i$

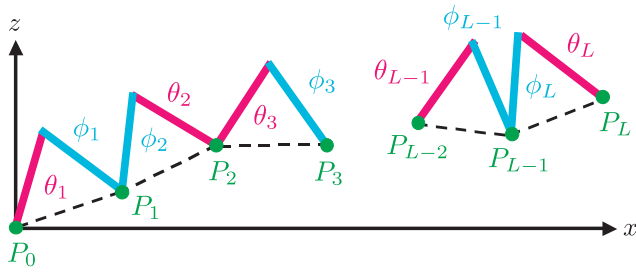


Figure 6 : Desired gait of compass-type biped robot

This problem setting can treat various walking surfaces, for example, flats [30]:  $\rho_i = 0$  ( $i = 1, \dots, L$ ), downward slopes [32]:  $\rho_i = \rho^- < 0$  ( $i = 1, \dots, L$ ), and upward slopes in [32]:  $\rho_i = \rho^+ > 0$  ( $i = 1, \dots, L$ ). In this paper, we consider gait generation on periodically unlevel grounds as depicted in Fig. 7 with the parameter:

$$\rho_i = \begin{cases} \rho, & i = 1, 3, 5, \dots, L-1, \\ -\rho, & i = 2, 4, 6, \dots, L, \end{cases} \quad (28)$$

where  $\rho > 0$  and  $L$  is an odd number. Since a periodically unlevel ground contains both downward and upward slopes, this type of gait generation problems is expected to be more difficult to solve in comparison with the downward and upward slopes cases [32]. Based on the setting above, we consider the following problem on the gait generation for the CCBR.

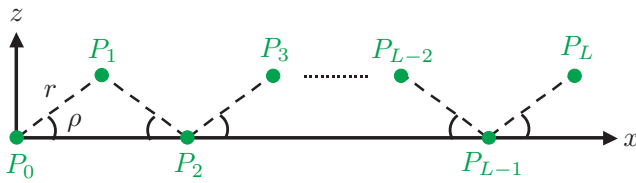


Figure 7 : Setting of Periodically Unlevel Grounds

**Problem 1:** For the continuous compass-type biped robot (CCBR) (14)–(16), find a control input  $v^{(i)}$  ( $i = 1, \dots, L$ ) such that the swing leg of the CCBR lands at the reference grounding points  $P_i$  ( $i = 1, \dots, L$ ) on a periodically unlevel ground of (28) with a stable and natural gait.  $\square$

In order to solve Problem 1 above, we shall consider a method based on discrete mechanics. The method consists of two steps: (i) calculation of a discrete control input by solving a finite dimensional constrained nonlinear optimization problem (Subsection IV-B), (ii) transformation a discrete control input into a zero-order hold input by discrete Lagrange-d'Alembert principle (Subsection IV-C).

### B. Gait generation problem for the DCBR

As the first step, we consider a problem on generation of a discrete gait for the DCBR in stead of the CCBR. The discrete gait generation problem for the DCBR is stated as follows.

**Problem 2:** For the discrete compass-type biped robot (DCBR) (21)–(26), find a sequence of the control input  $u_k^{(i)}$  ( $i = 1, \dots, L$ ,  $k = 1, \dots, N-1$ ) such that the swing leg of the DCBR lands at the reference grounding points  $P_i$  ( $i = 1, \dots, L$ ) with a stable and natural discrete gait.  $\square$

Our main purpose is that we obtain the mathematical formulation of Problem 2 as an optimal control problem. In order to do this, we focus attention on a periodical motions of the DCBR. It must be noted that the DCBR walks on upward and downward slopes alternately, and hence we consider one upward slope and one downward slope as a set (see Fig. 8). If the initial angular velocities of the swing leg at the  $i$ -th and  $(i+2)$ -th swing phases are pretty much the same, a stable gait of the DCBR can be generated as shown in Fig. 8. So, we introduce a cost function of a square of difference between initial angular velocities in the  $i$ -th and  $(i+2)$ -th swing phases:

$$J = (\dot{\phi}_1^{(i+2)} - \dot{\phi}_1^{(i)})^2 + (\dot{\theta}_1^{(i+2)} - \dot{\theta}_1^{(i)})^2. \quad (29)$$

However, the cost function (29) contains the angular velocities in the  $(i+2)$ -th swing phase. To avoid this, we eliminate  $\dot{\phi}_1^{(i+2)}$ ,  $(\dot{\theta}_1^{(i+2)})$  by using the  $(i+1)$ -th impact phase model<sup>1</sup>:

$$\begin{aligned} a_-^{(i+1)}(\phi_N^{(i+1)}, \theta_N^{(i+1)}) \begin{bmatrix} \dot{\phi}_N^{(i+1)} \\ \dot{\theta}_N^{(i+1)} \end{bmatrix} \\ = a_+^{(i+1)}(\phi_N^{(i+1)}, \theta_N^{(i+1)}) \begin{bmatrix} \dot{\phi}_1^{(i+2)} \\ \dot{\theta}_1^{(i+2)} \end{bmatrix}. \end{aligned} \quad (30)$$

Solving (30) for  $\dot{\phi}_1^{(i+2)}$  and  $\dot{\theta}_1^{(i+2)}$ , and substituting this into the cost function (29), we have

$$J = (a_{11}^{(i+1)} \dot{\phi}_N^{(i+1)} + a_{12}^{(i+1)} \dot{\theta}_N^{(i+1)} - \dot{\phi}_1^{(i)})^2 + (a_{21}^{(i+1)} \dot{\phi}_N^{(i+1)} + a_{22}^{(i+1)} \dot{\theta}_N^{(i+1)} - \dot{\theta}_1^{(i)})^2 \quad (31)$$

where

$$(a_+^{(i+1)})^{-1} a_-^{(i+1)} =: \begin{bmatrix} a_{11}^{(i+1)} & a_{12}^{(i+1)} \\ a_{21}^{(i+1)} & a_{22}^{(i+1)} \end{bmatrix}.$$

We can see that the new cost function (31) does not contain  $\dot{\phi}_1^{(i+2)}$ ,  $\dot{\theta}_1^{(i+2)}$  and is represented by only variables in the  $i$ -th and  $(i+1)$ -th swing phases. Consequently, Problem 2 can be formulated as (32)–(48). In the optimization control problem (32)–(48), (32) is the cost function to be minimized, (33)–(38) are the  $i$ -th swing phase model, (39)–(44) are the  $(i+1)$ -th swing phase model, and (46) is the  $i$ -th impact phase model. Moreover, (46) and (47) indicates constraints that prevent a reverse behavior of the swing leg and realize a natural gait. (48) are given data on initial and desired angles of Leg 1 and 2, which can be obtained from data of the reference grounding points  $P_i$  ( $i = 1, \dots, N$ ),

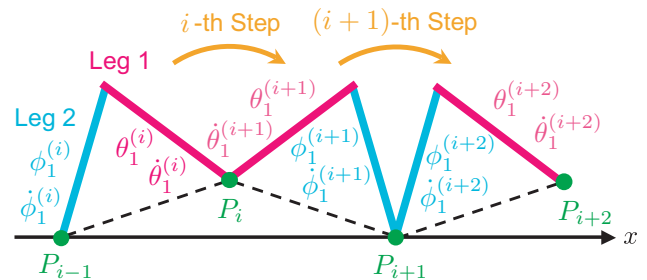


Figure 8 : A gait on a periodically unlevel ground.

<sup>1</sup>Since Leg 1 is the swing leg and Leg 2 is the supporting one in the  $(i+1)$ -th swing phase, the  $(i+1)$ -th impact model can be obtained by exchanging  $\theta$  for  $\phi$  in (27).

$$\begin{aligned} \min \quad & J = (a_{11}^{(i+1)} \dot{\phi}_N^{(i+1)} + a_{12}^{(i+1)} \dot{\theta}_N^{(i+1)} - \dot{\phi}_1^{(i)})^2 + (a_{21}^{(i+1)} \dot{\phi}_N^{(i+1)} + a_{22}^{(i+1)} \dot{\theta}_N^{(i+1)} - \dot{\theta}_1^{(i)})^2 \quad (32) \\ \text{s.t.} \quad & D_2 L^d(\theta_{k-1}^{(i)}, \theta_k^{(i)}, \phi_{k-1}^{(i)}, \phi_k^{(i)}) - D_1 L^d(\theta_k^{(i)}, \theta_{k+1}^{(i)}, \phi_k^{(i)}, \phi_{k+1}^{(i)}) + u_{k-1}^{(i)} + u_k^{(i)} = 0 \quad (k = 2, \dots, N) \quad (33) \\ & D_4 L^d(\theta_{k-1}^{(i)}, \theta_k^{(i)}, \phi_{k-1}^{(i)}, \phi_k^{(i)}) - D_3 L^d(\theta_k^{(i)}, \theta_{k+1}^{(i)}, \phi_k^{(i)}, \phi_{k+1}^{(i)}) - u_{k-1}^{(i)} - u_k^{(i)} = 0 \quad (k = 2, \dots, N) \quad (34) \\ & D_2 L^d(\theta_1^{(i)}, \dot{\theta}_1^{(i)}, \phi_1^{(i)}, \dot{\phi}_1^{(i)}) + D_1 L^d(\theta_1^{(i)}, \theta_2^{(i)}, \phi_1^{(i)}, \phi_2^{(i)}) + u_1^{(i)} = 0 \quad (k = 2, \dots, N) \quad (35) \\ & D_4 L^d(\theta_1^{(i)}, \dot{\theta}_1^{(i)}, \phi_1^{(i)}, \dot{\phi}_1^{(i)}) + D_3 L^d(\theta_1^{(i)}, \theta_2^{(i)}, \phi_1^{(i)}, \phi_2^{(i)}) - u_1^{(i)} = 0 \quad (k = 2, \dots, N) \quad (36) \\ & -D_2 L^c(\theta_N^{(i)}, \dot{\theta}_N^{(i)}, \phi_N^{(i)}, \dot{\phi}_N^{(i)}) + D_1 L^d(\theta_{N-1}^{(i)}, \theta_N^{(i)}, \phi_{N-1}^{(i)}, \phi_N^{(i)}) + u_{N-1}^{(i)} = 0 \quad (37) \\ & -D_4 L^c(\theta_N^{(i)}, \dot{\theta}_N^{(i)}, \phi_N^{(i)}, \dot{\phi}_N^{(i)}) + D_3 L^d(\theta_{N-1}^{(i)}, \theta_N^{(i)}, \phi_{N-1}^{(i)}, \phi_N^{(i)}) - u_{N-1}^{(i)} = 0 \quad (38) \\ & D_2 L^d(\theta_{k-1}^{(i+1)}, \theta_k^{(i+1)}, \phi_{k-1}^{(i+1)}, \phi_k^{(i+1)}) - D_1 L^d(\theta_k^{(i+1)}, \theta_{k+1}^{(i+1)}, \phi_k^{(i+1)}, \phi_{k+1}^{(i+1)}) + u_{k-1}^{(i+1)} + u_k^{(i+1)} = 0 \quad (k = 2, \dots, N) \quad (39) \\ & D_4 L^d(\theta_{k-1}^{(i+1)}, \theta_k^{(i+1)}, \phi_{k-1}^{(i+1)}, \phi_k^{(i+1)}) - D_3 L^d(\theta_k^{(i+1)}, \theta_{k+1}^{(i+1)}, \phi_k^{(i+1)}, \phi_{k+1}^{(i+1)}) - u_{k-1}^{(i+1)} - u_k^{(i+1)} = 0 \quad (k = 2, \dots, N) \quad (40) \\ & D_2 L^d(\theta_1^{(i+1)}, \dot{\theta}_1^{(i+1)}, \phi_1^{(i+1)}, \dot{\phi}_1^{(i+1)}) + D_1 L^d(\theta_1^{(i+1)}, \theta_2^{(i+1)}, \phi_1^{(i+1)}, \phi_2^{(i+1)}) + u_1^{(i+1)} = 0 \quad (k = 2, \dots, N) \quad (41) \\ & D_4 L^d(\theta_1^{(i+1)}, \dot{\theta}_1^{(i+1)}, \phi_1^{(i+1)}, \dot{\phi}_1^{(i+1)}) + D_3 L^d(\theta_1^{(i+1)}, \theta_2^{(i+1)}, \phi_1^{(i+1)}, \phi_2^{(i+1)}) - u_1^{(i+1)} = 0 \quad (k = 2, \dots, N) \quad (42) \\ & -D_2 L^c(\theta_N^{(i+1)}, \dot{\theta}_N^{(i+1)}, \phi_N^{(i+1)}, \dot{\phi}_N^{(i+1)}) + D_1 L^d(\theta_{N-1}^{(i+1)}, \theta_N^{(i+1)}, \phi_{N-1}^{(i+1)}, \phi_N^{(i+1)}) + u_{N-1}^{(i+1)} = 0 \quad (43) \\ & -D_4 L^c(\theta_N^{(i+1)}, \dot{\theta}_N^{(i+1)}, \phi_N^{(i+1)}, \dot{\phi}_N^{(i+1)}) + D_3 L^d(\theta_{N-1}^{(i+1)}, \theta_N^{(i+1)}, \phi_{N-1}^{(i+1)}, \phi_N^{(i+1)}) - u_{N-1}^{(i+1)} = 0 \quad (44) \\ & a_-^{(i)}(\theta_N^{(i)}, \phi_N^{(i)}) \begin{bmatrix} \dot{\theta}_N^{(i)} \\ \dot{\phi}_N^{(i)} \end{bmatrix} = a_+^{(i)}(\theta_N^{(i)}, \phi_N^{(i)}) \begin{bmatrix} \dot{\theta}_1^{(i+1)} \\ \dot{\phi}_1^{(i+1)} \end{bmatrix} \quad (45) \\ & \phi_1^{(i)} < \phi_2^{(i)} < \dots < \phi_{N-1}^{(i)} < \phi_N^{(i)} \quad (46) \\ & \theta_1^{(i+1)} < \theta_2^{(i+1)} < \dots < \theta_{N-1}^{(i+1)} < \theta_N^{(i+1)} \quad (47) \\ \text{given} \quad & \theta_1^{(i)}, \phi_1^{(i)}, \theta_N^{(i)}, \phi_N^{(i)}, \theta_1^{(i+1)}, \phi_1^{(i+1)}, \theta_N^{(i+1)}, \phi_N^{(i+1)} \quad (48) \end{aligned}$$

It turns out that the optimization control problem (32)–(48) is represented as a finite dimensional constrained nonlinear optimization problem with respect to the  $(6N + 6)$  variables:  $\theta_1^{(i)}, \dots, \theta_N^{(i)}, \theta_1^{(i+1)}, \dots, \theta_N^{(i+1)}, \phi_1^{(i)}, \dots, \phi_N^{(i)}, \phi_1^{(i+1)}, \dots, \phi_N^{(i+1)}, u_1^i, \dots, u_{N-1}^i, u_1^{i+1}, \dots, u_{N-1}^{i+1}, \dot{\theta}_1^{(i)}, \dot{\phi}_1^{(i)}, \dot{\theta}_N^{(i)}, \dot{\phi}_N^{(i)}, \dot{\theta}_1^{(i+1)}, \dot{\phi}_1^{(i+1)}, \dot{\theta}_N^{(i+1)}, \dot{\phi}_N^{(i+1)}$ . Therefore, we can solve it by the sequential quadratic programming [23], [33], and obtain a sequence of discrete control input  $u_1^{(i)}, \dots, u_{N-1}^{(i)}, u_1^{(i+1)}, \dots, u_{N-1}^{(i+1)}$ .

### C. Transformation to continuous-time zero-order hold input

The previous subsection presents a synthesis method of a discrete control to generate a discrete gait of the DCBR by solving a finite dimensional constrained nonlinear optimization problem. However, since the control input is discrete-time, it cannot be utilized for the CCBR. Therefore, we here consider transformation of a discrete control input into a continuous one.

There exist infinite methods to generate a continuous control input from a given discrete one, and a continuous control input generated from a given discrete input has to be consistent with laws of physics. Hence, in this paper, we deal with a zero-order hold input in the form:

$$v^{(i)}(t) = v_k^{(i)}, \quad (i-1)kh \leq t < (i-1)(k+1)h, \quad (49)$$

which is one of the simplest continuous inputs. We need to derive a relationship between a discrete input  $u_k^{(i)}$  ( $k = 1, 2, \dots, N-1$ ) and a zero-order hold input (49). By using discrete Lagrange-d'Alembert's principle which is explained in Section II, we can have the following theorem.

**Theorem 1:** A zero-order hold input (49) that satisfies discrete Lagrange-d'Alembert's principle is given by

$$v_k^{(i)} = \frac{2}{h} u_k^{(i)}. \quad (50)$$

(Proof) During the time interval  $(i-1)kh \leq t < (i-1)(k+1)h$ , substituting (20) and (49) into the definition of the left discrete external force in (9):

$$F^{d-}(q_k, q_{k+1}) = \frac{h}{2} F^c \left( (1-\alpha)q_k + \alpha q_{k+1}, \frac{q_{k+1} - q_k}{h} \right),$$

we obtain

$$u_k^{(i)} = \frac{h}{2} v_k^{(i)}.$$

Hence, we have (50).  $\square$

By using (50) in Theorem 1, we can easily calculate a zero-order hold input from  $u_k^{(i)}$ ,  $i = 1, \dots, N-1$  which are obtained by solving a finite dimensional constrained nonlinear optimization problem (32)–(48). In addition, it must be noted that since we use discrete Lagrange-d'Alembert's principle to prove Theorem 1, a zero-order hold input with a gain (50) is consistent with laws of physics.

## V. NUMERICAL SIMULATIONS

### A. Problem formulation

In this section, some numerical simulations on a gait generation on a periodically unlevel ground for the CCBR based on our new method proposed in the previous section, and confirm the effectiveness of it. First, this subsection gives the problem setting. we set parameters as follows; the physical parameters of the CCBR:  $m = 2.0$  [kg],  $M = 10.0$  [kg],  $I =$

$0.167[\text{kgm}^2]$ ,  $a = 0.5[\text{m}]$ ,  $b = 0.5[\text{m}]$ ,  $l = 1.0[\text{m}]$ , the parameters of discrete mechanics:  $\alpha = 1/2$ ,  $h = 0.005[\text{s}]$ ,  $N = 80$ . We consider two types of periodically unlevel grounds. The one is set as  $r = 1.0[\text{m}]$ ,  $\rho = 5[\text{deg}]$ ,  $L = 8$  (Simulation I), and the other is set as  $r = 1.0[\text{m}]$ ,  $\rho = 10[\text{deg}]$ ,  $L = 8$  (Simulation II). Initial conditions are  $\theta_1^{(1)} = -0.5321[\text{rad}]$ ,  $\phi_1^{(1)} = 2.0273[\text{rad}]$ ,  $\dot{\theta}_1^{(1)} = 0.1830[\text{rad}]$ ,  $\dot{\phi}_1^{(1)} = 2.1820[\text{rad}]$ .

### B. Simulation results

Next, numerical simulations are shown in order to check the availability of our new approach. Figs. 9–11 show the results of Simulation I. Fig. 9 illustrates the time series of Leg 1 and 2 ( $\theta$  and  $\phi$ ). Fig. 10 shows the plot of solution trajectory in the phase space of  $\theta - \phi$ . In Fig. 11, a snapshot of the continuous gait is depicted. From these results, we can confirm that a stable gait on periodically unlevel grounds for the CCBR can be generated by the proposed approach.

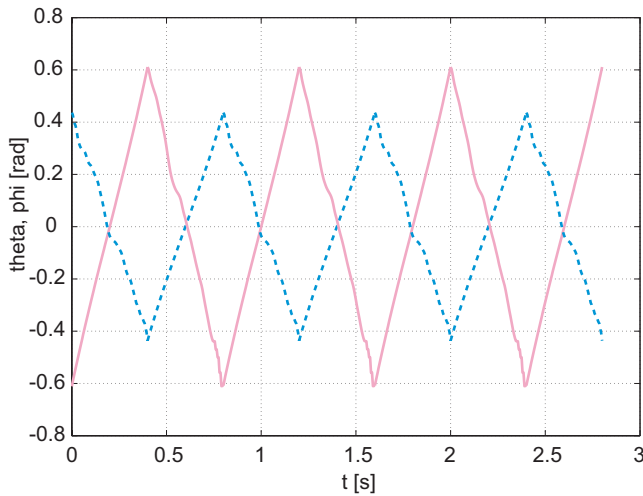


Figure 9 : Time series of  $\theta$  and  $\phi$  (Simulation I; red line:  $\theta$ , blue line:  $\phi$ )

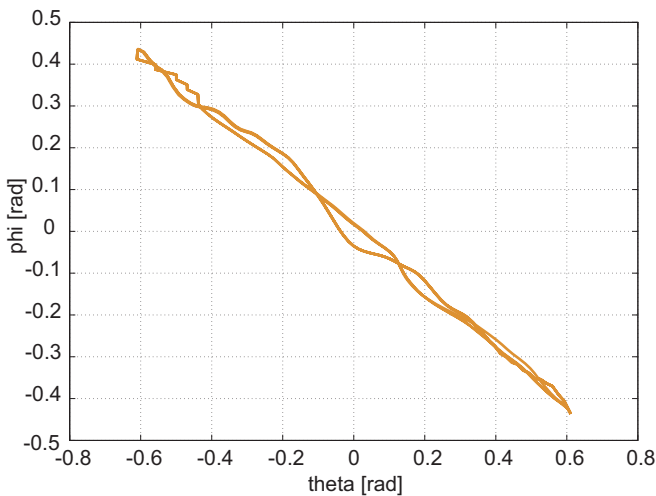


Figure 10 : Solution trajectory on  $\theta - \phi$ -space (Simulation I)

Figs. 12–14 illustrate the results of Simulation II. Fig. 12 depicts the time series of Leg 1 and 2 ( $\theta$  and  $\phi$ ). Fig. 13 shows

the plot of solution trajectory in the phase space of  $\theta - \phi$ . In Fig. 14, a snapshot of the continuous gait is illustrated. From these results, we can also see that the proposed method can generate a stable gait for the CCBR.

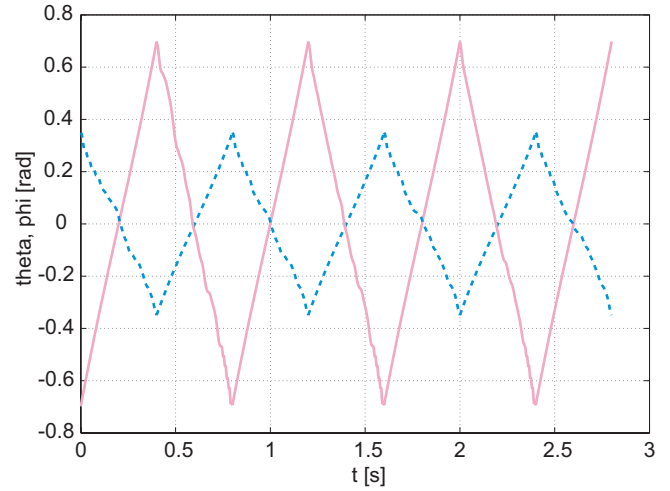


Figure 12 : Time series of  $\theta$  and  $\phi$  (Simulation II; red line:  $\theta$ , blue line:  $\phi$ )

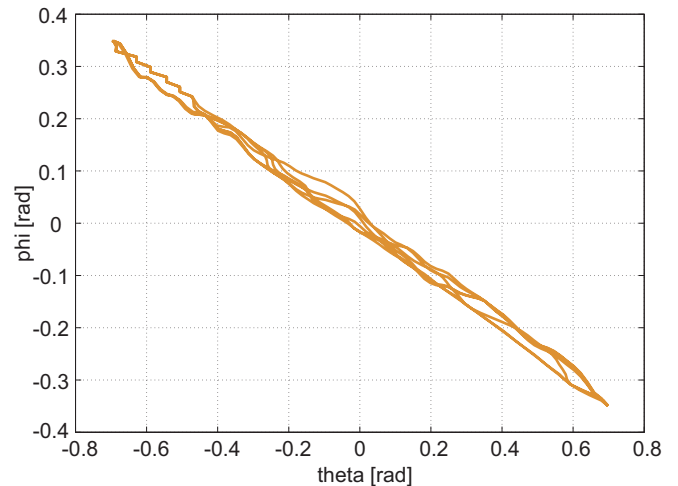


Figure 13 : Solution trajectory on  $\theta - \phi$ -space (Simulation II)

## VI. CONCLUSIONS

This paper has dealt with a gait generation problem for the compass-type biped robot on periodically unlevel grounds. We have formulated a discrete gait generation problem for the DCBR as a finite dimensional constrained nonlinear optimization problem. A transformation method from a discrete control input into a zero-order hold input has been introduced from the viewpoint of discrete Lagrange-d'Alembert principle. By numerical simulations, we have verified generation of a stable gait and the effectiveness of our new approach.

In association with this work, we will tackle the following problems: stable gait generation of the CCBR irregular grounds, experimental evaluation of the proposed control method, and applications of discrete mechanics to more human-like robots.

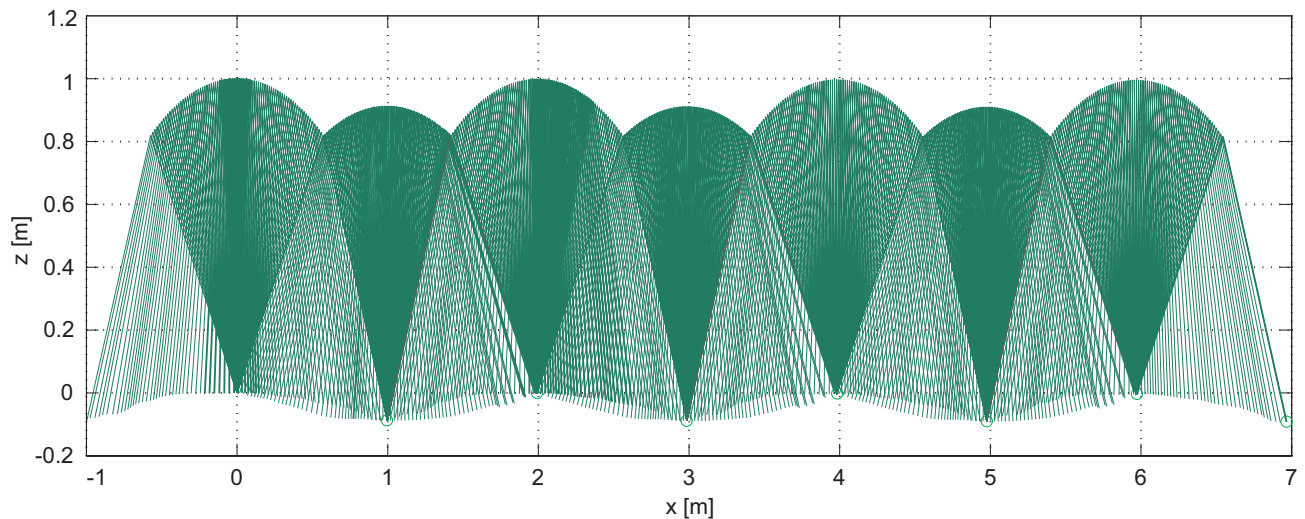


Fig. 11 : Snapshot of Gait (Simulation I)

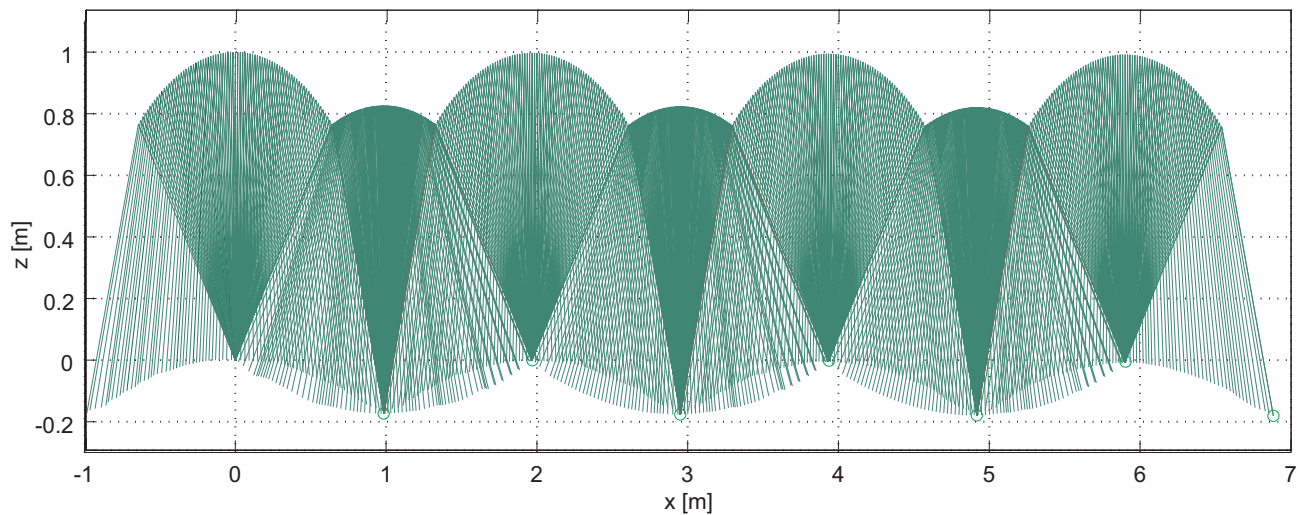


Fig. 14 : Snapshot of Gait (Simulation II)

## REFERENCES

- [1] T. McGeer, "Passive Dynamic Walking," *The International Journal of Robotics Research*, Vol. 9, No. 2, pp. 62-82, 1990.
- [2] A. Goswami, B. Thuilot, and B. Espiau, "A Study of the Passive Gait of a Compass-like Biped Robot: Symmetry and Chaos," *International Journal of Robotics Research*, Vol. 17, No. 12, pp. 1282-1301, 1998.
- [3] S. H. Collins, A. Ruina, R. Tedrake, and M. Wisse, "Efficient Bipedal Robots based on Passive-Dynamic Walkers," *Science*, Vol. 307, pp. 1082-1085, 2005.
- [4] H. Gritli, N. Khraief, and S. Belghith, "Period-Three Route to Chaos induced by a Cyclic-Fold Bifurcation in Passive Dynamic Walking of a Compass-Gait Biped Robot," *Communications in Nonlinear Science and Numerical Simulation*, Vol. 17, pp. 4356-4372, 2012.
- [5] A. Goswami, B. Espiau and A. Keramane, "Limit Cycles in a Passive Compass Gait Biped and Passivity Mimicking Control Laws," *Autonomous Robots*, Vol. 4, pp. 273-286, 1997.
- [6] M. Garcia, A. Chatterjee, A. Ruina, and M. J. Coleman, "The simplest walking model: stability, complexity, and scaling," *ASME Journal of Biomech. Eng.*, Vol. 120, No. 2, pp. 281-288, 1998.
- [7] J. W. Grizzle, G. Abba, and F. Plestan, "Asymptotically Stable Walking for Biped Robots: Analysis via Systems with Impulse Effects," *IEEE Trans. on Automatic Control*, Vol. 46, No. 1, pp. 51-64, 2001.
- [8] E. R. Westervelt, J. W. Grizzle, and C. Canudas de Wit, "Switching and PI Control of Walking Motions of Planar Biped Walkers," *IEEE Transactions on Automatic Control*, Vol. 48, No. 2, pp. 308-312, 2003.
- [9] J. Hass, J. M. Herrmann, and T. Geisel, "Optimal Mass Distribution for Passivity-based Bipedal Robots," *International Journal of Robotics Research*, Vol. 25, No. 11, pp. 1087-1098, 2006.
- [10] A. T. Safa, M. G. Saadat, and M. Naraghi "Passive Dynamic of the Simplest Walking Model: Replacing Ramps with Stairs," *Mechanism and Machine Theory*, Vol. 42, pp. 1314-1325, 2007.
- [11] D. G. E. Hobbelen and M. Wisse, "Swing-leg Retraction for Limit Cycle Walkers Improves Disturbance Rejection," *IEEE Transactions on Robotics*, Vol. 24, No. 2, pp. 377-389, 2008.
- [12] Q. Huang, K. Yokoi, S. Kajita, K. Kaneko, H. Arai, N. Koyachi, and K. Tanie, "Planning Walking Patterns for a Biped Robot," *IEEE Transactions on Robotics and Automation*, Vol. 17, No. 3, pp. 280-289, 2001.
- [13] P. Sardain and G. Bessonnet, "Forces Acting on a Biped Robot. Center

- of Pressure – Zero Moment Point,” *IEEE Transactions on Systems, Man, and Cybernetics, Part A: Systems and Humans*, Vol. 34, No. 5, pp. 630-637, 2004.
- [14] K. Erbatur and O. Kurt, “Natural ZMP Trajectories for Biped Robot Reference Generation,” *IEEE Transactions on Industrial Electronics*, Vol. 56, No. 3, pp. 835-845, 2009.
- [15] C. M. A. Pinto, A. P. Santos, “Modelling Gait Transition in Two-Legged Animals,” *Communications in Nonlinear Science and Numerical Simulation*, Vol. 16, pp. 4625-4631, 2011.
- [16] G. Taga, Y. Yamaguchi, and H. Shimizu, “Self-organized Control of Bipedal Locomotion by Neural Oscillators in Unpredictable Environment,” *Biological Cybernetics*, Vol. 65, pp. 147-159, 1991.
- [17] W. T. Miller, “Real-time Neural Network Control of a Biped Walking Robot,” *IEEE Control Systems Magazine*, Vol. 14, No. 1, pp. 41-48, 1994.
- [18] J. Nakanishi, J. Morimoto, G. Endo, G. Cheng, S. Schaal, and M. Kawato, “Learning from Demonstration and Adaptation of Biped Locomotion,” *Robotics and Autonomous Systems*, Vol. 47, pp. 79-91, 2004.
- [19] J. Morimoto and C. G. Atkeson, “Learning Biped Locomotion: Application of Poincare-map-based reinforcement learning,” *IEEE Robotics & Automation Magazine*, Vol. 14, No. 2, pp. 41-51, 2007.
- [20] J. E. Marsden, G. W. Patrick, and S. Shkoller, Multisymplectic Geometry, Variational Integrators and Nonlinear PDEs, *Communications in Mathematical Physics*, Vol. 199, pp. 351-395, 1998.
- [21] C. Kane, J. E. Marsden, M. Ortiz, and M. West, “Variational Integrators and the Newmark Algorithm for Conservative and Dissipative Mechanical Systems,” *International Journal for Numerical Methods in Engineering*, Vol. 49, pp. 1295-1325, 2000.
- [22] J. E. Marsden and M. West, “Discrete Mechanics and Variational Integrators,” *Acta Numerica*, Vol. 10, pp. 3571-5145, 2001.
- [23] O. Junge, J. E. Marsden, and S. Ober-Blöbaum, “Discrete Mechanics and Optimal Control,” *Proc. of 16th IFAC World Congress, Praha, Czech*, Paper No. We-M14-TO/3, 2005
- [24] A. M. Bloch, M. Leok, J. E. Marsden and D. V. Zenkov, “Controlled Lagrangians and Stabilization of the Discrete Cart-Pendulum System,” *Proc. of 44th IEEE CDC-ECC*, Seville, Spain, pp. 6579-6584, 2005.
- [25] A. M. Bloch, M. Leok, J. E. Marsden and D. V. Zenkov, “Controlled Lagrangians and Potential Shaping for Stabilization of the Discrete Mechanical Systems,” *Proc. of 45th IEEE CDC*, San Diego, U.S.A., pp. 3333-3338, 2006.
- [26] T. Kai and Y. Yamamoto, “On Analysis and Control of the Cart-Pendulum System Modeled by Discrete Mechanics,” *Proc. of NOLTA 2007*, Vancouver, Canada, pp. 485-488, 2007.
- [27] T. Kai and K. Bito, “Solvability Analysis and Stabilization of the Cart-Pendulum Modeled by Discrete Mechanics with Friction,” *Proc. of NOLTA 2008*, Budapest, Hungary, pp. 305-308, 2008.
- [28] T. Kai and T. Shintani, “Stabilization Control and Experiments of the Cart-Pendulum based on Discrete Mechanics,” *Proc. of NOLTA 2009*, Sapporo, Japan, pp. 82-85, 2009.
- [29] T. Kai and T. Shintani, “Discrete Gait Generation for the Compass-Type Biped Robot Modeled by Discrete Mechanics,” in *Proc. of NOLTA 2010*, Krakow, Poland, pp. 434-437, 2009.
- [30] T. Kai and T. Shintani, “Discrete Mechanics Approach to Gait Generation for the Compass-type Biped Robot,” in *Proc. of IFAC World Congress 2011*, Milano, Italy, pp. 434-437, 2011.
- [31] T. Kai and T. Shintani, “A Discrete Mechanics Approach to Gait Generation for the Compass-Type Biped Robot,” *Nonlinear Theory and Its Applications, IEICE*, Vol. 2, No. 4, pp. 533-547, 2011.
- [32] T. Kai and T. Shintani, “A Gait Generation Method for the Compass-type Biped Robot on Slopes via Discrete Mechanics,” in *Proc. of IEEE CDC 2011*, Orlando, USA, pp. 675-681, 2011.
- [33] C. B. Gurwitz, *Sequential Quadratic Programming Methods Based on Approximating a Projected Hessian Matrix*, General Books, 2001.

# The Paradox of the Fuzzy Disambiguation in the Information Retrieval

Anna Bryniarska

Department of Electrical and Computer Engineering  
Opole University of Technology  
Opole, Poland

Email: a.bryniarska@doktorant.po.edu.pl

**Abstract**—Current methods of data mining, word sense disambiguation in the information retrieval, semantic relation, fuzzy sets theory, fuzzy description logic, fuzzy ontology and their implementation, omit the existence of paradox called here the paradox of the fuzzy disambiguation. The paradox lies in the fact that due to fuzzy data and the experts knowledge it can be obtained precise knowledge. In this paper to describe this paradox, is introduced a conceptual apparatus. Moreover, there is formulated an information retrieval logic. There are suggested certain applications of this logic to search information on the Web.

**Index Terms**—fuzzy disambiguation paradox, Description Logic, FuzzyDL, Information Retrieval Logic, Semantic Web.

## I. INTRODUCTION

Recently information retrieval (*IR*) on the Semantic Web usually means searching a reliable source of information. So far systems of information retrieval and systems of semantic relation indicated only for the most semantically similar source of searched information [13], [14].

To define the semantic relationships is typically used measurement of the keywords incidence. However, meaning of these words is exactly identified and represents certain knowledge. Therefore, these *IR* methods cannot always be used.

Sometimes, the information retrieval about an object can lead to uncertain knowledge described in the appropriate, ontology language. In spite of this uncertainty, it can be found a disambiguated source of information about this object. In this way, the compliance with the description of the object model (compliance with the thesaurus) is obtained. The situation described above is called here **the paradox of the fuzzy disambiguation in the information retrieval**. Methods of data mining [11], word sense disambiguation in information retrieval [2], [7], [8], [13], [16], semantic relation [7], [8], fuzzy sets theory and fuzzy logic [10], fuzzy description logic [3], [4], [17], [18], and also their implementation (i.e. in OWL language), do not concern about this paradox. The following are two examples to illustrate this paradox.

### A. Example 1

**Data from user of X iron:** the fabric *Y* shrunk and waved after ironing.

**Data from expert:** some threads of the fabric *Y* shrink, but only in the water steam at 100°C. Only program 1 uses the water steam.

Data from user of the *X* iron are uncertain, if we want to find out which program was used for ironing. However, from these uncertain data indicate a precise data: during ironing was turned on the program 1 with the steam. Reasoning in this case uses particular data from the expert. The situation that when ironing the fabric was only heated by the iron is excluded with the experts knowledge.

### B. Example 2

Whether “Ralf Möller”, a German bodybuilder and TV actor and “Ralf Möller”, a professor at the Hamburg University of Technology, is the same person?

**Data from Web resources:** Ralf Möller, the actor, born in 1959 r.; Ralf Möller, the professor, born when the German Chancellor was Ludwig Erhard (from history it was between 1963 and 1966).

**Data from expert:** Any attribute for a single person has only one value.

Data on the Web resources are ambiguous and uncertain. Names of people are:  $name(person1) = \text{“Ralf Möller”}$  for the actor,  $name(person2) = \text{“Ralf Möller”}$  for the professor. Whether  $person1 = person2$ ? Complementing the uncertain knowledge of the attributes values of expert knowledge:  $birthDate(person1) = 1959$ ,  $birthDate(person2) > 1963$ , it can be concluded that  $person1 \neq person2$ . The result of reasoning is accurate information.

## II. RESIDUUM RULE IN IR

The information retrieval on the Semantic Web is based on finding a copy of data which are:

- 1) values of single attribute arguments, i.e. **concepts** – data representing knowledge of certain properties or object types,
- 2) values of multi attribute arguments, i.e. **roles** – data representing knowledge about relationships between objects.

Firstly, concepts and roles are described by the language of the *Description Logic (DL)* [1]. Secondly, the *DL* logic, describing concepts and roles, is extended for some first-order logic formulas. Then, in this extended logic, is created the **thesaurus** – language describing the reference concepts and roles. While the **ontology** describes the real, found on Web pages, concepts and roles which are searched. If the interpretation of

concepts and roles from the ontology, accordingly to experts knowledge and criteria, will result in the interpretation of concepts and roles of thesaurus, then this relationship is called **the residuum**. This interpretation determines the membership degree of the data copies (set of the Web addresses  $X$ ). This degree also includes the semantic structure of the resources, determined by the Semantic Web.

Due to fuzzy degree of knowledge, concepts and roles can be interpreted as fuzzy sets in the space  $X \cup X \times X$  of the Web addresses and their pairs. Then can be made **the fuzzification** of knowledge [5]. Whereas setting residuum is necessary to make the knowledge **defuzzification** [5]. Then for a given query, it can be indicate, a reliable-for-experts set of Web addresses representing this knowledge. Interpretation sets forming residuum will be further treated as an information search result. Then, the following search rule is applied.

Firstly, the question (search query) is compared to the thesaurus. Secondly, if for all interpretation the set of searched addresses is empty, then this question is compared to ontology, so that the compared entry has the most similar meaning to the thesaurus. Found, for this entry, the set of Web addresses represents knowledge which is identical or the most similar to the searched one. This rule of  $IR$  is called **the residuum rule**. Below is introduced **the information retrieval logic (IRL)** using this rule. Applying this logic to the information search is an attempt to develop a new, more universal  $IR$  method, using the artificial intelligence.

### III. LANGUAGE OF IRL

In the context of the Semantic Web research [1], [3]–[5], the representation of knowledge in the Semantic Web can be defined by the attribute language ( $AL$ ) of the Description Logic ( $DL$ ) [1]. Then knowledge is represented by concepts **TBox**, roles **RBox** and assertions **ABox**. The Semantic Web might be extended by edges representing relationships between concepts and roles. Descriptions of these edges are called **axioms**. Then knowledge is represented by two systems: the terminology called **TBox** and the set of assertions called **ABox**. Where the assertion is the relationship between the concept or the role and their instances.

Further is presented the syntax of the language  $AL$  for the  $IRL$ , analogously to the fuzzy Description Logic ( $fuzzyDL$ ) [3]. Articles [10], [11] show the semantic and the interpretations of this language which are called the fuzzification and the defuzzification.

#### A. Syntax of TBox

The following names are included to the set of concepts and roles names:

*The universal concept*  $\top$  (Top) and *the empty concept*  $\perp$  (Bottom).

The universal concept includes all instances of concepts and the empty concept informs about no instance of a concept.

Let  $C, D$  be the names of the concepts,  $R$  be the name of a role, and  $m$  be the modifier. Then complex concepts are:

$\neg C$  – *the concept negation*; it means all instances of concepts which are not an instance of the concept  $C$ ;

$C \cap D$  – *the intersection of concepts*  $C$  and  $D$ ; it means all instances of both concepts  $C$  and  $D$ ;

$C \sqcup D$  – *the union of concepts*  $C$  and  $D$ ; it means all instances either of the concept  $C$  or the concept  $D$ ;

$\exists R.C$  – *the existential quantification*; it means all instances of the concept  $C$  which are in role  $R$  with at least once occurrence of the concept  $C$ ;

$\forall R.C$  – *the universal quantification*; it means all occurrence of the concept  $C$  which is in role  $R$  with some occurrence of the concept  $C$ ;

$m(C)$  – *the modification*  $m$  of the concept  $C$ ; it means the concept  $C$  which is modified by the word  $m$ . For example  $m$  can occur as a word: very, more, the most, high, higher or the highest.

Concepts which are not complex are called *atomic*.

#### B. Syntax of ABox

For any concepts instances  $t_1, t_2$ , the concept name  $C$  and the role name  $R$ , **the assertions** are “ $t_1 : C$ ”, “ $(t_1, t_2) : R$ ”. We read them:  $t_1$  is an instance of the concept  $C$ , the pair  $(t_1, t_2)$  is an instance of the role  $R$ .

For any concepts instances  $t_1, t_2$ , the concept name  $C$  and the role name  $R$ , **the assertions with membership degree**  $\alpha$  are “ $\langle t_1 : C, \alpha \rangle$ ”, “ $\langle (t_1, t_2) : R, \alpha \rangle$ ”. We read them:  $t_1$  is an instance with membership degree  $\alpha$  of the concept  $C$ , the pair  $(t_1, t_2)$  is an instance with membership degree  $\alpha$  of the role  $R$ .

#### C. Syntax of axioms TBox

For any concepts names  $C, D$  and any number  $\alpha \in [0, 1]$ , the axioms are:

$C \sqsubseteq D$  – the concept  $C$  is the concept  $D$ ,

$C = D$  – the concept  $C$  is identical with the concept  $D$ ,

$\langle C \sqsubseteq D, \alpha \rangle$  – the concept  $C$  is the concept  $D$  in the  $\alpha$  degree,

$\langle C = D, \alpha \rangle$  – the concept  $C$  is identical with the concept  $D$  in the  $\alpha$  degree,

#### D. Syntax of axioms RBox

For any roles  $R_1, R_2$  and any number  $\alpha \in [0, 1]$ , the axioms are:

$R_1 \sqsubseteq R_2$  – the role  $R_1$  is the role  $R_2$ ,

$R_1 = R_2$  – the role  $R_1$  is identical with the role  $R_2$ .

$\langle R_1 \sqsubseteq R_2, \alpha \rangle$  – the role  $R_1$  is the role  $R_2$  in the  $\alpha$  degree,

$\langle R_1 = R_2, \alpha \rangle$  – the role  $R_1$  is the role  $R_2$  in the  $\alpha$  degree,

#### E. Syntax of formula

Any assertion or axiom is a formula. For any formula  $\varphi, \phi$ , a variable  $x$  and a number  $\alpha \in [0, 1]$ , formulas are:

$\neg \varphi$  – the negation;

$\langle \varphi, \alpha \rangle$  – the formula  $\varphi$  true in the degree  $\alpha$ ;

$\forall x \varphi$  – the existential quantification of the formula  $\varphi$  for variable  $x$ ;

$\exists_x \varphi$  – the universal quantification of the formula  $\varphi$  for variable  $x$ ;

$\varphi \Rightarrow \phi$  – the implication;

$\varphi \wedge \phi$  – the conjunction;

$\varphi \vee \phi$  – the alternative;

$\varphi \Leftrightarrow \phi$  – the equivalence formulas.

#### IV. POSTULATES OF FUZZYDL AND FUZZY DISAMBIGUATION IN $IR$

The occurrence of the paradox of the fuzzy disambiguation in  $IR$  determine the following postulates (**P1** – **P9**):

**P1.** There is a thesaurus which is a set of certain reference terms and formulas of the  $IRL$  language. Thesaurus terms represent knowledge in the same area as searched information and can be found in a text document (from thesaurus).

**P2.** An ontology includes all terms and formulas of the  $IRL$  language, which are semantically related to the searched information. The ontology includes the thesaurus. All thesaurus formulas are constructed of certain terms and assertions from the base set  $Tez$ . Likewise, all ontology formulas are constructed of certain terms and assertions belonging to the base set  $Ont$ . The degree of semantic similarity of ontology expressions to the thesaurus expressions is determined by an expert system based on the experts knowledge.

**P3.** The space  $IR$  is a group of addresses of knowledge resources on the Web, semantically related to the terms and formulas representing the searched information. Knowledge resources are text documents available at these addresses.

**P4.** Finding information is to search the text document, which semantic structure (terms from the Semantic Web created by the ontology) is the most similar to the structure of the thesaurus document. If both documents contains expressions that are equally used by agents in the communication process, then these expressions represent the same knowledge. Furthermore information retrieval is searching for the text document that represent the same knowledge or most similar knowledge to the one from the thesaurus [6]. Therefore, the residuum rule of information retrieval is applied.

**P5.** The information retrieval of the intersection of concepts represents collective knowledge of these concepts. *Complementary formulas*  $\varphi, \phi$  are formulas  $\varphi \& \phi$  represent the collective knowledge represented by the data set of these formulas.

**P6.** According to the intuition and practice of  $IR$ , if  $x \in [0, 1]$  is the degree of the semantic similarity of the instance  $t_1$  of a concept  $C_1$  or formula  $\varphi$  to the concept instance or formula belonging to the thesaurus and  $y \in [0, 1]$  is the degree of semantic similarity of the instance  $t_2$  of a concept  $C_2$  or formula  $\phi$  to the concept instance or formula belonging to the thesaurus, then the degree of the concepts intersection  $C_1, C_2$  or complementary formulas  $\varphi \& \phi$  are a number  $x \bullet y$ . The operation  $\bullet : [0, 1] \times [0, 1] \rightarrow [0, 1]$  is some t-norm. This t-norm

has the following properties. For all  $x, y, z, x_0, y_0 \in [0, 1]$ :

$$x \bullet y = y \bullet x \quad (1)$$

$$(x \bullet y) \bullet z = x \bullet (y \bullet z) \quad (2)$$

$$x \leq x_0 \text{ and } y \leq y_0 \text{ implies } x \bullet y \leq x_0 \bullet y_0 \quad (3)$$

$$1 \bullet x = x; 0 \bullet x = 0 \quad (4)$$

Each t-norm determines uniquely its corresponding implication  $\rightarrow$  (the residuum), defining a similarity degree of the formulas implications, satisfying for all  $x, y, z \in [0, 1]$ :

$$z \leq (x \rightarrow y) \text{ iff } x \bullet z \leq y \quad (5)$$

or

$$(x \rightarrow y) = \sup\{t \in [0, 1] : x \bullet t \leq y\}. \quad (6)$$

The implication of these formulas is semantically similar to the thesaurus formulas, if the similarity degree of the implication predecessor is the closest to its successor. Furthermore, this means that in the found text document is the formula  $\varphi$ , which implies a certain formula  $\phi$  contained in this document, or represents the searched information. When  $\phi$  represents the searched information and is not contained in this document, then the formula  $\varphi$  is supplemented with the formula  $\theta$  representing the experts knowledge, so that the complementary formulas  $\varphi \& \phi$  have the same similarity degree as search formula  $\phi$  (the degree equal 1). Thus, in the case of imprecise implications predecessor  $\varphi$ , the successor is a sharp expression with the semantic similarity degree equal 1 (Example 1).

**P7.** If in the text document is a conjunction  $\varphi \wedge \phi$ , according to the classical propositional calculus, then  $\varphi \Rightarrow \phi$ . Thus, the conjunction is recognized by firstly recognizing the formula  $\varphi$  and secondly by recognizing the implication  $\varphi \Rightarrow \phi$ . Therefore, the conjunction  $\varphi \wedge \phi$  is recognized as  $\varphi \& (\varphi \Rightarrow \phi)$ . Further is assumed that:

$$\varphi \wedge \phi := \varphi \& (\varphi \Rightarrow \phi) \quad (7)$$

Hence, the similarity degree of the conjunction  $\varphi \wedge \phi$  to the thesaurus formulas is defined:

$$x \otimes y := x \bullet (x \rightarrow y), \text{ for } x, y \in [0, 1] \quad (8)$$

where  $x, y$  are the similarity degrees of formulas  $\varphi, \phi$  to the thesaurus formulas.

**P8.** If in the text document is an alternative  $\varphi \vee \phi$ , then based on propositional logic, it can be assumed that this alternative is recognized based on the following assignment:

$$\varphi \vee \phi := ((\varphi \Rightarrow \phi) \Rightarrow \phi) \wedge ((\phi \Rightarrow \varphi) \Rightarrow \varphi) \quad (9)$$

Hence, the similarity degree of the alternative  $\varphi \vee \phi$  to the thesaurus formulas is defined:

$$x \otimes y := ((x \rightarrow y) \rightarrow y) \otimes ((y \rightarrow x) \rightarrow x) \quad (10)$$

where  $x, y \in [0, 1]$  are the similarity degrees of formulas  $\varphi, \phi$  to the thesaurus formulas.

**P9.** The algebra  $BL = \langle L, \otimes, \oplus, \bullet, \rightarrow, 0, 1 \rangle$  is a regular residuated lattice (or a  $BL$ -algebra). It is the algebra such that:

- 1)  $\langle L, \otimes, \oplus, 0, 1 \rangle$  is a complete lattice with the largest element 1 and the least element 0;
- 2)  $\langle L, \bullet, 1 \rangle$  is a commutative semigroup with the unit element 1, i.e.  $\bullet$  is commutative, associative, and  $1 \bullet x = x$  for all  $x$ ;
- 3) the following conditions hold (for all  $x, y, z \in [0, 1]$ ):

$$z \leq (x \rightarrow y) \text{ iff } x \bullet z \leq y \quad (11)$$

$$x \otimes y = x \bullet (x \rightarrow y) \quad (12)$$

$$x \oplus y = ((x \rightarrow y) \rightarrow y) \otimes ((y \rightarrow x) \rightarrow x) \quad (13)$$

$$(x \rightarrow y) \oplus (y \rightarrow x) = 1 \quad (14)$$

In the BL-algebra can be defined operations of the completeness ' and the equivalence  $\leftrightarrow$ :

$$x' := (x \rightarrow 0) \quad (15)$$

$$x \leftrightarrow y := (x \rightarrow y) \bullet (y \rightarrow x) \quad (16)$$

## V. FUZZIFICATION

The expressions of the IRL logic are interpreted in the regular residuated lattice  $BL = \langle L, \otimes, \oplus, \bullet, \rightarrow, 0, 1 \rangle$  and in the chosen, ordered algebra of fuzzy sets:

$$\mathbf{F} = \langle F, \wedge^F, \vee^F, \neg^F, c^F, e^F, 0^F, 1^F, M, F_0 \rangle \quad (17)$$

Where for the space  $X \cup X \times X$ ,  $F$  is a family of fuzzy sets,  $\mu : X \cup X \times X \in [0, 1]$ , described as follow. For any fuzzy set  $\mu$  there are exactly two fuzzy sets  $\mu_1 : X \rightarrow [0, 1]$  and  $\mu_2 : X \times X \rightarrow [0, 1]$ :

$$\mu(x) = \begin{cases} \mu_1(x), & \text{for } x \in X \\ \mu_2(x), & \text{for } x \in X \times X \end{cases} \quad (18)$$

$F$  is a set of all fuzzy sets in the  $\mathbf{F}$  algebra, which only apply to mentioned bellow operations and relation, described by t-norm  $\bullet$  [8], conclusion, equality and modification norm.

The operation:

- 1)  $\wedge^F$  is intersection of fuzzy sets;
- 2)  $\vee^F$  is a sum;
- 3)  $\neg^F$  is a complement operation;
- 4)  $c^F$  is a function  $c^F : F \times F \rightarrow [0, 1]$  called the degree of containment of fuzzy sets [8];
- 5)  $e^F$  is a function  $e^F : F \times F \rightarrow [0, 1]$  called the degree of equality of fuzzy sets [8].

These operations are defined in the regular residuated lattice  $BL = \langle L, \otimes, \oplus, \bullet, \rightarrow, 0, 1 \rangle$  defined as follows. For any fuzzy sets  $\mu_A, \mu_B \in F$  and  $x \in [0, 1]$ :

$$(\mu_A \wedge^F \mu_B)(x) = \mu_A(x) \otimes \mu_B(x) \quad (19)$$

$$(\mu_A \vee^F \mu_B)(x) = \mu_A(x) \oplus \mu_B(x) \quad (20)$$

$$c^F(\mu_A, \mu_B)(x) = \mu_A(x) \rightarrow \mu_B(x) \quad (21)$$

$$e^F(\mu_A, \mu_B)(x) = \mu_A(x) \leftrightarrow \mu_B(x) \quad (22)$$

$$(\neg^F \mu_A)(x) = \mu_A(x) \rightarrow 0 \quad (23)$$

The symbol  $0^F$  is any fuzzy set only with values 0, the symbol  $1^F$  is any fuzzy set only with values 1,  $M$  is a set of one-argument operations  $f : [0, 1] \rightarrow [0, 1]$  called the **modification functions**;  $F_0$  is a subset of  $F$ .

Let  $X$  is a set of all objects (data copies), which are part of the Semantic Web and  $X \times X$  is a set of all ordered pairs of the set  $X$ . Then there can be described the interpretation  $I = (F, I)$  which:

**F1.** For the concept instances  $t$  assigns certain values  $t^I \in X$  and for the pair of instances  $(t_1^I, t_2^I)$  assigns pairs  $(t_1^I, t_2^I) \in X \times X$ . Most frequently concept instances are associated with data copies. These copies are considered by IT specialists as objects. Thus, the space  $X \cup X \times X$  is a set of Web resources which include documents with considered data. For example specific word in a computer screen is an instance of data copy indicated by the specific Web resource address. Also the relationship between this word and other word is indicated by a pair of Web resources addresses.

**F2.** For the concept name  $C$  assigns fuzzy set  $C^I : X \cup X \times X \rightarrow [0, 1]$ , that for any  $x, y \in X, C^I(x, y) = C^I((x, y)) = C^I(y)$ .

**F3.** For the role name  $R$  assigns a fuzzy set  $R^I : X \cup X \times X \rightarrow [0, 1]$ , equals 0 for arguments from  $X$ ,

**F4.** For the modifier  $m$  assigns a function  $m^I : [0, 1] \rightarrow [0, 1]$ , where  $m^I \in M$ ,

**F5.** For formulas  $\varphi$ , including assertions and axioms, assigns some number  $\varphi^I \in [0, 1]$ .

### A. Semantic of concepts Tbox

For any  $x \in X$ , concept names  $C, D$ , the role name  $R$  and the modifier  $m$ :

$$\top^I(x) = 1 \quad (24)$$

$$\perp^I(x) = 0 \quad (25)$$

$$(\neg C)^I(x) = (\neg^F C^I)(x) \quad (26)$$

$$(C \wedge D)^I(x) = (C^I \wedge^F D^I)(x) \quad (27)$$

$$(C \vee D)^I(x) = (C^I \vee^F D^I)(x) \quad (28)$$

$$(\exists R.C)^I(x) = \sup_{y \in X} (R^I \wedge^F C^I)(x, y) \quad (29)$$

$$(\forall R.C)^I(x) = \inf_{y \in X} (\neg^F R^I \vee^F C^I)(x, y) \quad (30)$$

$$(m(C))^I(x) = m^I(C^I(x)) \quad (31)$$

### B. Semantic of assertions ABox

For any instance  $t$  of the concept  $C$  and any instances  $t_1, t_2$  of the role  $R$ :

$$(t : C)^I = C^I(t^I) \quad (32)$$

$$((t_1, t_2) : R)^I = R^I(t_1^I, t_2^I) \quad (33)$$

### C. Semantic of axioms

For any concept names  $C, D$  and roles  $R_1, R_2$ :

$$(C \sqsubseteq D)^I = c^F(C^I, D^I) \quad (34)$$

$$(R_1 \sqsubseteq R_2)^I = c^F(R_1^I, R_2^I) \quad (35)$$

$$(C = D)^I = e^F(C^I, D^I) \quad (36)$$

$$(R_1 = R_2)^I = e^F(R_1^I, R_2^I) \quad (37)$$

#### D. Semantic of formulas

For any formulas (assertions and axioms)  $\varphi, \phi$  and degree  $\alpha \in [0, 1]$ :

$$(\neg\varphi)^I = \varphi^I \rightarrow 0 \quad (38)$$

$$(\varphi \wedge \phi)^I = \varphi^I \otimes \phi^I \quad (39)$$

$$(\varphi \vee \phi)^I = \varphi^I \oplus \phi^I \quad (40)$$

$$(\varphi \Rightarrow \phi)^I = \varphi^I \rightarrow \phi^I \quad (41)$$

$$(\varphi \Leftrightarrow \phi)^I = \varphi^I \leftrightarrow \phi^I \quad (42)$$

$$(\exists x\varphi(x))^I = \sup\{y \in [0, 1] : \text{exists the instance } t \text{ of the concept } T \text{ that } y = (\varphi(t))^I\} \quad (43)$$

$$(\forall x\varphi(x))^I = \inf\{y \in [0, 1] : \text{exists the instance } t \text{ of the concept } T \text{ that } y = (\varphi(t))^I\} \quad (44)$$

$$\langle \varphi, \alpha \rangle^I = \begin{cases} 1, & \varphi^I \geq \alpha \\ \varphi^I, & \varphi^I < \alpha \end{cases} \quad (45)$$

When the interpretation function  $I$  satisfies the conditions **F1 – F5** and (24)–(45), then it is called the fuzzification of the *IRL* logic language. If after the fuzzification as the result there are only characteristic functions, then this interpretation is called an exact. Then it is equivalent to the standard interpretation of description logic DL [2] and it satisfies the conditions **F1 – F5** and (24)–(37) are satisfied.

#### VI. BASIC INFORMATION RETRIEVAL LOGIC

The Information Retrieval System can be extended for searching reliable for experts subsets of  $X \cup X \times X$ , where  $X$  is a set of Web resources relating to a chosen field of knowledge. These subsets for a given query indicate reliable for experts Web addresses, representing the searched knowledge. Therefore, these sets can be used to reliable interpret the *IRL* expression.

For this purpose, as in the statistics, is used the confidence range  $V$ . It is considered that the most important is that all experts, on the basis of the confidence range  $V$ , accept the set of membership degrees of an object to the fuzzy set. This set represent fuzzification of the concept or the role, defined by the knowledge base  $K = \langle Tez, Fuz, V, Ont \rangle$ .  $Tez$  is a set of concepts and roles from the thesaurus and  $Ont$  is a set of concepts and roles from the ontology defined due to the postulate **P2**.  $Fuz$  is a set of possible-to-use interpretations (the fuzzification) defined due to postulates **P1 – P9**, conditions **F1 – F5** and (24) – (45). All *IRL* formulas consist of the set  $Tez \cup Ont$  and are interpreted in the **F** algebra by means of the fuzzification set  $Fuz$ . The formula  $\varphi$  is true in the knowledge base  $K$ , when for any fuzzification  $I \in Fuz, \varphi^I = 1$ . Since the formulas interpretations are at once the *BL-algebra* interpretations, algebra which is uniquely defined by these interpretations (the **F** algebra), we write  $val_{BL}(\varphi) = 1$ . Thus, the set of all *IRL* formulas belongs to the class of formulas sets of the fuzzy logic *BLV* interpreted in the *BL-algebra*. These logic were studied by Hájek [9]. In the *BLV* there are the following inference rules:

- 1) *Modus ponens*: from  $\varphi$  and  $\varphi \rightarrow \phi$  infer  $\phi$ ;
- 2) *Substitution rule*: we can substitute any formulas for the propositional variables;
- 3) *Generalization*: from  $\varphi$  infer  $\forall x\varphi(x)$ .

**Theorem (Soundness and Completeness).** Let  $\varphi$  be a formula of the *BLV*,  $T$  be a set of all formulas from the *BLV-theory*. Then the following conditions are equivalent (Proof. see [9]):

- 1) the formula  $\varphi$  is derived from  $T$ -theory with use of the inference rules;
- 2)  $val_{BL}(\varphi) = 1$  for each *BL-algebra* (with infinite intersection and infinite union) that is model for  $T$ .

The *IRL* is the two-variable fragment of the second-order logic. The values of all predicated variables are concepts and roles. However, the validities of a monadic predicate calculus with identity are decidable. When the formula with predicate variables and roles which are predicates would be removed, then we obtain the monadic predicate calculus. This fragment of the *IRL* is decidable. There are some fragments of the *IRL* of roles, which are decidable and some are known for their use [9], [12].

#### VII. DEFUZZIFICATION IN IRL

In this paper, the defuzzification is identified with the interpretation  $\langle K, Def \rangle$  in the *IRL* logic. This interpretation, for a given query, indicates a reliable-for-experts set of the Web addresses representing knowledge from the knowledge base  $K$ .

In this purpose, for the knowledge base  $K = \langle Tez, Fuz, V, Ont \rangle$  and for some fuzzification  $I \in Fuz$ , any concept  $C$  or any role  $R$ , have interpretation belonging to the set of the fuzzy confidence range  $V$ . It is accepted by all experts and is defined by:

$$V(C) \subseteq \{\alpha : \text{for some instance } t \text{ of the concept } C \text{ or } I \in Fuz, \alpha = (t : C)^I\} \quad (46)$$

$$V(R) \subseteq \{\alpha : \text{for some instances } (t_1, t_2) \text{ of the role } R \text{ or } I \in Fuz, \alpha = ((t_1, t_2) : R)^I\}. \quad (47)$$

Experts consider knowledge, which is in the fuzzy confidence range, as the exact knowledge and as part of the possible interpretations. The designation of such subsets will be identified with the knowledge defuzzification of the objects, belonging to the  $X$  or  $X \times X$  [5].

The function  $(.)^{Def}$  is called the **defuzzification interpretation** or the **defuzzification of the knowledge base**  $K = \langle Tez, Fuz, V, Ont \rangle$ , if following formulas are true. For any concepts  $C, D$ , roles  $R, R_1, R_2$ , instances of concepts  $t, t_1, t_2$ :

## VIII. CONCLUSION

The information retrieval system is a kind of **the information retrieval agent** on the Semantic Web, if it meets the postulates **P1 – P9**. Commonly, the information retrieval systems and semantic relation systems have indicated only semantically closest resources. This not is always the case. When searching information about any object you can get the fuzzy knowledge described in the ontology and this uncertainty can lead to the uniquely determined knowledge resource. In this way we obtain the knowledge disambiguation and compliance with the description of the object by the expression used in the thesaurus.

Introduced conceptual apparatus will be used to develop the information retrieval agent, supporting effective and intelligent use of search engines. Likewise, this research can be used to extend the software used in search engines or to create a new type of search engine.

## ACKNOWLEDGMENT

Anna Bryniarska is a recipient of a Ph.D. scholarship under a project funded by the European Social Fund.

## REFERENCES

- [1] F. Baader, D. Calvanese, D. L. McGuinness, D. Nardi and P. F. Patel-Schneider eds., *The description logic handbook: theory, implementation, and applications*, Cambridge University Press, 2003.
- [2] R. Baeza-Yates and B. Ribeiro-Neto, *Modern Information Retrieval*, Addison-Wesley, 1999.
- [3] F. Bobillo and U. Straccia, *A fuzzy description logic with product t-norm.*, the IEEE International Conference on Fuzzy Systems (Fuzz IEEE-07), pp. 652–657. IEEE Computer Society, 2007.
- [4] F. Bobillo and U. Straccia, *Fuzzy description logics with general t-norms and datatypes*, Fuzzy Sets and Systems 160 (23), pp. 3382–3402, 2009.
- [5] A. Bryniarska, *The algorithm of knowledge defuzzification in semantic network*, Information Systems Architecture and Technology, Networks Design and Analysis, pp. 23–32, Wroclaw, Poland, 2011.
- [6] A. Bryniarska, *An Information Retrieval Agent in Web resources.*, IADIS International Conference Intelligent Systems and Agents 2013, Proceedings, pp. 121–125, Prague, Czech Republic, 2013.
- [7] R. Ceglarek and W. Rutkowski, *Automated Acquisition of Semantic Knowledge to Improve Efficiency of Information Retrieval Systems*, In: Business Information Systems 10th International Conference, Proceedings, LNCS, Springer, pp. 329–341, 2006.
- [8] R. Ceglarek, K. Haniewicz and W. Rutkowski, *Semantic compression for specialized Information Retrieval systems*, In: Find out how to access preview-only content Advances in Intelligent Information and Database Systems Studies in Computational Intelligence, vol. 283, pp. 111–121, 2010.
- [9] M. Cerami, F. Francesc Esteva and F. Bou, *Decidability of a Description Logic over Infinite-Valued Product Logic*, Proceedings of the Twelfth International Conference on the Principles of Knowledge Representation and Reasoning (KR 2010), pp. 203–213, 2010.
- [10] P. Hájek, *Metamathematics of fuzzy logic*, vol. 4 of Trends in Logic-Studia Logica Library, Dordrecht: Kluwer Academic Publishers, 1998.
- [11] J. Han and M. Kamber, *Data Mining: Concepts and Techniques*, Morgan Kaufmann Publishers, 2001.
- [12] U. Hustadt, R. A. Schmidt and L. Georgieva, *A Survey of Decidable First-Order Fragments and Description Logics*, Journal on Relational Methods in Computer Science, Vol. 1, pp. 251–276, 2004.
- [13] S. K. Jayanthi and S. Prema, *Word Sense Disambiguation in Web Content Mining Using Brills Tagger Technique*, In: International Journal of Computer and Electrical Engineering, vol. 3, No. 3, pp. 358–362, 2011.
- [14] Ch. D. Manning, P. Raghavan and H. Schtze, *Introduction to Information Retrieval*, Cambridge University Press, 2008.
- [15] M. Sanderson, *Word Sense Disambiguation and Information Retrieval*, In: Proceedings of the 17th International ACM SIGIR, Dublin 1994.

$$\perp^{Def} = \emptyset, \top^{Def} = X \quad (48)$$

$C^{Def} = X_C$ , where

- 1)  $X_C \subseteq X$
- 2)  $x \in X_C$  iff exists fuzzification  $I \in Fuz$ ,  
such that  $(t : C)^I \in V(C)$  and  $x = t^{Def}$

$R^{Def} = (X \times X)_R$ , where

- 1)  $(X \times X)_R \subseteq X \times X$
- 2)  $(x, y) \in (X \times X)_R$  iff exists fuzzification  $I \in Fuz$ , such that  $((t_1, t_2) : R)^I \in V(R)$   
and  $x = t_1^{Def}, y = t_2^{Def}$

$$(\neg C)^{Def} = X \setminus C^{Def} \quad (51)$$

$$(C \vee D)^{Def} = C^{Def} \sqcup D^{Def} \quad (52)$$

$$(C \wedge D)^{Def} = C^{Def} \sqcap D^{Def} \quad (53)$$

$$(\exists R.C)^{Def} = \{x \in X : \text{exists } y \text{ such that } (x, y) \in R^{Def} \text{ and } y \in C^{Def}\} \quad (54)$$

$$(\forall R.C)^{Def} = \{x \in X : \text{exists } y, \text{ if } (x, y) \in R^{Def}, \text{ then } y \in C^{Def}\} \quad (55)$$

$$(t : C)^{Def} \text{ iff } t^{Def} \in C^{Def} \quad (56)$$

$$((t_1, t_2) : R)^{Def} \text{ iff } (t_1^{Def}, t_2^{Def}) \in R^{Def} \quad (57)$$

$$(C \sqsubseteq D)^{Def} \text{ iff } C^{Def} \sqsubseteq D^{Def} \text{ and } (C = D)^{Def} \text{ iff } C^{Def} = D^{Def} \quad (58)$$

$$(R_1 \sqsubseteq R_2)^{Def} \text{ iff } R_1^{Def} \sqsubseteq R_2^{Def} \text{ and } (R_1 = R_2)^{Def} \text{ iff } R_1^{Def} = R_2^{Def} \quad (59)$$

For any formulas  $\phi, \varphi$  and degrees  $\alpha \in [0, 1]$ :

$$\langle \phi, \varphi \rangle^{Def} \text{ iff } \phi^I \geq \alpha \text{ for any } I \in Fuz \quad (60)$$

$$(\neg \phi)^{Def} \text{ iff (not } \phi^{Def}) \quad (61)$$

$$(\phi \wedge \varphi)^{Def} \text{ iff } (\phi^{Def} \text{ and } \varphi^{Def}) \quad (62)$$

$$(\phi \vee \varphi)^{Def} \text{ iff } (\phi^{Def} \text{ or } \varphi^{Def}) \quad (63)$$

$$(\phi \Rightarrow \varphi)^{Def} \text{ iff (if } \phi^{Def} \text{ then } \varphi^{Def}) \quad (64)$$

$$(\phi \Leftrightarrow \varphi)^{Def} \text{ iff } (\phi^{Def} \text{ iff } \varphi^{Def}) \quad (65)$$

$$(\exists x \phi(x))^{Def} \text{ iff exists the instance } t \text{ of the concept } T \text{ such that } (\phi(t))^{Def} \quad (66)$$

$$(\forall x \phi(x))^{Def} \text{ iff for any instance } t \text{ of the concept } T : (\phi(t))^{Def} \quad (67)$$

It can be noticed that as a result of the defuzzification of the knowledge base  $K$  is some theory  $Theory(K)$  of sets from the space  $X \cup X \times X$ . In the process of information retrieval, the knowledge base  $K$  should be define in such way, that the defuzzification process of true formula in the base  $K$ , is thesis from  $Theory(K)$ : if for any fuzzification  $I \in Fuz$ ,  $\phi^I = 1$ , then there is  $\phi^{Def}$ . This knowledge base is called the **adequate knowledge base**. Furthermore, definition of this knowledge base allows to disambiguate fuzzy knowledge which is searched.

- [16] Ch. Stokoe, M. P. Oakes and J. Tait, *Word Sense Disambiguation in Information Retrieval Revisited*, SIGIR 2003, 2003.
- [17] U. Straccia, *A fuzzy description logic*, In Proc. of the 15th Nat. Conf. on Artificial Intelligence (AAAI-98), Madison, USA, pp. 594–599, 1998.
- [18] U. Straccia, *Reasoning with Fuzzy Description Logics*, In: Journal of Artificial Intelligence Research 14, pp. 137–166, 2001.